UNIVERSITY OF CALIFORNIA
RIVERSIDE

The Gray Area: Investigating Transitional Slip Behavior through Observational Seismology

A Dissertation submitted in partial satisfaction
of the requirements for the degree of

Doctor of Philosophy

in

Geological Sciences

by

Alexandra Hutchison

September 2018

Dissertation Committee:

Dr. Abhijit Ghosh, Chairperson
Dr. David D. Oglesby
Dr. James H. Dieterich

The Dissertation of Alexandra Hutchison is approved:

Committee Chairperson

University of California, Riverside

Acknowledgments

Mom and Dad. This thesis is for you. I love you and this would not have been possible without your steadfast guidance, support, and love.

Dr. Abhijit Ghosh, your manner of thinking and ability to deconstruct complex ideas into simple explanations is incredible. I am grateful for how you encouraged me to explore and challenge my limits.

Dr. Gordon Love, this PhD would never have happened without your unrelenting guidance and support. Thank you for always being a mentor and a friend.

I would like to express my deepest appreciation to my committee, Dr. David Oglesby and Dr. James Dieterich. Thank you both for providing constructive feedback on my work and being active participants in my development as a scientist over the course of my PhD.

Prof. Katherine Cashman - Working with you was the first time I began to have confidence in myself as a scientist. Thank you for teaching me to trust in myself. You are are an inspiration in all of the ways.

Prof. David Bailey. I remember my first geology class with you. You played a Bob Dylan song and we talked about asbestos and 9/11. You made geology relatable, tangible, and omnipresent. Thank you for awakening my fascination in Earth Sciences (and the cosmos) and for the continued support through the years.

Wally and Bruiser. Thank you for keeping the bed warm, the apartment lively, making sure I always had a friend, and the consistent enthusiasm at the door.

Friends. I'm so grateful for you: for feeding me food for my belly and my brain.

I'm too afraid to leave anyone out, but know that this PhD has a piece of all of you in it. For each moment that I doubted myself, or thought this wasn't worth it, or had a bad day, one of you was there to encourage me – even if not directly in the world of geophysics, just by being there, and I will never forget that kindness. You all are my family, my cult ;), my dream team, my mentors, my lovers, my inspirations, and my motivators. Thank you.

and to Laurent,)'(, *, and the desert. Thank you always.

Chapter 2: Hutchison, A. A., & Ghosh, A. (2017). Ambient Tectonic Tremor in the San Jacinto Fault, near the Anza Gap, Detected by Multiple Mini Seismic Arrays. Bulletin of the Seismological Society of America, 107(5), 1985-1993.

Chapter 4: Hutchison, A. A., & Ghosh, A. (2016). Very low frequency earthquakes spatiotemporally asynchronous with strong tremor during the 2014 episodic tremor and slip event in Cascadia. Geophysical Research Letters, 43(13), 6876-6882.

Chapter 5: in revision for Journal of Geophysical Research (Solid Earth)

Dedication

S.E.G | 1987-2016

ABSTRACT OF THE DISSERTATION

The Gray Area: Investigating Transitional Slip Behavior through Observational Seismology

by

Alexandra Hutchison

Doctor of Philosophy, Graduate Program in Geological Sciences
University of California, Riverside, September 2018
Dr. Abhijit Ghosh, Chairperson

Slow earthquakes essentially represent a gray area of the slip spectrum, where regular fast slip earthquakes and aseismic creep constitute the spectrum's end members. Since their discovery in 2003 [Rogers and Dragert, 2003], increasing seismic observations, in addition to models, geodetic observations, and laboratory studies, have helped elucidate the nature of these events that vary quite vastly amongst themselves. Empirically, however, they share a linear moment rate scaling law that distinguishes them from regular earthquakes [Ide *et al.*, 2007]. Slow earthquakes include, but are not limited to, low frequency earthquakes (LFEs), tremor, very low frequency earthquakes (VLFEs), slow slip events (SSEs), and episodic tremor and slip (ETS) events. Each type of these events has distinctive properties that makes their detection challenging. Furthermore, their relationships to each other remains unclear, particularly in terms of source properties. They may be important in the context of regular earthquakes and seismic hazard assessment as they appear to have a correlation with large events. Some slow earthquakes have been observed spatiotemporally preceding regular earthquakes such as the 2011 M_w 9.0 Tohoku earthquake [Kato *et al.*, 2012] and the

2014 M_w 8.1 Iqueique earthquake [Ruiz *et al.*, 2014]. Additionally, a region near the trench known to produce VLFEs ruptured coseismically during the Tohoku earthquake producing a larger earthquake and tsunami than was previously anticipated [Ide *et al.*, 2012]. Ultimately, more observations and studies are required to understand the mechanical properties of slow earthquake source physics and to understand their greater role in the earthquake cycle.

The research shared herein describes a variety of observations of slow earthquakes in discrete tectonic settings. The first section of this thesis examines a locked section of the San Jacinto Fault – a non-plate boundary transform fault – called the Anza Gap. The study begins in chapter 2 by introducing the detection of ambient tectonic tremor [Hutchison and Ghosh, 2017], likely acting as a seismic manifestation of slow-slip or deep creep. The latter chapter within this section, chapter 3, examines a series of teleseismically triggered tremor and small earthquakes leading up to the June 10, 2016 M_w 5.2 Borrego earthquake. This cascade of tremor and foreshocks is interpreted to signify seismic manifestations of deep creep triggered by the energy from two distant earthquakes that occurred earlier in the day. The second section of this thesis focuses on VLFEs in the Cascadia subduction zone, a plate boundary where the Juan de Fuca plate is subducting beneath the North American plate. The first chapter in this section (chapter 4) uses grid search centroid moment tensor inversion during the 2014 ETS event to detect VLFEs. Unlike previous studies where VLFEs and tremor are spatiotemporally coincident, tremor and VLFE are only quasi-coincidentally occurring during this ETS event, indicating for the first time that VLFE and tremor may have discrete sources. Chapter 5 successfully employs matched filter analysis for VLFEs detection in Cascadia, indicating that VLFEs are repeating events, generating a high

resolution temporal catalog for the 2011 and 2014 ETS events. These data are compared to SSE data in both ETS events. VLFEs acts as an accurate proxy for both SSEs, even when tremor does not. This further indicates that tremor and VLFEs may have discrete source mechanics, though they may both be related through slow-slip. In addition, an inter-ETS VLFE catalog shows sustained background VLFE activity throughout the inter-ETS period. Finally, in Chapter 6, a grid-search centroid moment tensor inversion VLFE catalog is created between the 2011 and 2014 ETS events. This allows for further investigation of VLFE behavior, particularly during inter-ETS periods. These new observations further underscore a quasi-spatiotemporal relationship between VLFE and tremor, suggesting an underlying process that uniting these events. Through these observations, I propose that there are ongoing small, and largely undetectable SSEs that are manifested through inter-ETS slow earthquake seismic signatures, "mini-ETS" events, and that these events would fill the gap in the slow earthquake scaling law [Ide *et al.*, 2007]. These observations support the Colella *et al.*, [2011] rate- and state- dependent friction models that suggest a non-linear scaling relationship between moment and duration. I also propose slow-slip is the driving mechanism uniting all slow earthquake activity, or the gray area, of the slip spectrum [e.g. Wech and Bartlow, 2014, Wech *et al.*, 2009, Bartlow *et al.*, 2011].

Contents

List of Figures

Part I

Introduction

Chapter 1

Introduction

1.1 Introduction

The earthquakes that we are most familiar with, the ones that rattle the ground, and can topple buildings only represent one end member of slip behavior that can occur along a fault interface. Though not necessarily obvious to us through our immediate experiences, other types of fault slip behaviors are emerging as the scientific community becomes equipped with improving detection technology, better instrument distribution, and ever-evolving analytic techniques. Not only do these observations allow us to characterize fault behavior, but also to better parameterize the mechanisms responsible for the apparent fault slip behavior. On the opposite end of the fault spectrum of the earthquakes some of us are experientially familiar with is aseismic slip, a type of fault motion that produces creep, which cannot be observed with seismicity, but rather through strain alone. Finally, in the last decade and a half, an entire gray area in the slip spectrum has emerged that manifests elements of both seismic and aseismic slip and obeys its own set of unique scaling laws. As

with any topic in science, new behaviors provide new tool sets to investigate new principles and even explore new approaches to understanding old ones. This dissertation explores this gray area of the slip spectrum with observations of various types of behaviors from this still largely unexplored part of the slip spectrum, providing insights about the state of stress and material properties of the source region, elucidating pieces of information about the source mechanisms and relationships of these more obscure events: slow earthquakes.

1.1.1 The Slip Spectrum

Until the discovery of slow earthquakes, or the "gray area" of the slip spectrum, in 2002-2003 [Obara and Kazushige, 2002; Rogers and Dragert, 2003], slip was considered bimodal and was either thought to produce or not to produce seismic energy. Many models were created and experiments performed to determine the best parameterization for encompassing this bi-modality of slip behavior. Different properties can have various impacts on how and when a fault will slip including its stress field and physical properties that are often dependent on depth and geologic setting. With increasing depth, temperature and pressure increase in the Earth's lithosphere, resulting in increasingly plastic materials. In other words, with increasing depth, materials tend to deform in a less brittle – or elastic – manner. Instead, materials begin to take on more viscous rheologies, meaning that slip occurs with little to no frictional resistance or elastic deformation. Some places in the shallow crust also experience such behavior due to the material properties of the geologic setting of the fault, or it has been suggested this can be due to the presence of fluids and increased effective normal stress. Such behavior characterizes the creeping side of the slip spectrum. On the other side of the slip spectrum, at shallow depths (<40 km), the seis-

mogenic zone is the part of the fault capable of producing seismic energy due to its brittle nature that mandates elastic deformation. Most simply put, this variety of deformation, largely resulting from the rigidty and strength of shallower lithospheric materials and their frictional properties is what is responsible for this end of the slip spectrum that produces regular earthquakes.

"The gray area" of the slip spectrum consists of behavior inclusive of elements of the rigid, locked, upper crust and the more plastic, freely sliding, lower crust. Its behavior is revealed through a unique sub-spectrum of events that can emit seismic energy, but also sometimes consist only of discrete creeping events.

The first observations of slow earthquakes occurred in southwest Japan, where low frequency and long period tremors that did not fit the classical understanding of earthquakes had source locations and focal mechanisms consistent with the subducting Philippine plate. Moreover, the events occurred near the Mohorvich discontinuity at 30 km, where the material properties of the lithosphere begin to transition into more viscous material [Obara and Kazushige, 2002]. Some of these events lasted for weeks, which sharply contrasted with regular earthquakes, which typically do not have signal durations longer than several hundred seconds. Shortly thereafter, similar seismic signals were observed with simultaneous GPS observations from the Earth's surface, directly above a similar depth in the Cascadia subduction zone. In this case, these coincidental crustal deformation and elusive tremor signals were episodic, and further, the Earth's crust in this region above this particular transition depth range of the subducting slab (30-40 km) would move opposite plate motion [Rogers and Dragert, 2003]. Since the region of crust corresponding to shallower depths of

the subducting slab continued to move in the direction of subduction, it seems intuitive that this up-dip segment of the fault, the locked zone, may experience an increase in stress during these, what are now termed, episodic tremor and slip (ETS) events [Obara and Kato, 2016].

There is a growing body of evidence showing that these slow earthquakes often do spatiotemporally precede regular earthquakes in different shapes and sizes. Two slow earthquakes led up to the mainshock of the M_w 9.0 Tohoku earthquake in 2011 [Kato *et al.*, 2012]. A foreshock sequence associated with multiple slow-slip events spatiotemporally preceeded the M_w 8.1 Iquique earthquake in 2014 [Ruiz *et al.*, 2014; Kato and Nakagawa, 2014]. Such phenomena is not unique to subduction zones either. In 1999, the M_w 7.9 Izmit earthquake was also preceeded by 44 minutes of slow earthquakes activity characterized by long period signals that increased in their number until the mainshock. Finally, one of the most enigmatic types of slow earthquakes: a very low frequency earthquake (VLFE) essentially transitioned into a M_w 3.7 earthquake in a strike-slip setting in Alaska [Tape *et al.*, 2018].

The fact that these transitional slip behaviors can occur in the same part of the fault interface as regular earthquakes raises questions about the mechanisms that entertain one flavor of slip behavior as opposed to another, even sometimes in rapid succession. Curiously, during the 2011 Tohoku earthquake, the fault ruptured coseismically up-dip into a region previously associated with VLFE activity. This additional rupture area produced both a larger earthquake and larger tsunami than was previously thought possible [Ide *et al.*, 2011]. Again, such fault behavior should cause us to reassess our basic understanding

of traditional fault mechanics: the fault interface and its materials behave differently with respect to time and different conditions. This concept can be unpacked further by examining the many types of slow earthquakes that have been observed and beginning to investigate why at times some of these events are observed together and why in certain settings, only one type of slow earthquake is observed.

1.1.2 Slow Earthquakes

Slow earthquakes empirically follow a scaling relationship that differentiates them from regular earthquakes based on their moment rate, or how much moment is produced per unit time. In the case of regular earthquakes, their moment is proportional to their duration cubed. However, in the case of slow earthquakes, their moment has a linear relationship with their duration, such that the name slow earthquake is quite fitting [Ide *et al.*, 2007]. This empirical relationship has been countered, however, with the proposition that there is a variety of slip that can occur with a moment to event duration ratio that lies on a continuum between the typical earthquake moment scaling rate and the linear relationship portrayed in the slow earthquake scaling law; in other words, slip is not bimodal [Peng and Gomberg, 2010]. Slow earthquake is really an umbrella term that encompass all of the events that do not behave quite like continuous creep or like regular earthquakes, but that tend to follow this scaling law. Starting with the largest events: slow slip events (SSEs), which are discrete aseismic slip events that can produce a wide range of magnitude events, as large as M_w 7.0. SSEs have distinct mechanics that separate them from continuous creep. These essentially represent a rupture patch that is slowly passing through the fault interface producing no seismic energy. Seismic slow earthquakes tend to be smaller

magnitudes. Very low frequency earthquakes (VLFEs) produce the largest moment of the seismic slow earthquakes. Characteristically they produce energy between 0.02 – 0.05 Hz and their signal durations are 90 s, thus producing events in the range of M_w 3-4. Low frequency earthquakes (LFEs) produce short duration signals, usually lasting no more than 10 seconds, and typically are depleted of energy outside the 1-10 Hz range. They are very small events, sometimes with negative magnitudes. Tremor is thought to consist of many clustered LFEs, as it is a longer duration signal that can last for hundreds to thousands of seconds over periods of weeks, but due to the fact it is difficult to isolate events, it is also challenging to quantify the moment release of tremor. These types of "gray area" -or slow earthquake seismic activity- have distinctive seismic signature that distinguish them from regular earthquakes (figure 1.1). Ultra low frequency earthquakes (ULFEs) have also been observed, but on the electromagnetic spectrum, outside of the scope of this dissertation. Though, it should be noted that ULFEs have been investigated in the context of precursory earthquake behavior [e.g. Frasier-Cain *et al.*, 1990]. This research can be conducted, for example, by differentiating magnetic emissions presumably of seismic origin from plasma space waves. In one particular study, the emissions thought to originate seismically were actually in the 0.02 - 0.05 Hz frequency band, which we associate with VLFEs [Hayakawa *et al.*, 1996].

VLFEs, LFEs, and tremor are often associated with SSEs in the sense that if an SSE front passes through an asperity with a particular set of mechanical properties, it may produce one of these signals. This concept is often cited as the principle behind ETS events. In some settings and at some times, however, tremor and VLFE occur simultaneously, while

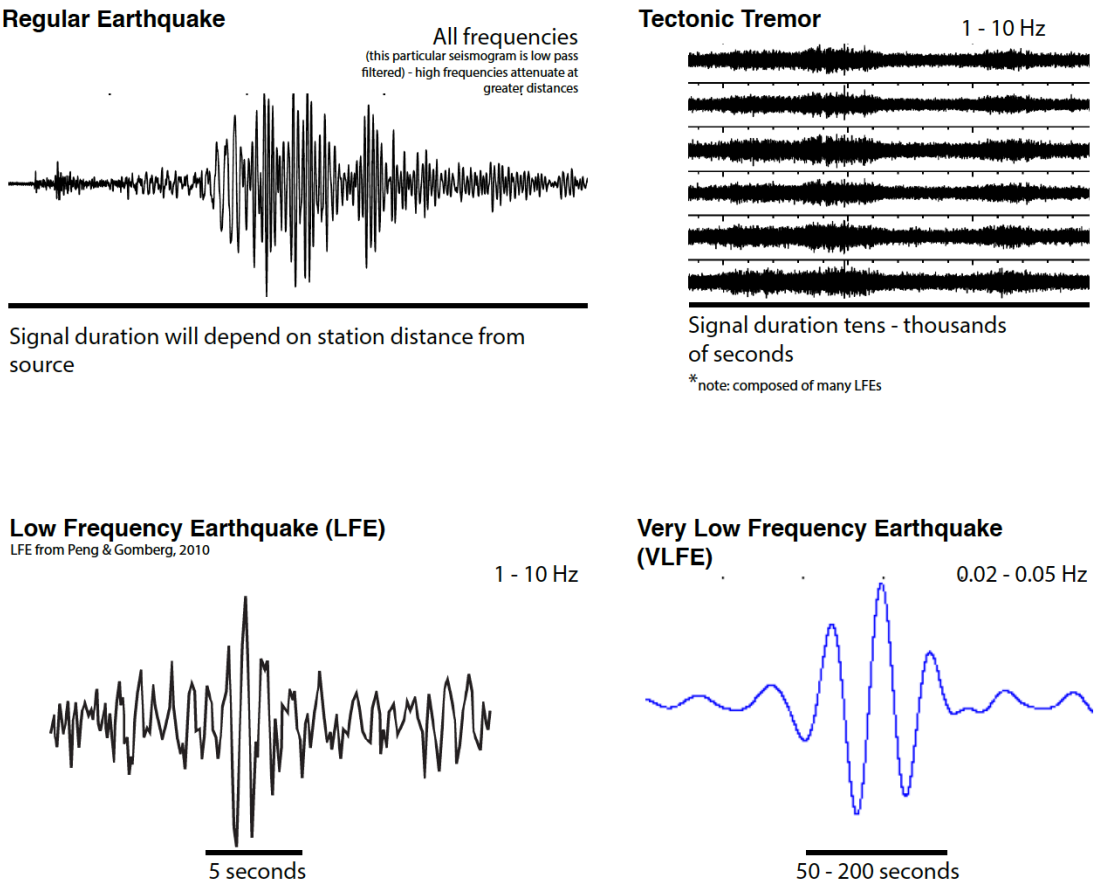

Figure 1.1: This figure gives examples of each of the main types of seismic slow earthquakes compared to a regular earthquake. The upper left hand corner demonstrates a regular earthquake in the upper left hand corner. They emit energy at all frequency bands, but higher frequencies attenuate at greater distances. There are distinct and impulsive P- and S- wave arrivals. A low frequency earthquake (LFE) is shown in the lower left hand corner [Peng and Gomberg, 2010]. They emit energy between 1-10 Hz and have short signal durations (5-10s). In the upper right hand corner is an example of tremor. Tremor consists of the clustered arrivals of many LFEs and thus has the same frequency content. Tremor, like the other events, must be coherent across multiple stations, preferably network stations. It can last from tens to thousands of seconds. Finally, an example of a very low frequency earthquake (VLFE) is shown in the lower right hand corner. It is completely depleted of high frequency energy and primarily emits energy in the 0.02 - 0.05 Hz frequency band. The signal duration typically lasts from 50 - 200 seconds.

at other times they do not, even in the same tectonic setting [Ghosh *et al.*, 2015; Hutchison and Ghosh, 2016, respectively]. This must be a reflection of characteristics of the plate interface during the ETS event, though as we are only beginning to expand the middle part of the slip spectrum, these questions are still fundamental and many observations are still required to build up the repertoire of knowledge required to understand the variety of transitional fault behaviors. This thesis combines observations of slow earthquakes in various tectonic settings to make inferences about relationships between different types of activity within the middle of the slip spectrum and how they relate to one another and to regular earthquakes.

1.1.3 Methods for Detection of Slow Earthquakes

Since several types of slow earthquakes including VLFEs and tremor, the subjects of this dissertation, do not have P- and S- arrivals, they are more challenging to detect. Typical location methods that look implement P- and S- wave travel times to different stations become useless when locating VLFEs and tremor. Several methods that are used throughout this dissertation include envelope cross correlation [Wech and Creager, 2008], beamforming and various subtypes of beamforming (i.e. multi-beam backprojection and beam backprojection [Ghosh *et al.*, 2009; 2012]), and grid-search centroid moment tensor inversion. The following is a brief introduction to each of these location methodologies.

Envelope Cross Correlation

Given that tremor is many LFEs, events that do contain P- and S- waves, arriving in overlapping clusters, it is becomes essentially impossible to separate these phase arrivals

embedded within tremor. Envelope cross correlation (ECC) instead exploits the fact that tremor must have a coherent signal across many network stations within the general source region. First, the algorithm takes the envelope of the tremor signal, filtered in the frequency band with the best signal to noise ratio (SNR). It then time shifts all of the envelopes that show the coherent tremor signal such that they are aligned according to their highest cross-correlation coefficient. In other words, they are aligned so that the envelopes match up in time as closely as possible. Next, using a 1-D velocity S-wave model, the algorithm performs a grid search of the source region to determine which grid node best fits the time shift that was applied to each seismogram (e.g. station) to achieve the optimal cross correlation coefficient.

This method has limitations. First, it is entirely limited by the velocity model. Using a 1-D velocity model means that any lateral heterogeneities are unaccounted for. ECC can provide relatively good horizontal locations, but lacks vertical resolution. Next, if the algorithm is set to run in an automated time-shifting fashion, it may pick up small local or regional earthquakes that are not in the earthquake catalog.

Beamforming

Beamforming is method that is applied across many types of physics. The basic principle behind beamforming is essentially the generation of a vector that represents the timing for which energy in a specific frequency band arrives at each individual detection instrument within an array. In other words, the order and rate in which the signal reaches each instrument can provide vector of a given magnitude and direction that offers a sense of direction, and in the case of seismology, slowness. Beamforming is essentially summing

the energy of the seismograms vector space. A coherent source will produce constructive interference such that energy reaches each of the seismometers in an ordered fashion, producing a beam in the direction of the source. Conversely, noise will have deconstructive inference such that energy will reach seismometers simultaneously from different directions, producing an incoherent beam, or multiple beams for the same time window.

Slowness is the inverse of velocity. It is used instead of velocity in the case of beamforming because it is a way to represent the wave front, which most accurately captures the order in which instruments are reached by a given source (figure 1.2). A shallowly sloping wave front, or low slowness, corresponds to a high velocity source (high angle with respect to the surface of the Earth). Thus, a low slowness source represents a high velocity source. High velocity sources tend to occur deeper in the crust. When identifying slow earthquakes, it is important that they have low slowness values since they tend to have source locations and the bottom of of the locked zone. Shallow sources have steeper wave fronts and lower velocity sources. Lower velocities tend to correspond to shallower sources in the crust.

Given that beamforming can be used to give an independent constraint on depth, without relying on a velocity model, it can be useful for determining the relative depth of an event. This is helpful for ruling out events that may appear like tremor in a seismogram, but are actually anthropogenic noise coming from the surface.

For an exact location based on beamforming, beam backprojection uses the vector in the slowness space produced by beamforming and projects it onto a fault model. The back projection is based on a projection of slowness values projected onto the fault based on a velocity model [Ghosh *et al.,* 2009; 2012]. Given that beam backprojection relies on both

a fault model and a velocity model, the there is a margin of error based on the accuracy of the fault model and the velocity model.

Finally, multi-beam beackprojection (MBBP) utilizes the intersection point of the back azimuth of the slowness vector of multiple arrays to determine a location. This method does not require a velocity model or a fault model, but does require multiple arrays. As such it can be highly accurate, but given the requirements for implementation, it is more difficult to implement. [Ghosh *et al.,* 2009; 2012]

Grid Search Centroid Moment Tensor Inversion

VLFEs are detected in a frequency band with a very low SNR. VLFEs have only 1-3 peaks and troughs, which can also contribute to difficulty in their detection and location. One method to detect VLFEs divides the possible source region into a 3D grid and then compares observed seismograms with synthetic seismograms from each individual grid node. The grid node with the highest match between the synthetic and observed seismograms is then considered the source location.

The important part of this method is ultimately the generation of synthetic seismograms. This process involves the convolution of a source-time function and a Green's Function based on a velocity model of choice. For each grid node, a unique synthetic is generated that represents the path between each each station and that respective grid node.

Each grid node is considered the source such that when the grid-search begins the observed seismograms are compared to the synthetics from each grid-node (i.e. each possible source). The highest match, or variance reduction, between the observed and the synthetic is then considered the source. The moment tensor is calculated for each grid-node.

Additional work is required to select actual events, but that criteria is discussed later in this dissertation.

1.1.4 Summary of Projects

This dissertation contains several studies that utilize slow earthquakes as a means to determine more about the properties of the source region and also more about the source properties of slow earthquakes themselves. It incorporates and combines multiple detection and location methodologies, which reflects the inherent difficulty of detecting these elusive events. These projects can be divided into two study regions. The first subproject focuses on the San Jacinto Fault (SJF) in Southern California and primarily focuses on the discovery of ambient tremor in the Anza Gap [Hutchison and Ghosh, 2017] using envelope cross correlation (ECC) [Wech and Creager, 2010] and various types of location methods in the slowness space including beam backprojection and multi-beam backprojection [Ghosh *et al.*, 2009; Ghosh *et al.*, 2012]. The next subproject looks at teleseismically triggered tremor and a foreshock sequence of microseismic eventic events that spatiotemporally evolve towards the nucleation site of a M_w 5.2 earthquake, which occurred on the southern edge of the Anza Gap. This study again utilizes beam backprojection and various spectral analyses. The second section of this dissertation examines a different type of slow earthquake, VLFEs in Cascadia [Hutchison and Ghosh, 2016]. The first subproject employs grid-search centroid moment tensor inversion method [e.g. Ito *et al.*, 2007] to generate a VLFE catalog during the 2014 ETS event to examine any spatiotemporal relationship between VLFEs and tremor. The resulting catalog is the first time VLFE and tremor are observed with asynchronous spatiotemporal distributions. The next subproject incorporates a matched-filter

method to determine create a higher resolution temporal catalog to examine VLFE activity during the ETS with respect to both tremor and GPS observations of slow-slip. It also evaluates VLFE activity during the inter-ETS period. The findings indicate that during both the 2011 and 2014 ETS events, VLFEs are consistent with slow-slip, even if tremor is not, as is the case during the 2014 ETS event. The matched-filter search detects consistent inter-ETS activity and asperity reactivation during subsequent ETS events [Hutchison & Ghosh, in revision, JGR.]. Finally, using the grid-search centroid moment tensor inversion, I generate a catalog from the 2011 ETS event through the 2014 ETS event to generate a long term catalog of template events to begin a long term characterization of VLFE activity in the Puget Sounds region of Cascadia.These findings show both VLFE behavior that is spatiotemporally coincident with tremor at times during ETS events, but that demonstrates a quasi-spatiotemporal coincidence with tremor during the inter-ETS period. This is interpreted to signify a response to changes in the stress field both during or after other slow-earthquake activity.

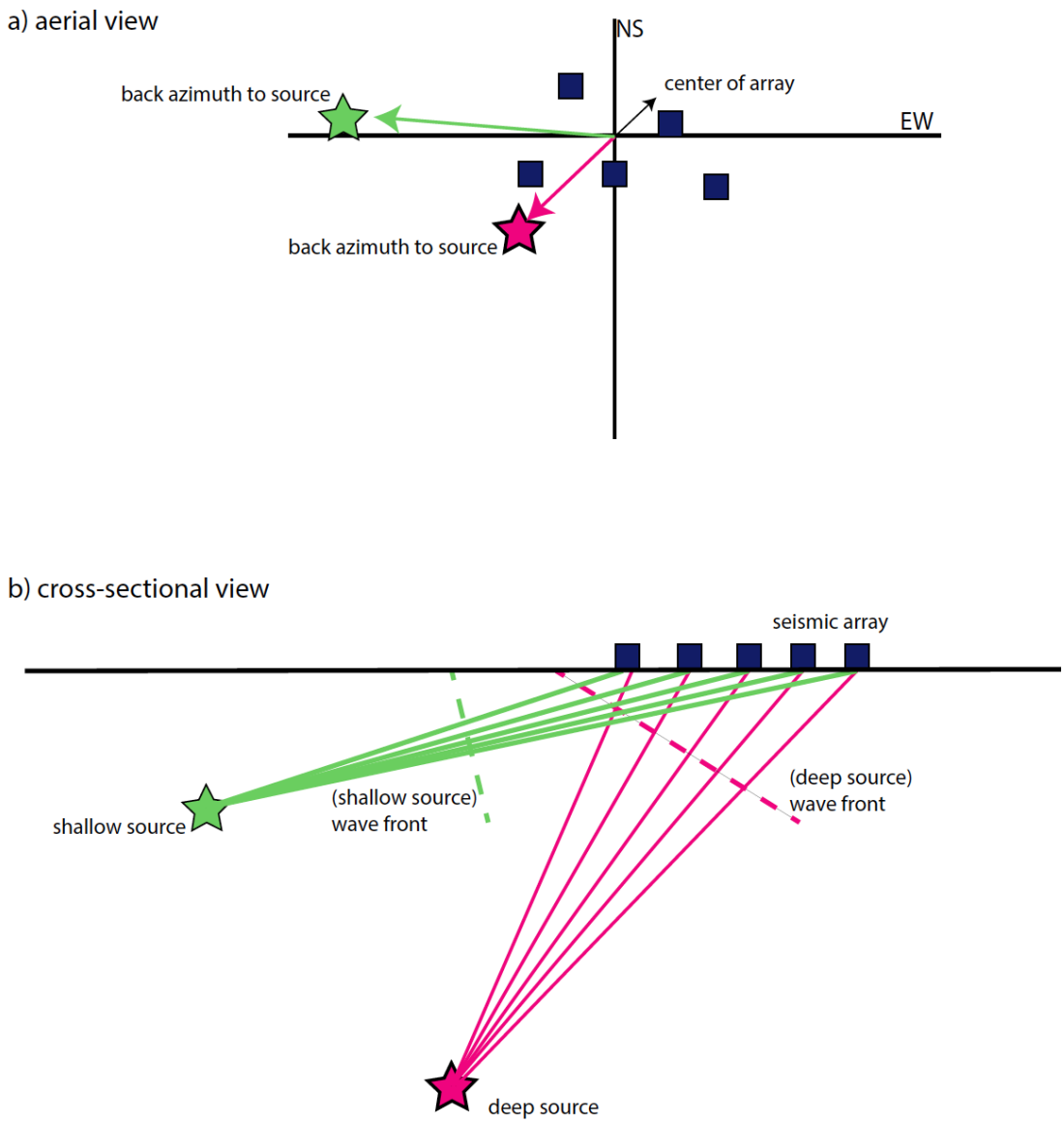

Figure 1.2: This is a schematic diagram of the way beamforming works. Two sources are given (one with a green star and one with a pink star, stations are displayed by navy blue squares). a) Gives an aerial perspective of how energy from a source will hit stations of an array in a particular order such that a back azimuth between the center of the array and the source can be produced. b) Gives a cross-sectional perspective of how a relative sense of depth can be determined through beamforming. Deep sources (pink) will have a shallow sloping wave front, and thus a lower slowness; shallower sourcer (green) will have a steeper wave front, and thus a higher slowness. Shallower wave fronts (and low slowness) correspond to higher velocity sources, which correlate with greater depths. Steeper wave fronts have high slowness values and correspond to low velocity sources, which typically correspond to source locations that are shallower in the crust.

Part II

Distinctive Seismic Behavior of the San Jacinto Fault near the Anza Gap

Chapter 2

Ambient Tectonic Tremor in the Anza Gap

2.1 Tectonic tremor in the San Jacinto Fault, near the Anza Gap, detected by multiple mini seismic arrays

2.1.1 Abstract

We detect multiple short duration ambient tremor events in the San Jacinto Fault near the Anza Gap applying multiple independent detection and location methods including multi-beam backprojection [*Ghosh et al.*, 2009a; 2012], envelope cross correlation [*Wech & Creager*, 2008], spectral analyses and visual inspection of existing network stations and high-density mini seismic array data. Different methods provide similar source locations for each of the tremor events in our catalog. All of the events have low peak slowness values indicating that they originate from a deep source, aiding in the elimination of potential

surface noise sources that may cause false detections. The tremor events are depleted of high frequency energy in the displacement amplitude spectrum compared to a small local earthquake at a similar location, a characteristic of tectonic tremor [*Shelly et al.*, 2007]. All tremor events are located near the northwestern boundary of the Anza Gap, where the Hot Springs Fault terminates. Recent studies may be interpreted to indicate that deep creep may be occurring at depth in this region [*e.g. Meng & Peng*, 2016; *Jiang & Fialko*, 2016; *Lindsay et al.*, 2014]. Another study by Inbal *et al.*, [2017] provided evidence for a slow-slip event in the Anza Gap following the El Mayor-Cucapah earthquake, suggesting the potential for transient behavior in the region, of which we interpret tremor to be a seismic manifestation.

2.1.2 Introduction

The San Jacinto Fault Zone (SJFZ) is a part of the San Andreas Fault System and is currently the most seismically active fault in southern California [*Sanders & Kanamori*, 1984; *Thatcher et al.*, 1975]. It is broken into many segments, all of which have experienced $M_w > 5.5$ earthquakes over the last 200 years [*Doser*, 1992], except for a 20 km region of the fault, the Anza seismic gap, which lies just northwest of the very seismically active triple junction of the Coyote Creek, Clark, and Buck Ridge segments of the SJFZ. There is no evidence that the Anza Gap is relieving stress through surface creep [*Sanders & Kanamori*, 1984], though this observation does not necessarily indicate whether or not strain is accumulating at depth. In fact, it appears there is strain accumulation in the Anza Gap at depth that may either indicate deep creep or a lower shear modulus [*Lindsay et al.*, 2014]. The Anza Gap's seismic quiescence, while being constrained on both sides by seismically

active fault strands has prompted many studies that forecast a M_w 6.5(+) earthquake for the area [*Thatcher et al., 1975*; *Sanders & Kanamori*, 1984]. Tremor has previously been identified between the creeping segment and the locked segment of the San Andreas Fault [*Nadeau & Dolenc*, 2005] and likely indicates stress loading on the locked segment of the fault. The ability to identify, locate and characterize tremor in this region can help with future seismic hazard assessment and understanding the state of stress in space and time near the Anza Gap, elucidating the presence of a fault segment with transitional seismic behaviors.

With the implementation of multiple tremor detection and location methods, we identified several discrete instances of non-volcanic tremor (NVT) during June 2011 along the San Jacinto Fault (SJF) near the Anza Gap. Wang *et al.*, [2013] identified and located triggered tremor during the passage of surface waves generated by the 2002 M_w 7.9 Denali earthquake. The triggered tremor occurred northwest of Anza, close to the location of the events found and described in this study. NVT is thought to be composed of many low frequency earthquakes (LFEs) [Shelly *et al.*, 2007], which are a type of slow earthquake that appear to obey a scaling law [Ide *et al.*, 2007] that is different from that of regular earthquakes. Slow earthquakes are typically known to occur in the transition zone of a fault at the base of the seismogenic zone. Different models are proposed to explain the dynamics of slow earthquakes [Ghosh *et al.*, 2010a; 2010b; Gershenzon *et al.*, 2011; Rubin, 2011;], but the underlying physics controlling slow earthquakes remains enigmatic. The slow earthquake scaling law characterizes the relationship between the duration and moment release of a family of events including tremor, LFEs, slow-slip events (SSEs), very low

frequency earthquakes (VLFEs), silent earthquakes, and ultra low frequency earthquakes (ULFEs). Tremor has been detected in Japan [i.e. Brown *et al.*, 2009], Costa Rica [Walter *et al.*, 2011], Cascadia [Wech & Creager, 2008], the Aleutian Islands, and Mexico – primarily in subduction regimes. Although less common, tremor has also been detected in strike-slip environments such as the SAF near Cholame [Nadeau & Dolenc, 2005; Nadeau & Guilhem, 2009]. The discovery of tremor in the SJF adds to the body of knowledge enveloping tremor in strike-slip settings, particularly given the recent findings that may suggest triggered deep creep in the region. Meng & Peng, [2016] found an aftershock region that extended below the locked zone, indicating that deep slip may be triggered by a main shock. Further, Jiang & Fialko [2016] observed microseismic eventicity several kilometers beneath the inferred locking depth (10-11 km). In the SJF, we see NVT in the Anza Gap, a segment of the fault that has no record of a noteworthy seismic event since 1890, when a complete large earthquake catalog has existed in California [Doser, 1992; Sanders & Kanamori, 1984, Thatcher *et al.*, 1975]. This lack of seismicity prompted scientists to forecast a M_w 6.5 or greater for this section of the SJF [Thatcher *et al.*, 1975; Sanders & Kanamori, 1984].

2.1.3 Data

This study uses seismic data from the Anza Network (AZ), the Caltech Regional Seismic Network (CI), the MAOTECRA Network (ZZ), which consists of three separate mini seismic arrays, and the Plate Boundary Observatory Borehole Network (PB). The network stations consist of short period (AZ, ZZ) and extra short period, defined by a sample rate of 100 Hz, (PB) sensors. The PB network stations consist of borehole stations, which are useful for elimination of surface noise that is prevalent in the area. The analyses

included in this study are from June 2011 when data from all three networks and all three of the mini seismic arrays in the MAOTECRA network are available. Availability of both array and network data is crucial for the detection and location methods employed in this study. Multiple arrays are required for locations using multi-beam backprojection (MBBP), while using the maximum number of network stations available increases the accuracy of the envelope cross correlation (ECC) location. All of the stations surround the area of interest, the Anza Gap, where we detect tremor. (figure 2.1)

2.1.4 Methods

This study began with simple visual inspection of MAOTECRA array data to identify tremor-like signals. Then we applied the MBBP method [Ghosh *et al.*, 2009a] on each of the arrays for the respective time windows to confirm a coherent beam, a low slowness value (indicating a deep source), and derive a location by identifying where the azimuths from the beams of each of the arrays intersect. To further confirm the events, we apply ECC method to network data from the AZ, CI, and PB network stations to determine if the ECC location is consistent with the location determined through the MBBP method. We cross-referenced candidate time windows with the Southern California Seismic Network (SCSN) catalog to rule out regional and local events and the Advanced National Seismic System (ANSS) catalog to eliminate teleseismic events. All signals were also examined in multiple frequency bands to rule out uncataloged events. Events that fit all of the evaluation criteria were added to our catalog.

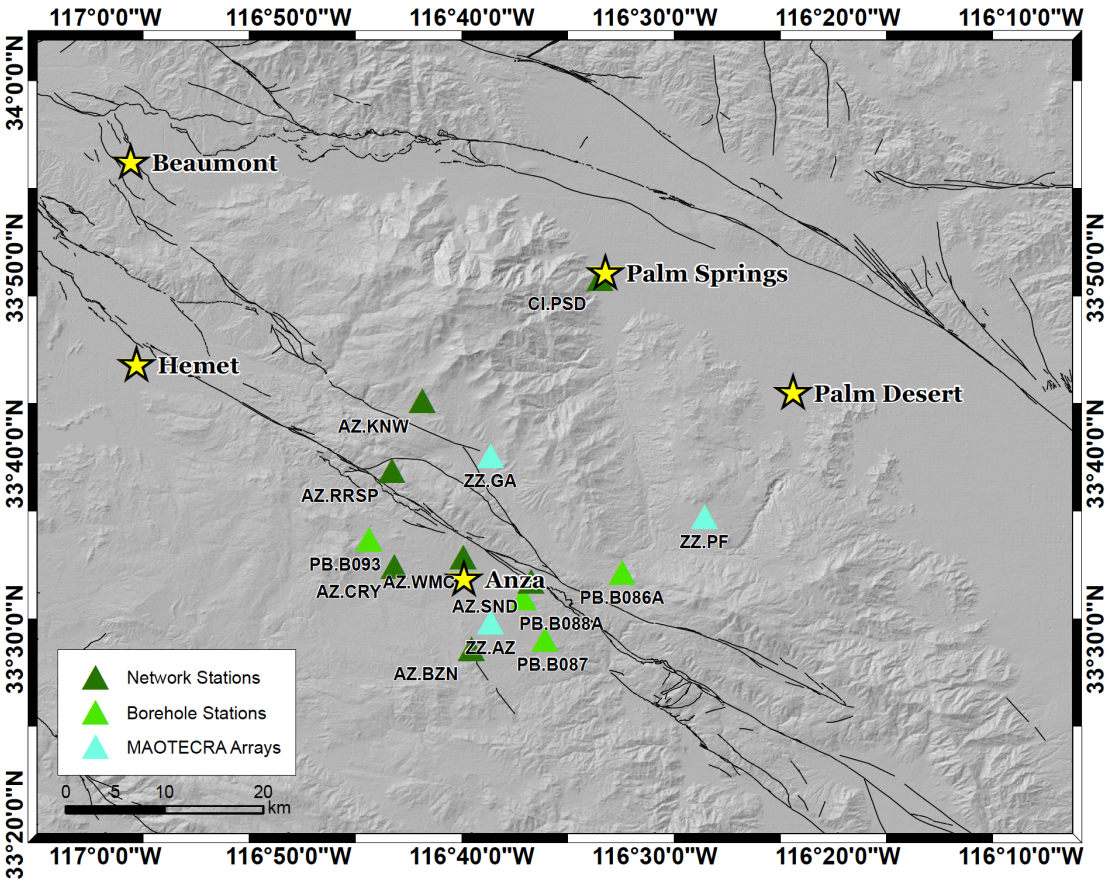

Figure 2.1: The region of interest, the Anza Gap, lies roughly within the red box. Locations of network stations and high-density arrays used for analyses in this study are also indicated on the map according to the legend. Each high-density array is labeled individually on the map.

Visual Inspection and Elimination of Noise and Earthquakes

Seismograms were inspected in tremor's characteristic frequency band of 2-8 Hz. Inspection of data from the mini arrays (MAOTECTRA) revealed several tremor-like events,

coherent across multiple stations. Seismic signals from time windows of interest were flagged and evaluated across all of the MACOTECRA mini-arrays and were then examined in the Anza (AZ), CalTech, and the Plate Boundary Observatory Borehole (PB) Networks. Waveforms that showed coherence across at least three stations from three separate networks or arrays (if they were in the MAOTECRA network) remained in our candidate list.

Anthropogenic noise is a significant problem in this area. Cristea-Platon *et al.*, [2013] found that train noise is often a source for false detection of tremor in the SJF and identified that the 3-5 Hz frequency band largely encompasses the seismic noise produced by trains, which unfortunately overlaps with the tremor frequency band of 2-8 Hz. The train signals identified by Cristea-Platon *et al.*, [2013] have durations of 5-20 mins, much longer than the tremor events cataloged in this study. Nonetheless, to avoid train noise altogether, we examined the higher end of the tremor frequency band, 6-8 Hz. Results remained consistent in the 2-8 Hz frequency band, but by also using the 6-8 Hz band, we safely ruled out train noise. To further rule out trains as a source of false tremor detections, we compared our tremor signals to the seismic data from stations that are located along train tracks (e.g. CI.MGE). Coherent signals that include the seismogram near the train station were discarded from our catalog. Overall, very few of these candidates existed, likely due to the fact that these signals typically had very high slowness and were eliminated earlier in the cataloging process.

To rule out regional and local events, we compared our NVT catalog to the Advanced National Seismic System (ANSS) catalog and the Southern California Seismic Network (SCSN) catalog. Some events were eliminated if the azimuth from all beams pointed

south without converging. These events may be regular, small, attenuated earthquakes located in Mexico.

Multi-beam Backprojection

Beamforming is a method that boosts coherent signal and reduces incoherent noise in time series data, and is thus helpful in analyzing data with low signal-to-noise ratio. Beamforming uses the differential travel times of a wavefronts between stations to determine an apparent (horizontal) slowness and back azimuth [Rost & Thomas, 2002]. While this method alone cannot provide an exact location, beam backprojection technique uses slowness and azimuth obtained from the beamforming method to locate the general source of the signal [Ghosh *et al.*, 2009a, 2012]. Using a single array, azimuth and slowness are calculated for a sliding time window analysis [i.e. Ghosh *et al.*, 2009a].

Multi-beam backprojection (MBBP) is utilized when slowness vectors are available for multiple arrays; their point of intersection can be inferred as the approximate source location in the physical latitude-longitude-depth space [Ghosh *et al.*, 2012; Ryberg *et al.* 2010]. We performed MBBP on the tremor candidates identified through visual inspection. The point of intersection of the back azimuths of the high-density mini arrays was recorded as the MBBP location in 2-D space (latitude-longitude). During June 2011, the MAOTECRA had three arrays with available data, thus three arrays were used to determine locations. Using MBBP [Ghosh *et al.*, 2009a; 2012], we were able to constrain approximate depths for the events. In order to do so, we generated an approximate model of the SJF by creating a vertical fault with a strike of 310° (figure 2.7 - appendix). We used a 1-D velocity model [Scott *et al.*, 1994] to map slowness values onto the fault for each of the mini

arrays. It should be noted, however, that depths are not very as well constrained. This is mainly due to the very short time period (about a month) all three arrays were operational simultaneously. This short time period does not allow decent calibration of the arrays to obtain well-constrained depth estimates of the tremor sources.

We also performed uncertainty tests for the MBBP method. We used a bootstraping method combined with a clustering algorithm to estimate updated tremor locations and associated uncertainties in NS and EW directions. Note that we only used the PF and AZ arrays for this exercise, since we were able to use GA array only for one tremor event. The NS uncertainty for MBBP is +/- 9.5 km and the EW uncertainty for MBBP is +/- 8.7 km.

Envelope Cross Correlation

To further confirm the tremor candidates, we applied envelope cross correlation to the candidate time windows. This method was used to detect and locate tremor in southwest Japan [Obara, 2002] and Cascadia [Wech & Creager, 2008]. In this study, however, time windows were manually selected for analysis to confirm locations, as opposed to an automated ECC algorithm that can be used for preliminary detections. Envelope cross correlation uses a grid search algorithm that treats each grid as a potential epicenter. The algorithm then searches for the source-receiver travel times that best match the travel-times of the envelope of the original seismograms. There is no original template in this method, instead seismograms are compared to each other, then time shifted before the grid-search is performed to determine the source location (i.e. grid node) that produces the highest cross correlation coefficient amongst the envelopes. Here, it is important to use a frequency band that well-constrains the signal of interest. In this case, we are interested in tremor,

which produces energy from 2-8 Hz. However, train noise is also produced from 3-5Hz [Cristea-Platon *et al.*, 2013], so our analyses were conducted between 6-8 Hz. We also use a sliding time window of 100 seconds with 50 seconds of overlap, given the findings of our initial visual inspection where we found signals that lasted on the order of 100 seconds. In this analysis, we used a 1-D velocity model from Scott *et al.*, [1994].

We perform a bootstrap analysis to estimate uncertainty of the tremor locations. The average uncertainty in the EW direction is +/- 6.2 km and the average uncertainty in the NS direction is +/- 6.7 km. To further test the robustness of our ECC locations we relocated the events using a different 1-D velocity model. The laterally homogenous model was derived from the Allam & Ben-Zion [2012] 3-D velocity model for the region by averaging S-wave velocities between the source and receiver for discrete depth intervals. Locations between both velocity models were agreeable, though the Allam & Ben-Zion, [2012] location had slightly larger uncertainties (figure 2.2).

Spectral Analyses

Tremor is shown to be depleted in high frequency energy compared to regular earthquakes [Shelly *et al.*, 2007]. To ensure the tremor candidates fit this criterion, we performed displacement-amplitude spectral analyses of each of the tremor events and compared the results to that of a regular earthquake with a source location near the source region of tremor. The earthquake used for comparison is a ML 1.69 that occurred on June 5, 2011 at 14.6 km depth. Finally, we stacked all the tremor events in the catalog and compared the resulting spectra to the same earthquake. To rule out that the signals were background

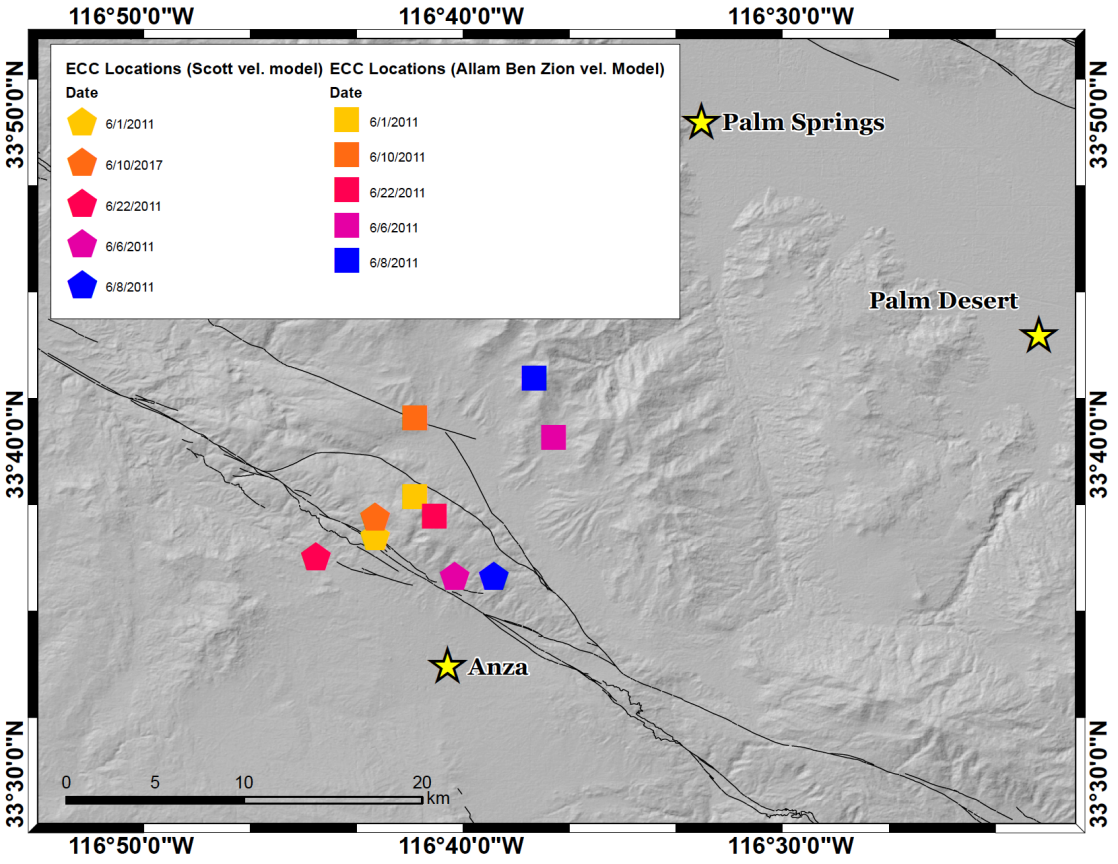

Figure 2.2: The final ECC location, determined after all of the bootstrap iterations for each event, are represented as either a square for the approximated 1-D Allam and Ben-Zion (2012) velocity model and as a pentagon for the Scott *et al.* (1994) velocity model. While there is a marked different, both velocity models give location in the same region within the NW boundary of the Anza Gap.

noise (BGN), we stacked five time windows of background noise and compared the resulting displacement amplitude frequency spectra to the tremor catalog and the stacked tremor.

2.1.5 Results

Using multiple methods described above, we find five tremor events that occur along the SJF near the Anza Gap. Each of the events in our catalog offer a coherent seismic transient in a minimum of two out of three arrays in addition to providing similar ECC and

MBBP locations (figure 2.3). These locations are in the same general area as a slow slip event detected following the 2010 El Mayor-Cucapah earthquake [Inbal *et al.*, 2011] and the deep creep inferred by Meng and Peng, [2016]. All of the events have low slowness values, indicating that they are from a deep source. Further, we use beam-backprojection method [Ghosh *et al.*, 2009a, 2012] to determine approximate depths for the tremor sources. The depths for these tremor events range between 13 and 24 km (figures 2.8, 2.9 - appendix), beneath the 12km locking depth in this area [e.g. Fialko *et al.*, 2006]. The results of our stacked and individual spectral analyses show rapid depletion of high frequency energy, which is to be expected of tremor (figure 2.4).

In figure 2.5, we give an example of tremor from June 22 at 00:52. All three arrays show a relatively low slowness value, and the slowness vectors all point to a similar location along the fault that correspond relatively well to the ECC location, along the northwest edge of the Anza Gap. The signal is visible across all three arrays within the MAOTECRA network and is even visible in network stations, though only stations from the three high-density arrays are included in this seismogram that is filtered from 2-8 Hz. The same tests from an example of tremor on June 6, 2011 at 13:34 are given in figure 2.6. (For the rest of the tremor events see figures 2.10-2.12 - appendix).

2.1.6 Discussion

The occurrence of tremor generally signifies transient deformation resulting from slow slip in the transition zone [e.g. Ide *et al.*, 2007]. Deep creep is regularly observed with

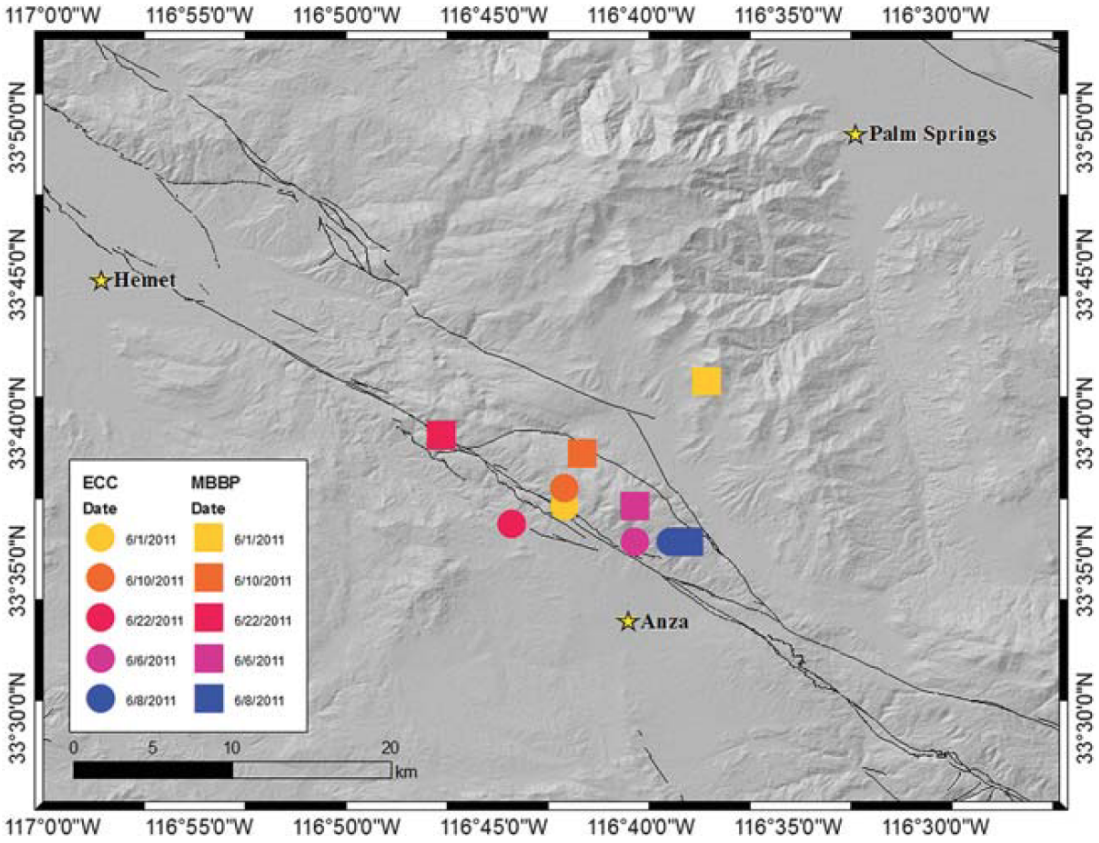

Figure 2.3: This map gives the ECC and MBBP locations of each of the five tremor events detected through this study. Each event has a specific color assigned to it, the pentagon represents the ECC location and the diamond represents the MBBP location. Both methods give similar locations for the tremor events.

NVT along major plate boundaries [Beroza & Ide, 2011; Shelley *et al.*, 2009]. Therefore, ambient tremor in this region of the SJF is likely a product of such behavior. A recent study by Meng & Peng [2016] that mapped aftershocks of moderate sized earthquake along the SJF near the Anza Gap, found anomalously large aftershock areas, elucidating the possibility that deep creep may be driving additional aftershock activity. Such deep creep can potentially produce tremor.

The extended aftershock zone indicate that this region is influenced at depth by

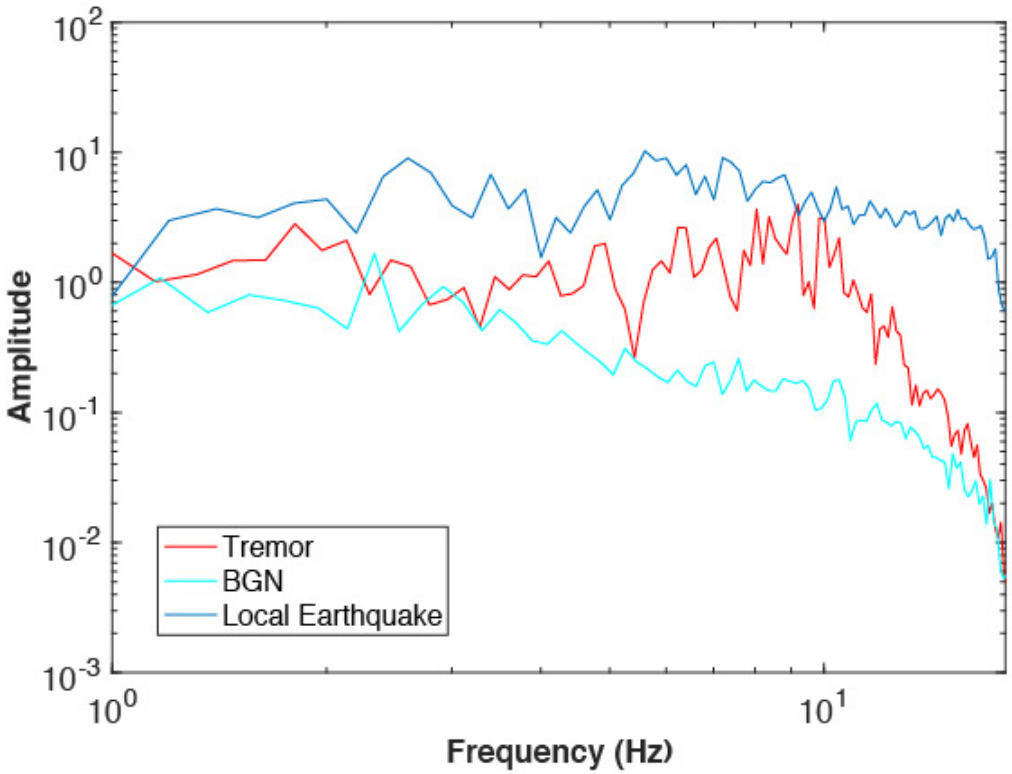

Figure 2.4: A comparison of displacement-amplitude frequency spectra from a local earthquake ML 1.69 earthquake (blue) that occurred on June 4, 2011 at 14.6 km depth, near many of the tremor events, to a stacked frequency spectra of the tremor events included in this study (red). The tremor shows a depletion of energy in high frequencies with respect to the local earthquake, a signature of NVT (*Shelley et al.*, 2007). Both signals are then compared to a stacked background noise (BGN) spectrum using five random BGN time windows (cyan). The tremor has higher energy in all frequencies than the BGN.

main shock activity of intermediate sized earthquakes below 12km depth. Whether or not the interpretation that this seismicity beneath the inferred locking depth indicates triggered deep creep, there appears to be feedback between the surrounding seismically active segments of the SJF and the edges of the Anza Gap. It is notable that the depth of the extended aftershock zone determined by Meng and Peng [2016] is consistent with the upper bound of tremor depths detected in this study (13km – 24km) and lie within the Anza Gap, like the tremor identified here.

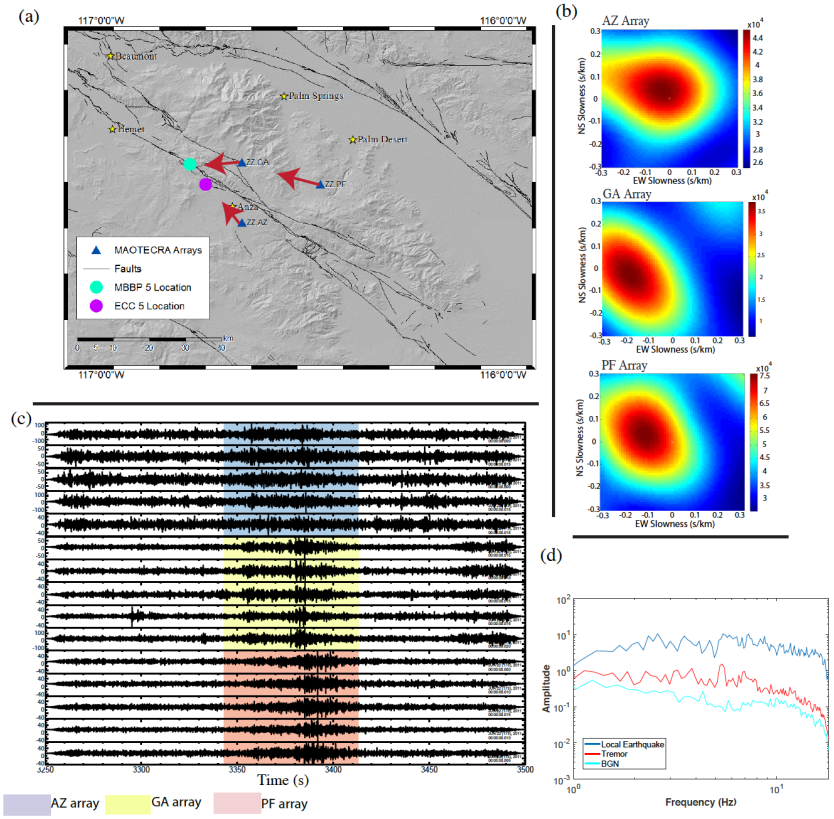

Figure 2.5: This figure gives an example of a tremor detection from June 4, 2011 and its associated testing for its addition into the tremor catalog. The three beams on the right give the azimuths in the slowness space for the tremor time window for the respective high-density array. The map on the left gives the envelope cross correlation location (pink point) for this time window across network stations. The slowness vectors from each of the arrays are indicated with a red arrow, their magnitudes illustrated by the length of their slowness vector on the map. All of the slowness vectors point towards a similar location on the fault that closely agrees with the ECC location. The seismograms (lower left) show the time window from five stations from each of the MAOTECRA arrays: AZ, GA, and PF (blue, yellow, and red respectively), with a 2-8 Hz filter on the vertical channel (SHZ). By detecting the event in a 6-8 Hz frequency band, we show that it exists outside of frequencies characteristics of train noise (3-5 Hz). The displacement-amplitude frequency spectrum of the tremor event (red) shows a decrease of energy in higher frequencies compared to the ML 1.69 earthquake that occurred in a similar location (blue) at 14.6 km depth; a stacked frequency band of background noise is also shown (cyan).

In other regions such as Cascadia [Rogers & Dragert, 2003] and southwest Japan [Obara *et al.*, 2004], tremor occurs episodically during periods of slow-slip. Inbal *et al.*,

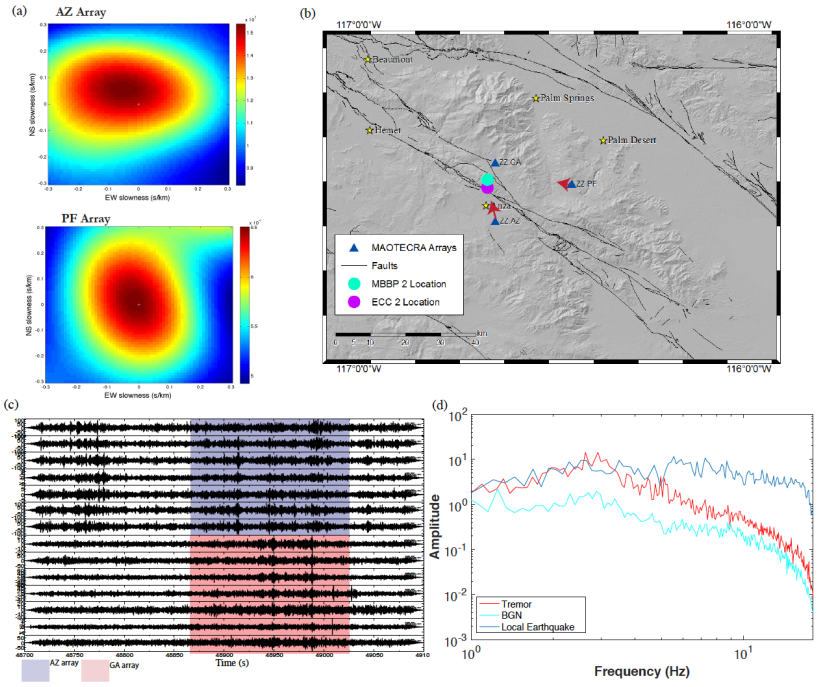

Figure 2.6: These figures are from the June 6, 2011 tremor event. The two upper left panels give the beams from the PF and AZ arrays. The yellow star indicates the location of maximum energy in the slowness space. The right panel gives the slowness vectors (red arrows) from each array and their point of intersection is the inferred MBBP location. The seismogram contains stations from the AZ and GA arrays in the vertical channel and is filtered from 2-8 Hz. The lower right hand figure are displacement-amplitude frequency spectra comparing local background noise (cyan), a local ML1.69 earthquake that occurred at 14.6 km depth (blue), and the tremor event (red).

[2017] performed a joint inversion using both strain and seismic data from the Anza region following the El Mayor-Cucapah earthquake. The inversion suggests that the largest slip was constrained within the Anza Gap, indicating the presence of a transition zone, capable of producing transient events at depth. In particular, the slow slip event occurred at depths below 10km, consistent with the depths of tremor identified in this study. Tremor is often considered a manifestation of slow-slip [i.e. Rogers & Dragert, 2013; Obara *et al.*, 2004], and though these tremor observations do not temporally coincide with the observations of the

Inbal *et al.*, [2017] study, they may indicate a seismic manifestation of slow-slip at depth. In some places, such as the Hikurangi subduction margin, slow-slip is observed without tremor [Wallace & Beavan, 2010], thus further observations are required to determine if there is a one-to-one correlation between duration of slow slip events and tremor.

Triggered tremor was identified in the northwest section of the Anza Gap following the 2002 M_w 7.9 Denali earthquake at depths of 13 km [Wang *et al.*, 2013]. Triggered tremor in the SAF [Ghosh *et al.*, 2009b] has also been observed in locations similar to those of ambient tremor [i.e. Nadeu & Dolenc, 2005]. It is then not surprising that the locations of ambient tremor identified in this study are comparable to the tremor locations that were triggered by the Love waves from the Denali event. The spatial similarity of the triggered and ambient tremor suggests that this region has distinctive qualities, markedly like that of a transitional zone, which make it susceptible to such activity.

In the SAF, near Cholame, tremor activity seems to vary depending on regional earthquake activity. For example, there was a marked increase in tremor activity following the M_w 6.5 San Simeon earthquake [Nadeau & Dolenc, 2005]. SAF tremor tends to last for several to tens of minutes and occur less frequently than tremor observed in subduction zones [Nadeau & Dolenc, 2005]. Relative to both the SAF tremor and subduction zone tremor, the tremor in the SJF is characterized by short bursts of emergent energy, usually lasting from 50-100s. It is unclear what observable activity directly causes ambient tremor in this region, though a larger catalog would help establish such a relationship.

The Anza Gap is also a region that has no record of large earthquakes ($M > 6.0$) since 1890, when all large earthquakes are known, though the record prior to this date may

be incomplete [i.e. Sanders & Kanamori, 1984; Toppozada *et al.*, 1981]. There is no surface evidence of aseismic slip [Thatcher *et al.*, 1975; Sanders and Kanamori, 1984] around the Anza Gap and it is bounded by two highly active segments of the SJF: the triple junction of the Coyote Creek, Clark, and Buck Ridge faults to the south, and the divergence of the Casa Loma Fault and the Hot Springs Fault to the north.

In this particular setting, regular seismic activity occurs on either side of the Anza Gap, while there is very little seismic activity within the gap itself. In other words, there are discrete types of behavior in the Anza Gap versus its surrounding segments. Consequently, the fault interface at depth at the edges of the Anza Gap may have mechanical properties that exhibit anomalous seismic disturbances. In other areas where there is a contrast in mechanical and rheological properties, we typically see seismic signatures of slow earthquakes, such as tremor, VLFEs, and LFEs [e.g. Ghosh *et al.*, 2012; Ghosh *et al.*, 2015; Hutchison & Ghosh, 2016; Shelly *et al.*, 2007]. However, due to the limited observation of tremor and slow slip in this area, their relationship cannot be established. Based on mounting evidence from other major faults, we suspect tremor to be associated with deep creep and/or slow-slip given recent findings that may suggest such behavior in this area [e.g. Lindsay *et al.*, 2014; Jiang & Fialko, 2016; Inbal *et al.*, 2017]. These types of transient behavior and an increase in shear stress from other surrounding segments of the fault over time of the fault may bring the Anza Gap closer to a critical stress where failure becomes increasingly likely.

Our results show that multiple methods converge on a similar location for each of the discrete tremor events found in this study. In particular, the beamforming results

of from the MAOTECRA high-density arrays effectively demonstrate consistent results with low slowness values, indicating the signals are originating from deep in the crust. Furthermore, beam-backprojection gives a depth range (13-24km) that lies beneath the locked zone, estimated at 12km and even beyond the seismogenic zone estimated at a depth of 17 km [Fialko, 2006; Wdowinski, 2009]. Additionally, we find that ambient NVT occurs in short duration episodes along the SJF, in the Anza Gap, in the same region where Wang *et al.*, [2013] detected triggered tremor following the 2002 Denali earthquake, where Meng & Peng [2016] present compelling evidence for deep creep, and where Inbal *et al.*, [2017] found evidence for a slow-slip event. The depths reported by these studies, 13 km [Wang *et al.*, 2013], 10+ km [Inbal *et al.*, 2017], and > 12km [Meng & Peng, 2016], also coincide with the depths of tremor determined in this study, suggesting that these behaviors likely correlate.

The difficulty associated with tremor detection in the Anza Gap is that it is not detected as frequently as it is along the SAF near Cholame [Nadeau & Dolenc, 2005; Nadeau & Guilhem, 2009, Shelley *et al.*, 2009]. In addition, many sources of anthropogenic noise make it difficult to distinguish tremor from background signals. Typically, NVT is detectable in the 2-8 Hz frequency band. The tremor detections here have a characteristic duration of 100 seconds. Due to the widespread presence of regional noise in the tremor frequency band, a tremor signal is often difficult to detect across network surface stations. The tremor here is likely very low amplitude. Tremor in this area is best detected through well-designed strategically located high-density mini seismic array data, with complementary borehole stations.

Since tremor occurs in the transition zone of a fault, beneath the locked zone, if we are able to produce a longer record of tremor activity and accurately constrain the depth of tremor events, and thus generate a better sense of potential rupture area, state of stress and the extent of the seismogenic zone, we will be better equipped to assess seismic hazard. It should be noted that this is an extremely reserved catalog from only one month of data, and may thus underestimate tremor activity.

2.1.7 Summary

This study provides evidence from multiple independent seismic methods for five discrete short duration episodes of tremor during June 2011. All five of the events occur near the Anza Gap, which are especially close to the locations of tremor triggered by the 2002 Denali earthquake [Wang *et al.*, 2013]. We find that in visual inspection, the signals are best detected through high-density array data in the 6-8 Hz frequency band, so as to avoid inclusion of regional noise. The signals are also, though less reliably, visible in borehole stations. These findings suggest that there may be slow slip, characteristic of a transition zone, occurring at depth in the region surrounding the Anza Gap. Inbal *et al.*, [2017] used a joint inversion from seismic and strain data to find evidence for slow slip events in the Anza Gap, suggesting that the tremor may be a seismic manifestation of such activity. Recent studies [Meng & Peng, 2016; Jiang & Fialko, 2016] give evidence that could be interpreted to indicate a creeping region at depth along the SJF that may also drive the types of seismic observations presented here. Further studies using similar methodologies is needed to develop complete robust catalogues that fully characterize long-term tremor behavior, and potentially investigate the relationship of tremor to other tectonic processes

in the region.

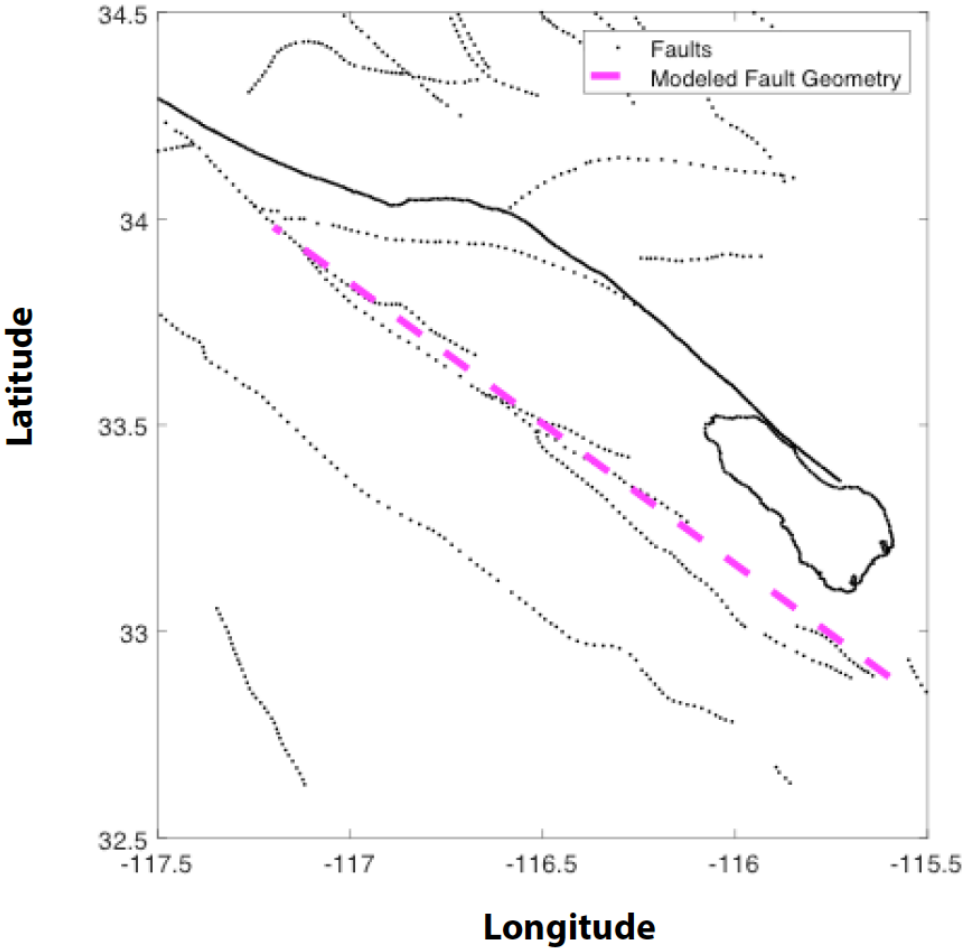

Figure 2.7: This is a map view of the approximated vertical fault used in the beam-backprojections used to determine tremor depth.

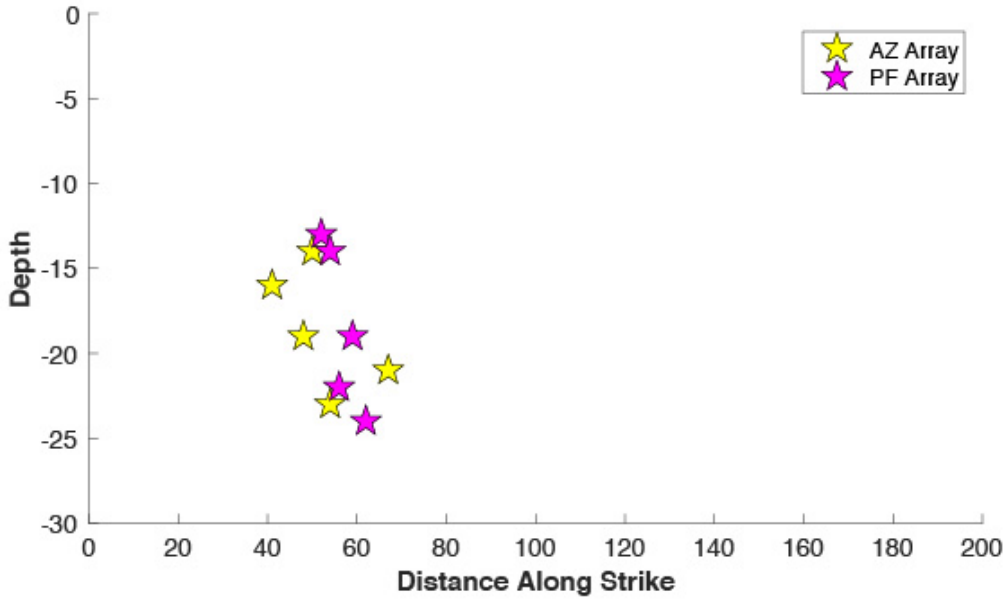

Figure 2.8: This cross-section, which is an approximation of the SJF (S1), that gives the locations of the five tremor events detected along the fault interface. The locations are from the PF (magenta) and AZ (yellow) arrays. They consistently lie within the Anza Gap and range in depth between 13-24 km.

2.1.8 Appendix: Supplementary Material

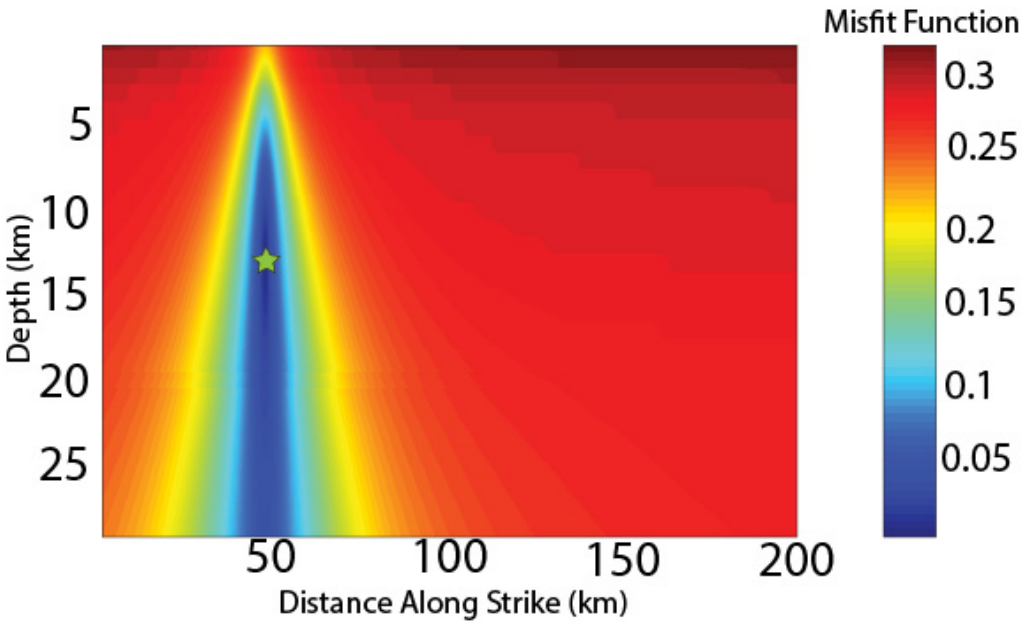

Figure 2.9: Cross-sectional figures giving the beam-backprojection depth along strike for the June 1, 2011 tremor event on the AZ array. The colorbar represents the misfit function for the beam-backprojection. This analysis was performed for each tremor event on the PF and AZ arrays giving a depth range of 13-24 km.

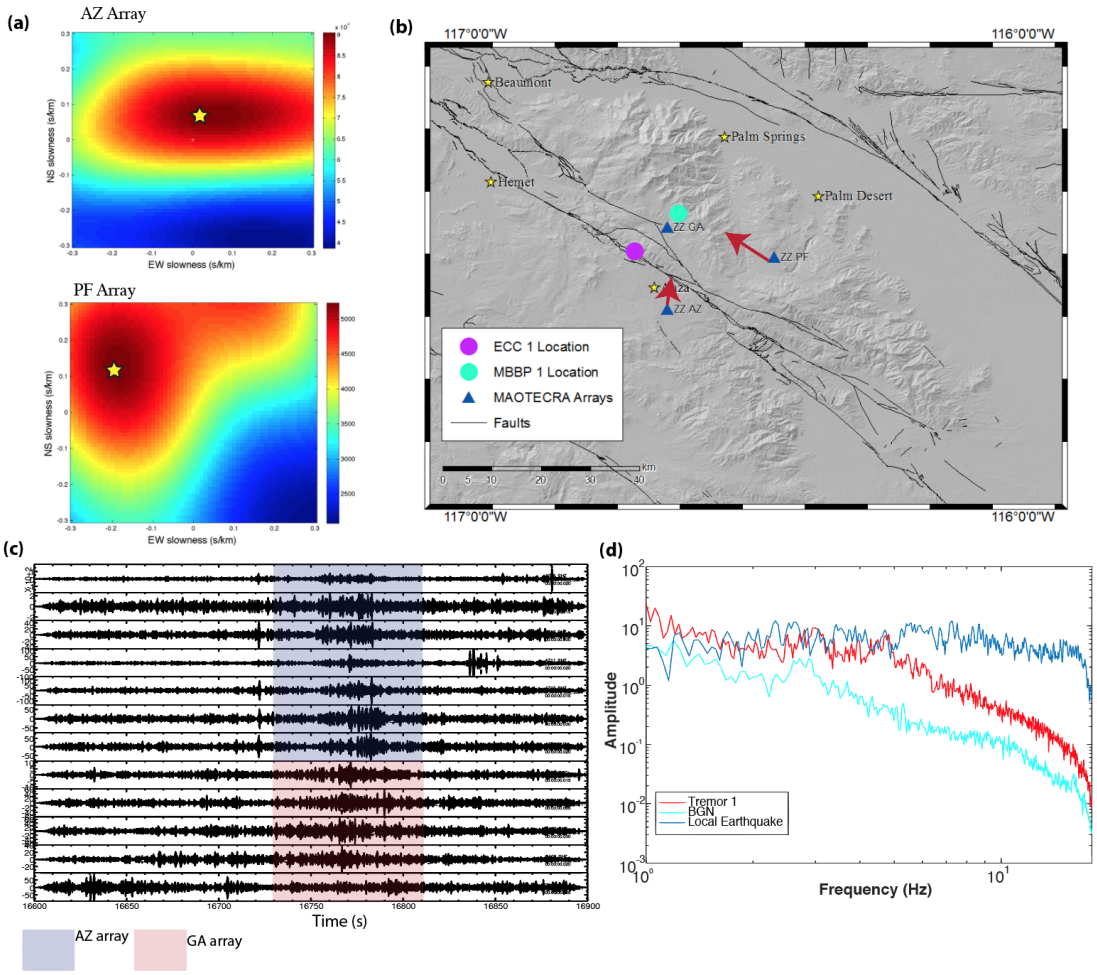

Figure 2.10: These figures are from the June 1, 2011 tremor event. A) The beams from the PF and AZ arrays. The yellow star indicates the location of maximum energy in the slowness space. B) The slowness vectors from each array, their intersecting point is the inferred MBBP location (light blue circle). The ECC location is shown with a purple circle. C) The seismogram contains stations from the AZ and GA arrays in the vertical channel and is filtered from 6-8 Hz. D) A displacement-amplitude frequency spectra comparing local background noise (cyan), a local ML1.69 earthquake that occurred at 14.6 km depth (blue), and the tremor event (red).

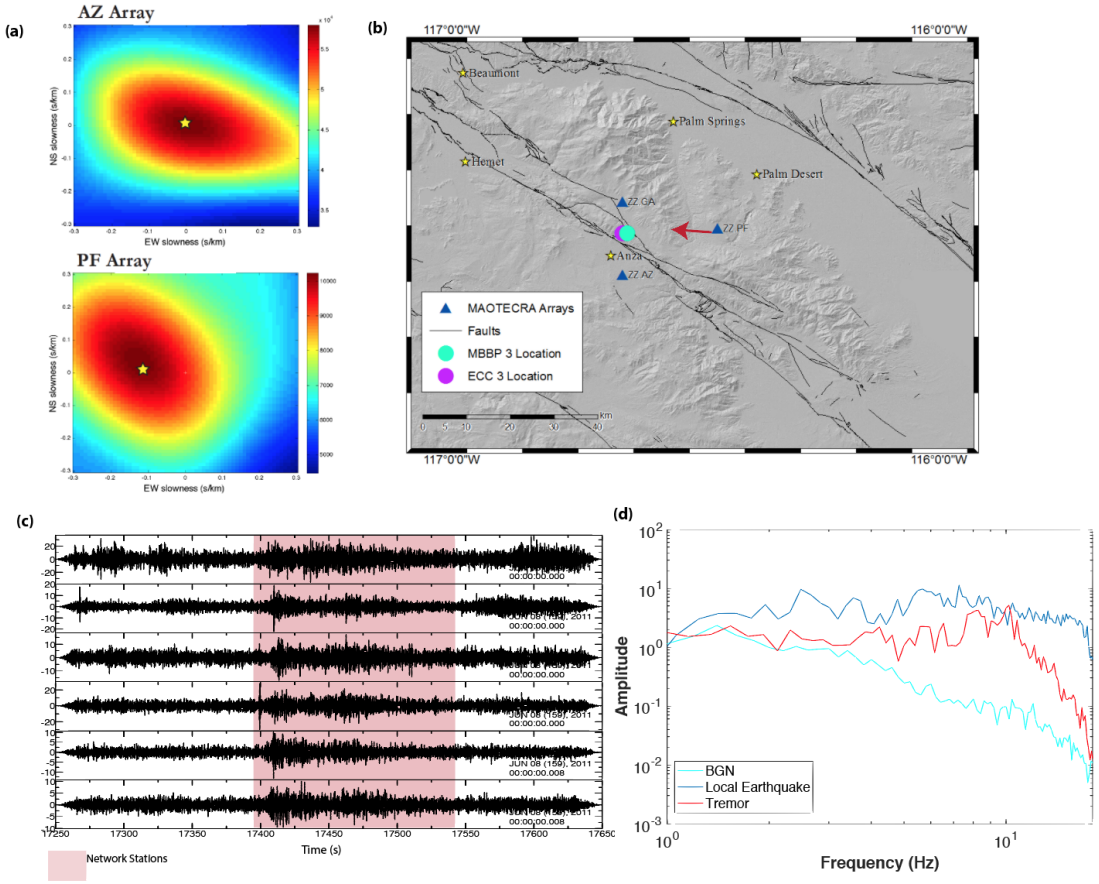

Figure 2.11: These figures are from the June 8, 2011 tremor event. A) The beams from the PF and AZ arrays. The yellow star indicates the location of maximum energy in the slowness space. B) The slowness vectors from each array and their point of intersection is the inferred MBBP location (light blue circle). The ECC location is given with a purple circle. C) The seismogram contains stations from network stations on the vertical channel and is filtered from 2-8 Hz. D) Displacement-amplitude frequency spectra comparing local background noise (BGN) (cyan), a local ML1.69 earthquake that occurred at 14.6 km depth (blue), and the tremor event (red).

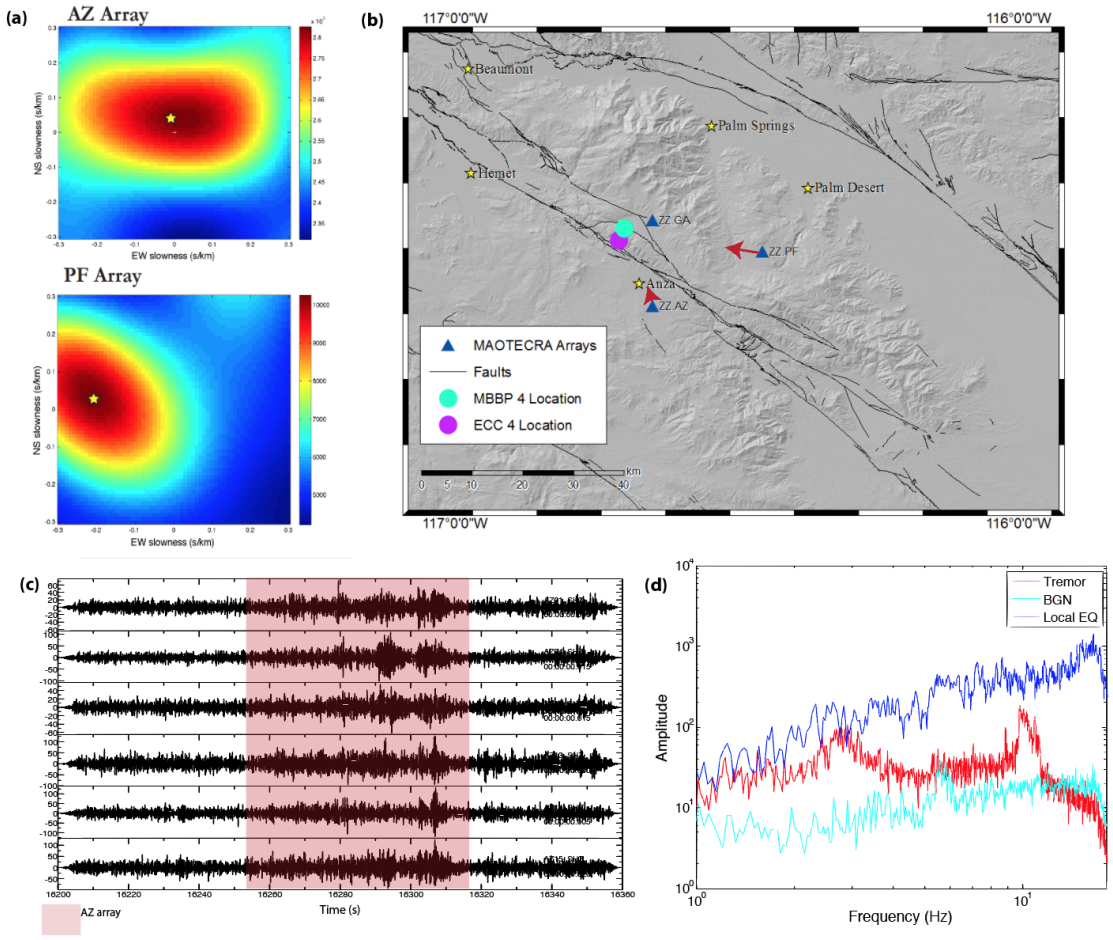

Figure 2.12: These figures are from the June 10, 2011 tremor event. A) The beams from the PF and AZ arrays. The yellow star indicates the location of maximum energy in the slowness space. B) The slowness vectors from each array and their point of intersection is the inferred MBBP location (light blue circle). The ECC location is given with a purple circle. C) The seismogram contains stations from the AZ array on the vertical channel and is filtered from 2-8 Hz. D) The lower right hand figure is a spectra comparing local background noise (BGN) (cyan), a local ML1.69 earthquake that occurred at 14.6 km depth (blue), and the tremor event (red).

Chapter 3

Foreshocks and Triggered Tremor Preceding the 2016 M_w 5.2 Borrego Earthquake

3.0.1 Abstract

On June 10, 2016, we observe tremor in the Anza Gap triggered by the passage of Rayleigh waves from the M_w 6.1 earthquake in Puerto Morazán, Nicaragua. The tremor is followed by a number of microseismic events that occur in the Anza Gap and near the trifurcation region of the San Jacinto Fault (SJF). A second teleseismic event, a M_w 6.2 from the Solomon Islands, passes through the area, occuring approximately 2 hours later. During the passage of the second teleseismic event, microseismic eventicity continues. Several hours after the seismic activity tapers off, the M_w 5.2 Borrego earthquake occurs. The microseismic events that occur during the teleseismic events are located both near the

Anza Gap and close to the source of the Borrego earthquake. This is the second instance of triggered tremor observed in the SJF and unlike the first observation it is triggered by Rayleigh waves. The increase in dynamic stress, 25 kPa, is consistent with values calculated for the region by Wang *et al.*, [2013] following the first instance of triggered tremor after the 2002 Denali Earthquake, indicating a greater fault strength or higher ambient stress, or a combination of the two, than that of the Cholame section of the San Andreas Fault (SAF), where triggered tremor will typically requires only an increase of 10-20 kPa in dynamic stress. Given previous studies may be interpreted to suggest deep creep in the region, it is possible that these teleseismic events triggered a creep event, that may have ultimately triggered the Borrego earthquake [Shelly *et al.*, 2011], though this possibility requires further investigation.

3.0.2 Introduction

Nonvolcanic tremor (NVT) is a type slow earthquake, a family of seismic and aseismic events that result from shear slip within the transition zone of a fault. Empirically, these events have a constant moment rate [Ide *et al.*, 2007] and are depleted of energy in higher frequencies [Shelly *et al.*, 2007]. Slow earthquakes have been observed along most major subduction zones including in Japan [i.e. Shelly *et al.*, 2007; Brown *et al.*, 2009], the Alaska-Aleutian subduction zone [Brown *et al.*, 2013; Li and Ghosh, 2017], Mexico [i.e. Payero *et al.*, 2008], and Cascadia [i.e. Rogers and Dragert, 2003]. NVT has also been observed in strike-slip environments such as the San Andreas Fault (SAF) [Nadeau and Dolenc, 2005]. Moreover, ambient NVT has been observed in short-duration bursts in the Anza Gap of the San Jacinto Fault (SJF) [Hutchison and Ghosh, 2017].

In a similar way that the passage of seismic waves can dynamically trigger earthquakes [Hill *et al.*, 1993], they also trigger tectonic tremor. Local, regional, and teleseismic events have all triggered NVT. In the SAF, triggered tremor has been widely observed in the Cholame section, the portion of the fault that separates the aseismic southern section of the SAF from the central creeping section, but also along the creeping section [Peng *et al.*, 2009; Gomberg *et al.*, 2008; Ghosh *et al.*, 2009]. Triggered tremor in California is not unique to the SAF: following the 2002 Denali Earthquake, Love waves triggered tremor in the Anza Gap of the SJF [Wang et al, 2017].

The SJF, and moreover specifically the Anza Gap, is a region historically lacking in seismicity. There is no record of a major earthquake in the Anza Gap for over 200 years [Doser, 1992]. The aseismic nature of this segment of the SJF has resulted in several studies citing this region as a high seismic hazard, likely to result in a M_w 6.5 or greater [Thatcher *et al.*, 1975; Sanders & Kanamori, 1984]. The Anza Gap is bound by two highly seismically active regions, suggesting it has distinct mechanical properties or stress conditions, thus its edges are likely to have transitive properties (e.g. slow earthquakes). In addition to the teleseismically triggered tremor detected following the 2002 Denali earthquake, ambient tremor was also detected during the installation of three high density mini seismic arrays in June, 2011 [Hutchison and Ghosh, 2017]. Furthermore, slow slip was detected following the 2010 M_w 7.2 El Mayor-Cucapah earthquake [Inbal et al, 2017]. This region is capable of exhibiting behavior characteristic of the middle of the slip spectrum, suggesting that it may be susceptible to teleseismic triggering.

Here, we have a unique observation where NVT is triggered by the envelope of

Rayleigh waves from a regional event and is then followed by a number of microseismic events over the course of approximately three hours. Another teleseismic event passes through the region as the microseismic events continue. About three hours after the seismic activity ceases, a M_w 5.2 earthquake occurs in the region that was previously activated with microseismic eventicity. Here we see a cascade of seismic events that begin at a distance but result in a number of smaller local events that ultimately spatiotemporally precede a sizeable mainshock. The relationship between these events is examined in this study.

3.0.3 Data

We have several sources of seismic data used in this study. First, we use the Pinyon Flats Observatory Array (PY array), which consists of 13 borehole, broadband, three-component stations. In addition, we look for a coherent tremor signal in several nearby high broadband stations seismic stations (100 samples per second) from the Plate Boundary Borehole Seismic Network (PB) and the Anza Network (AZ) to validate our findings (figure 3.1).

3.0.4 Methods

Beamforming

We initially detected the events preceding the M_w 5.2 Borrego earthquake using a beamforming algorithm that first filters data, normalizes it, stacks it, then calculates the amplitude in the horizontal slowness space [Ghosh *et al.*, 2009; 2012]. While this cannot provide a precise location, it can give an azimuth and a sense of depth since a low slowness

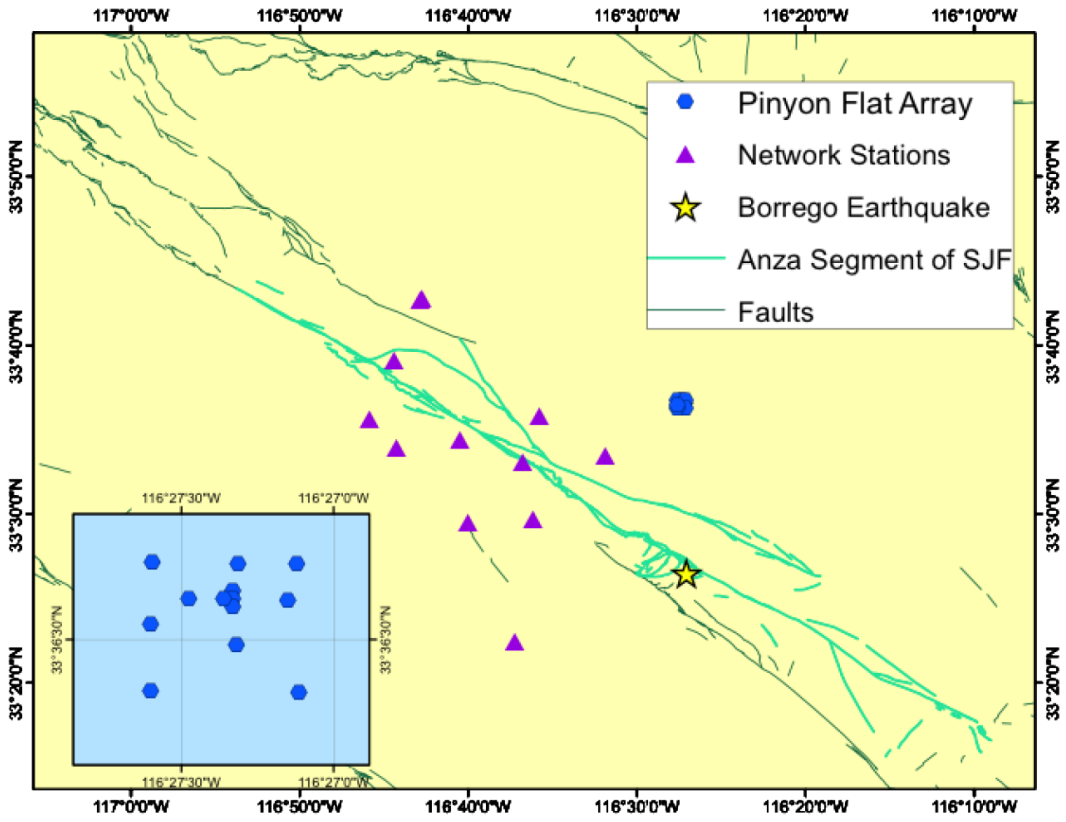

Figure 3.1: A map of the study region. The yellow star indicates the location of the M_w 5.2 earthquake that occurred on June 10, 2016. The blue point on the map represents the PY array, its station distribution is given in the inset map. The purple triangles represent stations used for comparison in visual inspection.

will typically correspond with a high velocity (i.e. deep) source. We initially performed this analysis from 0.01-20 Hz to have a complete dataset with maximum amplitude in the horizontal slowness space for each time window, azimuth, and the data required for a robust spectrogram, inclusive of all potentially relevant frequencies (figure 3.2). Once the tremor and microseismic events were detected through the stacked beamforming and visual inspection, we select a smaller frequency band of to perform beamforming on the time windows of interest for a more precise location in the slowness space. The selected

frequency band is 1-10 Hz for microseismic eventicity, but for the triggered tremor we use a frequency band of 5-15 Hz, and more specifically 8-13 Hz to see the event across the network. The narrower frequency band eliminates distances the signal from the train frequency band, thought to be between 3-5 Hz [Cristea-Platon *et al.*, 2013] and an unknown energy source at 14 Hz that seems present throughout the entire day on the spectrogram but does not impact any of the results of the location analyses.

To ensure our locations are precise, we located the Borrego earthquake in the slowness space using the location given by the Southern California Seismic Network (SCSN) catalog and a local 1D velocity model and the same beamforming algorithm employed throughout this study [Scott *et al.*, 1994]. We also directly beamform the Borrego earthquake. Because both the theoretical location and the observed location of the earthquake are nearly the same, we consider our array bias minimal.

Beamback Projection

To determine an exact location, a vector from the center of the array to the azimuth of the maximum amplitude in the slowness space is projected onto the nearest fault. For an estimate of the SJF fault, we estimate a 2D vertical fault with a strike of 310° . We use the same vertically homogeneous velocity model used for beamforming to map slowness values onto the fault model. To determine the location of the event in question, the beamback projection algorithm identifies the location with the smallest misfit function between the slowness values mapped on the fault and the projected slowness from the array [Ghosh *et al.*, 2009; 2012].

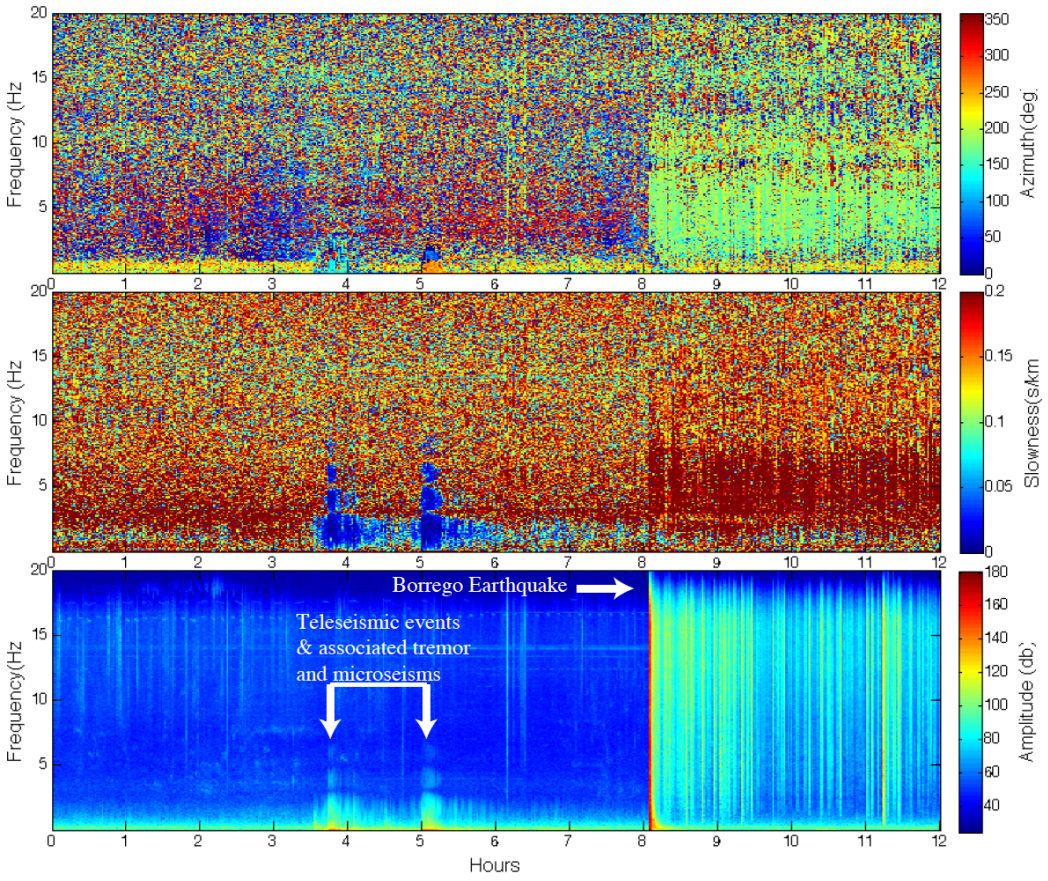

Figure 3.2: This figure shows the raw stacked beamforming results from the first 12 hours of June 10, 2016. All three panels give time vs. frequency on the x and y axes, respectively. The colormaps from top to bottom represent azimuth, slowness, and energy. Thus, the bottom panel is a spectrogram. The two teleseisms and the earthquake are marked in the lower panel, but stand out from the backround as well in the azimuthal and slowness plots. In both cases, they have low slowness, but the azimuth varies.

Time differentials and event triggering

To determine whether the tremor is in fact directly induced by the passage of teleseismic energy, a calculation is required to determine the time differential between the tremor source location and the receiver. The unfiltered, rotated teleseismic event in one

seismogram and the filtered tremor in a separate seismogram must be time shifted accordingly to determine if the tremor was in fact triggered by the passage of waves from the teleseismic event. This allows a direct comparison between the arrival of teleseismic energy and the activity of tremor in the suspected tremor source region. The time shift is done such that instead of the tremor signal arriving at the stations, it is shifted to arrive in the approximate source region using a local laterally homogeneous velocity model [Scott *et al.*, 1994]. Without this calculation, the timing at which the teleseismic event hit the tremor source region is not accounted for. Instead, the correlation between the tremor at the receiver location and the arrival of the teleseismic energy would be considered. [Ghosh *et al.*, 2009]. There is a possibility of delayed triggering as there are a number of signals throughout the day that resemble short bursts of tremor, but the first signal that appears to temporally coincide with the arrival of the Rayleigh wave energy is likely dynamically triggered without any delay. The exception would be if it were actually triggered by an earlier phase, but did not actually rupture until the arrival of the Rayleigh wave energy. Given the close relationship between the timing of the arrival of the surface wave energy and the tremor, dynamically triggered tremor is favored.

Spectral analyses

Whenever attempting to discern whether or not seismic activity is of the slow earthquake variety, it is always important to look at the frequency distribution of that event. In comparison to regular earthquakes, slow earthquakes are depleted of energy in high frequency bands [Shelly *et al.*, 2007]. Here, we integrate the seismograms of the time window of the triggered tremor in question for displacement and compare it to the

integrated seismogram of a ML 1.69 that occurred on June 4, 2011 at a depth of 14.6 km. We also compare the local earthquake and the triggered tremor to five stacked and normalized random samples of background noise from the same region. Ultimately, this process helps to ensure that the tremor behaves in the frequency domain would be expected, given previous observations [Hutchison and Ghosh, 2017].

3.0.5 Results

Prior to the M_w 5.2 Borrego earthquake on June 10, 2016, a M_w 6.1 earthquake occurred in Puerto Morazán, Nicaragua at 3:25:23. The teleseismic energy from the P-wave from the event arrives at the PY array at 3:32:24. The background seismic activity near the array is unaffected until the introduction of teleseismic Rayleigh wave energy at 3:49:40. When examining the teleseismic energy from the Puerto Morazán earthquake, we determine the time differential between the tremor source region and the PY array and time shift the respective seismograms accordingly. Upon further examination of the radial and vertical components, there is a correlation between the envelope of Rayleigh wave energy and a tremor burst that lasts for several hundred seconds (figure 3.3). Here, we use a Love wave velocity of 4.1 km/s and a Rayleigh wave velocity of 3.5 km/s to determine time shifts for the unfiltered and low pass filtered seismograms [Peng *et al.*, 2008]. The Love wave velocity is applied for a time shift to the tranverse component, while the Rayleigh wave velocity is applied to the vertical and radial components. We then use S-wave travel times [Scott *et al.*, 1994] to determine the travel time for tremor from the source. Upon further inspection, it appears the tremor activity is distinguishable from teleseismic activity in the 5-15 Hz frequency band, though we specify this further to 8-13 Hz the best SNR across both

network stations and the high density array. We distinguish the tremor from teleseismic energy due to its high frequency since energy in higher frequencies tends to attenuate at larger distances, particularly in the frequency band where we identify this unique tremor-like signal.

Applying beam-backprojection, we determine that the triggered tremor is located in the Anza Gap section of the SJF (figure 3.4), where both ambient and triggered tremor have been previously observed [Hutchison and Ghosh, 2017; Wang *et al.*, 2013]. The teleseismically triggered tremor occurs at a depth of 10 km (figure 3.5) [Hutchison and Ghosh, 2017].

Following the local tremor, there is continued teleseismic energy for just over an hour, but during this hour, there are some very small earthquakes (i.e. microseismic events) that often occur almost directly south of the PY array. This location directly corresponds to the location of the M_w 5.2 earthquake that occurs later at 8:04:38 (figure 3.6). Additionally, microseismic eventicity occurs in a similar location to the triggered tremor, but at a much greater depth (>20 km) (figure 3.7), a depth and location also correspondent to ambient tremor [Hutchison and Ghosh, 2017].

At 4:17:45, a second earthquake with M_w 6.2 occurs in the Solomon Islands that emits teleseismic energy, with P-wave energy that arrives at the PY array at 5:04:00. There is no clear tremor directly associated with the second teleseismic event. There is a signal that somewhat resembles tremor, but it is difficult to establish an immediate triggered

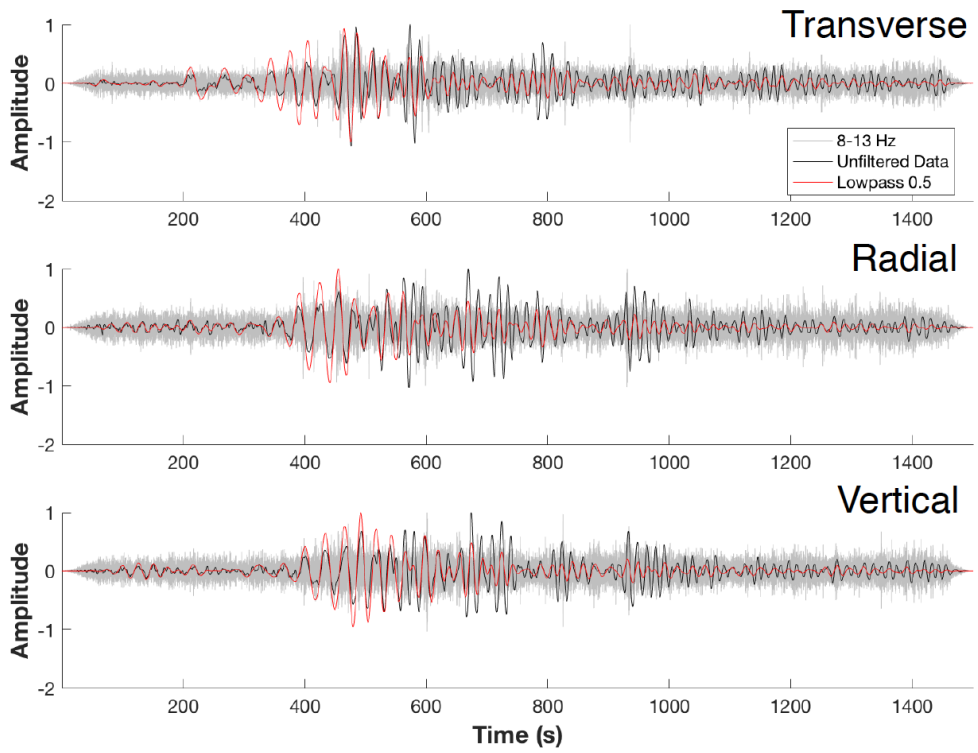

Figure 3.3: This plot gives rotated and time-shifted seismograms from station BPH05. The gray seismograms are filtered in a 8-13 Hz band pass, the black seismograms are the unfiltered data, and the red seismograms are lowpass to 0.5 Hz. All of the seismograms are time shifted to reflect the time differential to the receiver. For the transverse component, we use a Love wave velocity (4.1 km/s) to time shift the raw and low pass seismograms. For the radial and vertical components, we use a Rayleigh wave velocity (3.5 km/s) to time shift the raw and low pass seismograms. All of the plots plots filtered in the tremor frequency band are time shifted based on regional S-wave velocities. The tremor corresponds to the envelope of the Rayleigh wave.

relationship between the passage of teleseismic phases from this particular event and the onset of this tremor-like seismic activity. This may be due to convoluted signals from the remaining energy from the first teleseismic event. Although through slowness analyses, there is clearly some focused seismic energy in the 1-10 Hz frequency band that emulates that produced during the first teleseismic event, including small earthquakes (and/or mi-

croseismic events) (figure 3.8). There are two time periods where there is seismic energy that appears in the same location along strike, have the same azimuth pointed northwest towards the Anza Gap, and have very low slowness values (observable between 6-8 hours

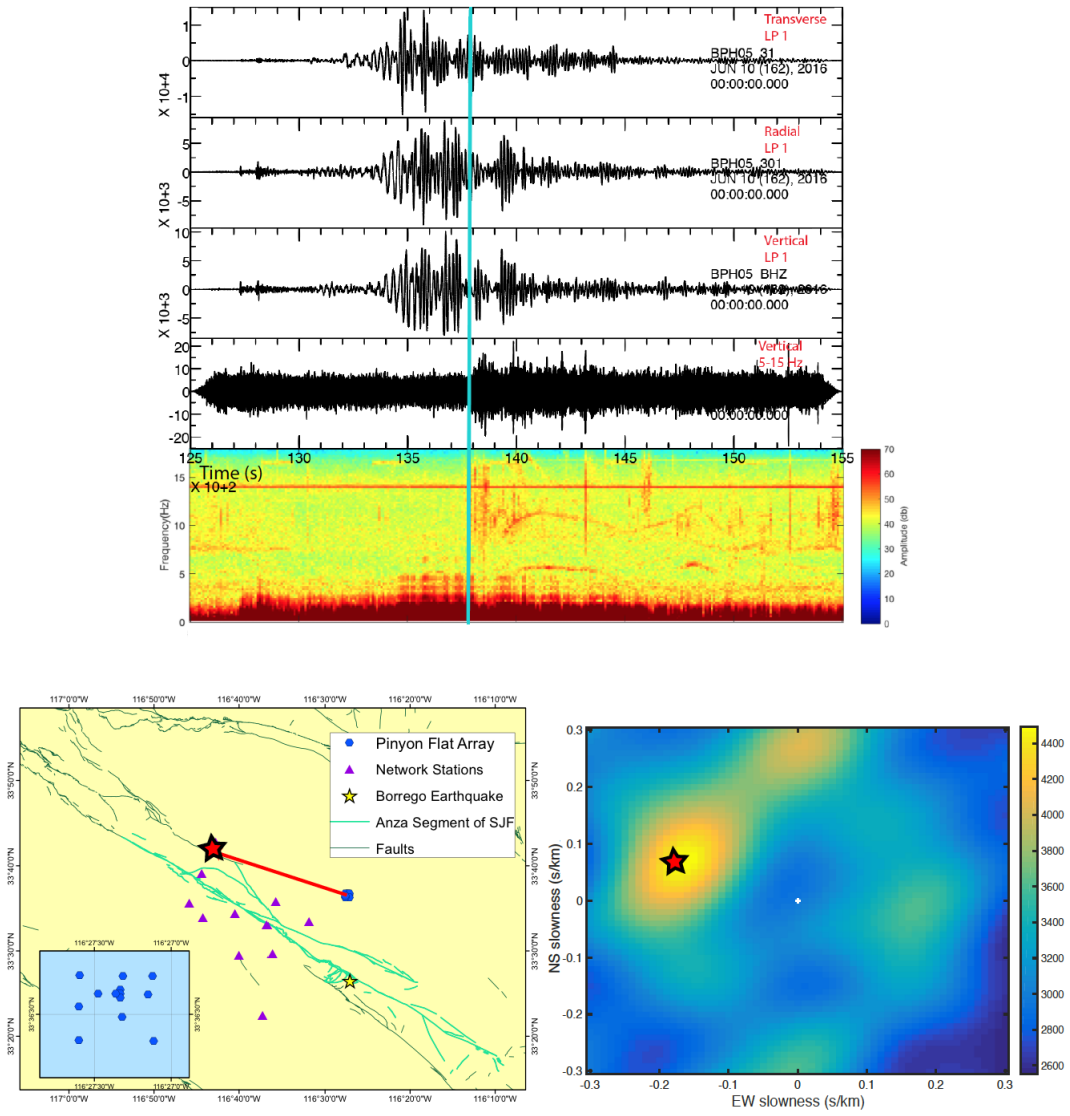

Figure 3.4: The top plot gives the raw rotated data from the first teleseismic event with a spectrogram from the same time window. There is a clear increase in energy in higher frequencies (8-15 Hz) after the arrival of the Rayleigh wave (indicated by a blue line). The bottom left plot gives the slowness vector of the tremor extended to the source fault on a map, giving a source location near the Anza Gap. The beam is shown in the bottom right.

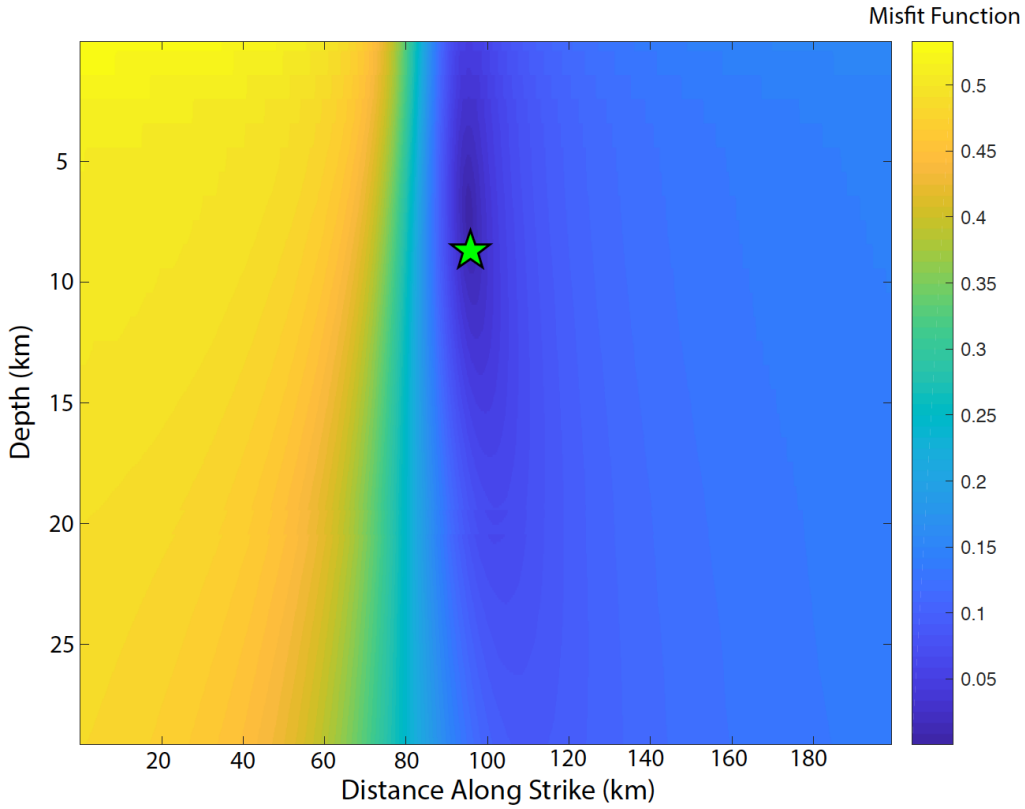

Figure 3.5: The beam backprojection depth of the triggered tremor window is plotted here. The colors along the fault represent a misfit function such that the lowest misfit function is the implied location of the tremor. The beam backprojection was conducted between 5-15 Hz with a local 1D shear wave velocity model [Scott *et al.*, 1994]. Here the tremor occurs at a depth of 9 km. This depth is somewhat shallower than previous triggered tremor locations (13 km, [Wang *et al.*, 2013], but is consistent with overall findings of slow-slip in the region. Inbal *et al.*, [2017] found geodetic evidence of slow slip following the EL Mayor Cucapah earthquake in this region at depths >10 km.

on figure 3.8). During this time period, some of the same microseismic eventicity continues with earthquakes from the same source at a depth >20km (figure 3.7), but also with some earthquake source locations beginning to evolve in the direction of the mainshock (figure 3.9).

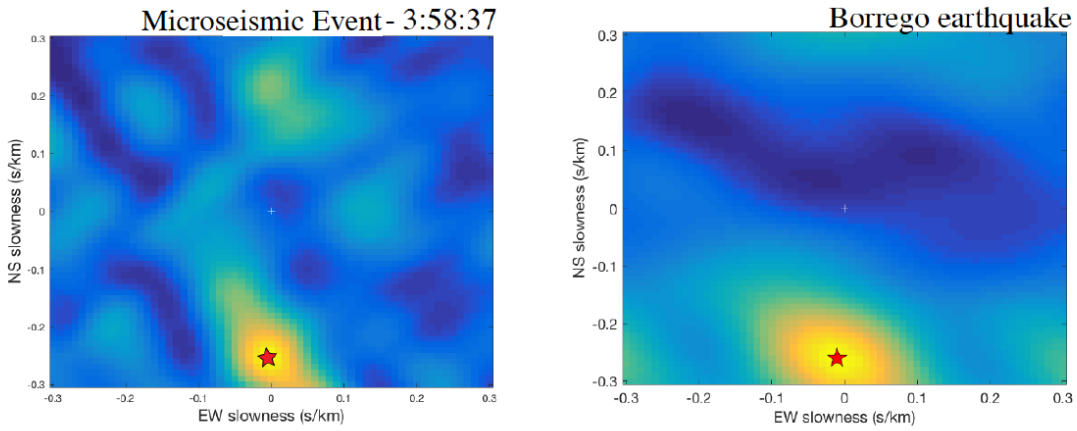

Figure 3.6: The beam on the left gives the beam from a microseismic event coincident with the first teleseismic event that occurs at 3:58:57. The beam on the right is the beam from the Borrego Earthquake. They are nearly identical. This is one of many microseismic events that shares the same source in the slowness space as the Borrego earthquake.

From the first tremor burst and through the duration of the second teleseism, until 6:06, there is a cascade of microseismic eventicity, lasting a total duration of 3 hours. To confirm the signal is consistent with network stations, we observe the activity on PY array stations and stations near the fault in the PB network (figure 3.10). The majority of the microseismic events occur in the same location as the triggered tremor, but deeper in the fault. In total, we observe a total of 26 events, including the first tremor burst and 25 microseismic events, 6 of which occur in the same location as the mainshock and 12 that occur near the Anza Gap, including one that is cataloged in the SCSN catalog.

It of interest to note that during the passage of teleseismic energy for both events, there is energy in the tremor frequency band that corresponds to a very low slowness, indicating that it has a deep source. These signals are difficult to characterize and we thus leave them out of these analysis. It can be difficult to differentiate between this activity and

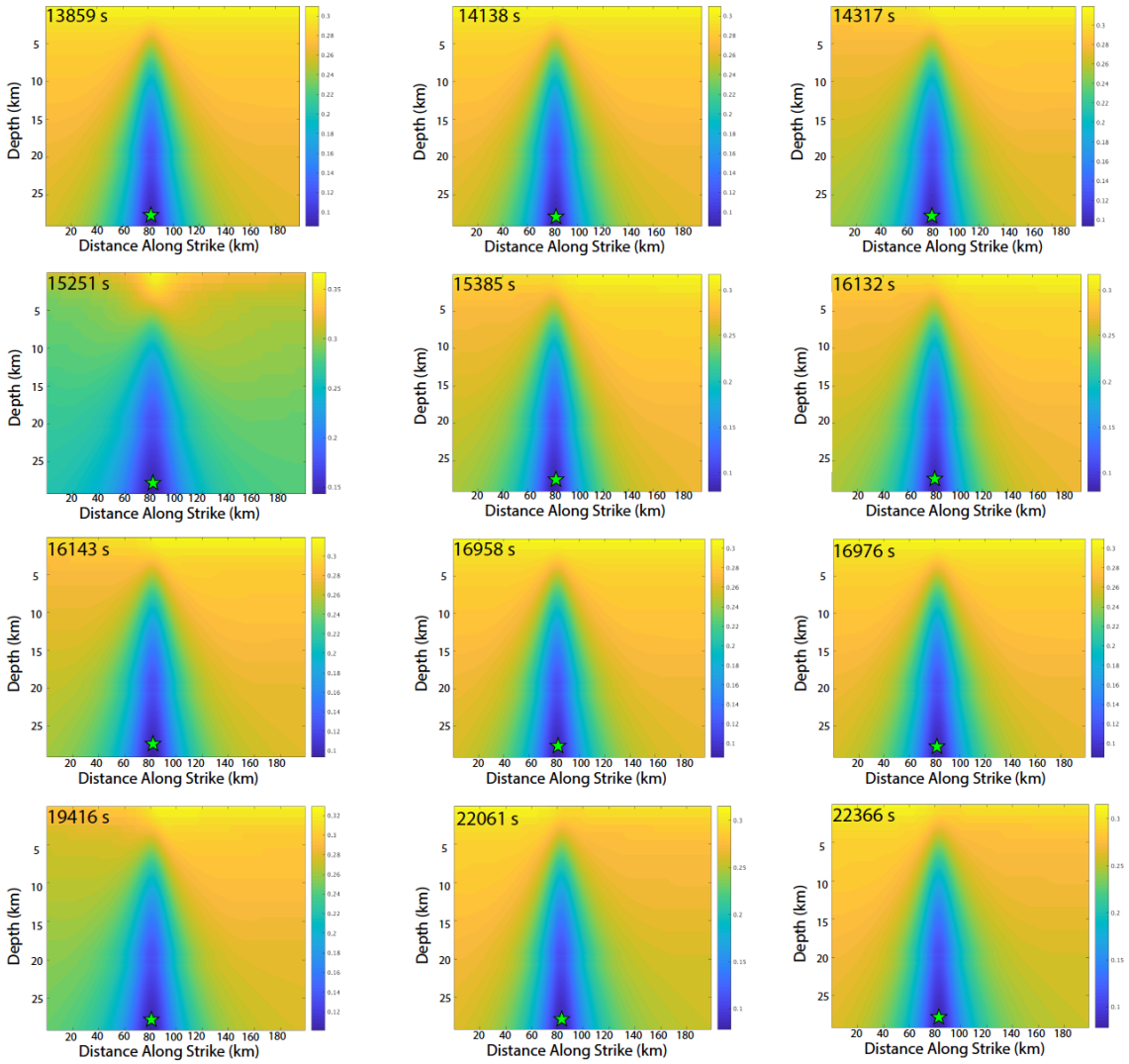

Figure 3.7: Twelve of the 24 microseismic events detected preceding the Borrego earthquake have similar locations along the fault. Using a 1-10 Hz frequency band for beam backprojection, we show that these events have nearly identical source locations from depth in the crust 24 km and at the same position along strike. These depths are consistent with the upper bounds of ambient tremor previously detected in the region [Hutchison and Ghosh, 2017].

the teleseismic energy given the variety of ways tremor can manifest. We interpret these energy bursts to be from the teleseisms, but they may be tremor. Further study is required

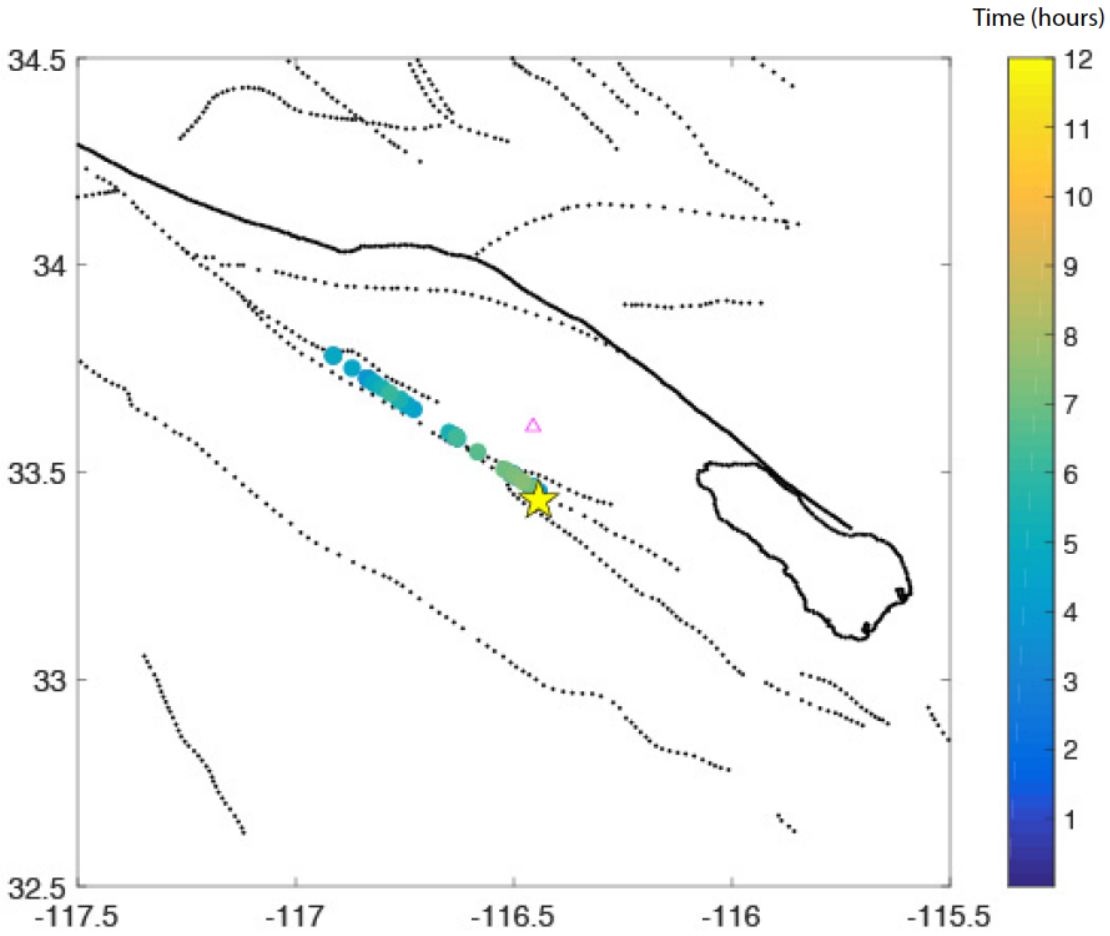

Figure 3.8: These points along the SJF represent the locations of the microseismic events that occur coincidentally with the passage of teleseismic energy. The colorbar represents time from the first twelve hours of the day. The first teleseismic energy arrives at 4 hours and we begin to microseismic events clustered at the Northwest corner of the Anza Gap. Until the mainshock at 8:04:38, seismicity propagates along strike to the southeast in the direction of the nucleation site of the M_w 5.2 earthquake.

to make this distinction.

The displace amplitude frequency spectra of this event is quite unique. It has more energy in low frequencies than the local earthquake coming from a similar depth (ML 1.69 at 14.6 km depth), but it depletes of higher frequencies very quickly. It's shape mimics that

of local noise, but it has much higher across all frequencies (figure 3.11).

3.0.6 Discussion

Triggered Events and Implications for State of Stress

Long period Love and Rayleigh waves in the 15-30s period band from teleseismic events can trigger events if their dynamic triggering stress lies between 0.01-1 MPa [Hill, 2012]. However, dynamic triggering can occur with dynamic stresses less than 0.1 kPa and a wide range surface wave period bands, with 15-200s often being the most effective at triggering [Hill & Prejean, 2015]. The dynamic strain equation is often employed to determine the peak dynamic strain from the teleseismic waves, $\epsilon \approx (V/Cs) * G$, where ϵ is strain, V is the peak particle velocity from a seismogram, Cs is surface wave velocity, and G is the shear modulus, generally estimated to be 30 GPa [Van der Elst & Brodsky, 2010]. After applying a time shift to the seismograms, it is clear that the tremor coincides with the envelope of the Rayleigh wave energy, which is best seen on the vertical and radial components. To calculate the largest peak ground velocity (V) during the Rayleigh wave (the triggering surface wave) is 0.00027 m/s and we use a Rayleigh wave velocity (Cs) of 3.2 km/s, which when multiplied by the shear modulus (G) gives a peak dynamic stress of 25 kPa.

Wang *et al.*, 2013 found that peak dynamic stress amplitudes between 17-35 kPa should be capable of triggering tremor along the SJF. The value of peak dynamic stress imparted by Rayleigh waves from the Puerto Morazán earthquake, 25kPa, falls right in the middle of this range of values. In the SAF, peak dynamic stress amplitudes required to

trigger tremor are estimated to range from 10-20 kPa [Peng *et al.*, 2008]. This value is slightly higher than what would be expected in the SAF, and is thus consistent with the findings from Wang *et al.* [2013] and Chao *et al.*, [2012] that indicate that the SJF requires a higher dynamic triggering stress than the SAF. A higher dynamic triggering stress is likely required because of higher fault strength. This is evidenced by the fact that the Cholame section of the SAF, where triggered tremor has been observed, is rich in direct evidence of slow slip at depth [e.g. Guilham & Nadeau, 2012; Shelly *et al.*, 2009], while there is no indication of such behavior in the SJF and only minimal indirect studies that introduce the possibility of deep creep [Lindsey *et al.*, 2014; Meng & Peng, 2016; Jiang & Fialko, 2016].

Curiously, the tremor caused by the Rayleigh waves generated by the Puerto Morazán earthquake has very different characteristics than the ambient tremor detected in the region [Hutchison & Ghosh, 2017]. Here, the tremor emits the most energy in a higher frequency band (5-15 Hz) than the ambient tremor (6-8 Hz). Their duration also vary by orders of magnitude where the triggered tremor is 1000s, while the ambient tremor is closer to 100s. This indicates that the two processes have different causal mechanisms, or that the magnitude of the causal mechanism is significantly different in each case. Finally, the depth of the triggered tremor is significantly shallower than that of the ambient tremor, which may indicate differences in the stress field over time; ambient tremor was detected in 2011, perhaps the configuration and state of stress has altered since. Alternatively, the differences of tremor depth may simply be a result of the fact that the rate weakening patches were closer to the surface and were thus more susceptible to changes in dynamic stress brought on by surface waves as opposed to the effects of long term process that may

influence static stress, which are likely to impact the behavior of ambient tremor. It is notable that the triggered tremor depth is more consistent with the triggered tremor depth detected by Wang *et al.*, [2013] following the 2002 M_w 7.9 Denali Earthquake.

Spectral analyses of the triggered tremor shows high energy at low frequencies (<1 Hz), characteristic of teleseismic events, due to the passage of long period energy at long distances. When compared to a local earthquake, the signal decays of high frequencies more quickly than the regular earthquake, which is characteristic of tremor. The signal is somewhat similar to that of a local ambient tremor event [Hutchison and Ghosh, 2017] and has more energy across all frequencies than the background, but energy depletes in a fashion to the background, though the slope is somewhat more linear. Thus, the combination of high energy in low frequencies, which may be from teleseismic energy, and a distribution that otherwise resembles tremor is likely indicative of teleseismically triggered tremor. It should be noted however, that there is a somewhat unique cyclical feature to this signal that may be an atypical feature worthy of deeper investigation (figure 3.11).

Curiously, a number of microseismic events that are temporally coincident with the energy from two teleseismic events occur in the Anza Gap region of the SJF and in the same location as the M_w 5.2 earthquake that occurs 3 hours after the cascade of seismic activity described in this paper. Numerous factors can affect the remote triggering of earthquakes; the extent to which each of these factors, or combination of them, is responsible for earthquake generation largely remains unknown. Such factors include, but are not limited to, the presence of fluids and associated pore fluid pressure effects, directivity effects, the geometry and frictional properties of of a fault, and the state of stress field [Brodsky

& van der Elst, 2014; Gomberg *et al.*, 2001]. As evidenced by the findings in this study, dynamic fluctuations in the stress field are capable of causing the fault to surpass Coulomb failure criteria. When an ordinary earthquake is triggered as a result of a teleseismic event, it is interpreted that the dynamic strain from the propagating waves of the triggering earthquake temporarily changes the stress field sufficiently to act as a clock advance for time until failure [Gomberg *et al.*, 1998].

Over time, the microseismic events, for the most part, nucleate increasingly close to the location of the mainshock (figure 3.9). This would indicate that these microseismic events are part of a foreshock sequence leading up to the nucleation of the mainshock of the Borrego earthquake. Previous studies have suggested that foreshock sequences can be representative of slow slip transient that can ultimately trigger a larger magnitude earthquake [McGuire *et al.*, 2005]. Curiously, of the 25 microseismic events that occur, 12 of the very small earthquakes occur in the same location along the fault at a similar depth of 23 km (figure 3.7). The repeating location and potential for creep suggests these may be repeating earthquakes [i.e. Anooshehpoor and Brune, 2001]. . If these are indeed repeating earthquakes, it is likely that they are a result of slipping rate-weakening patches within the setting of aseismic creeping of a larger rate-strengthening background [i.e. Chen and Lapusta, 2009]. Further studies using matched filter analyses would be useful to confirm whether or not these are indeed repeating earthquakes.

Delayed Triggering of the M_w 5.2 Borrego Earthquake

The evidence stacks such that it is likely that that the earthquake was a result of delayed remote triggering from dynamic stress changes associated with the two teleseismic

events of June 10, 2016. Triggered fault creep was previously suggested as a mechanism for delayed triggering of tremor and earthquakes [Shelly *et al.*, 2011]. Earthquakes were triggered by aseismic fault creep in several locations including New Zealand [Delahaye *et al.*, 2009], near the Salton Sea [Lohman *et al.*, 2007], and the central section of the SAF near San Juan Bautista [Peng & Gomberg, 2010]. Shelly *et al.*, [2011] proposes that creep is the primary event that is triggered by the dynamic stress change from the passage of teleseismic wave and that the tremor or earthquakes is a secondary process, likely resulting from the evolution of the creep event. Deep creep in this region would not be surprising, as recent findings could be interpreted to suggest such behavior [Lindsey *et al.*, 2014; Meng & Peng, 2016; Jiang & Fialko, 2016; Hutchison & Ghosh, 2017]. In this case, deep creep is supported by (suspected) repeated earthquakes at depth preceded by triggered tremor at the same location, but at a shallower depth.

Alternatively, the tremor and continued seismic activity that occurred during the teleseismic events sufficiently altered the stress field, providing the conditions required for the nucleation of a moderately sized earthquake. This would be a result of the static stress change resulting from the cascade of seismic events related to the teleseismic activity. This scenario seems unlikely since none of the events detected preceding the Borrego earthquake are likely large enough, even combined, to sufficiently change the stress field to generate a moderately sized event.

Finally, there remains the possibility that there is no relationship between these events and that the Borrego earthquake would have happened regardless of the teleseismic activity. Further, the triggered tremor signal remains an elusive one. Nonetheless, the

coincidence of small earthquakes occurring in a similar location near the Anza Gap and teleseismically triggered tremor are both likely to indicate conditions suggestive of a creep or slow slip event, which could ultimately trigger an earthquake.

3.0.7 Conclusion

A cascade of seismic activity in the Anza Gap and the trifurcation region of the SJF associated with two teleseismic events occurred on June 10, 2016. The activity started with tremor triggered by the envelope of the Rayleigh wave from the Puerto Morazán earthquake followed by microseismic events throughout the duration of the passage of the teleseismic energy and continued when a second teleseismic event from the Solomon Islands hit the region. As the teleseismic energy tapers off, so did the seismic activity until several hours later when a M_w 5.2 earthquake occurred where some of the microseismic events had occurred. We interpret these findings to suggest: (1) Dynamically triggered tremor from Rayleigh waves occurred in the region and that dynamic stress change required for triggering is on the order of previous studies in the region. (2) microseismic events are likely a result of the dynamic stress change, causing the respective part of the fault to surpass Coulomb failure criteria. (3) It is possible that these teleseismic events immediately triggered a deep creep event, resulting in seismic manifestations of such as a deep foreshock sequence of microseismic events that migrate in the direction of the mains shock. Additionally, some of the events such may have been repeating earthquakes, which would require additional studies using matched filtering, for example. These events may be manifestations of a delayed triggering mechanism for the M_w 5.2 Borrego earthquake.

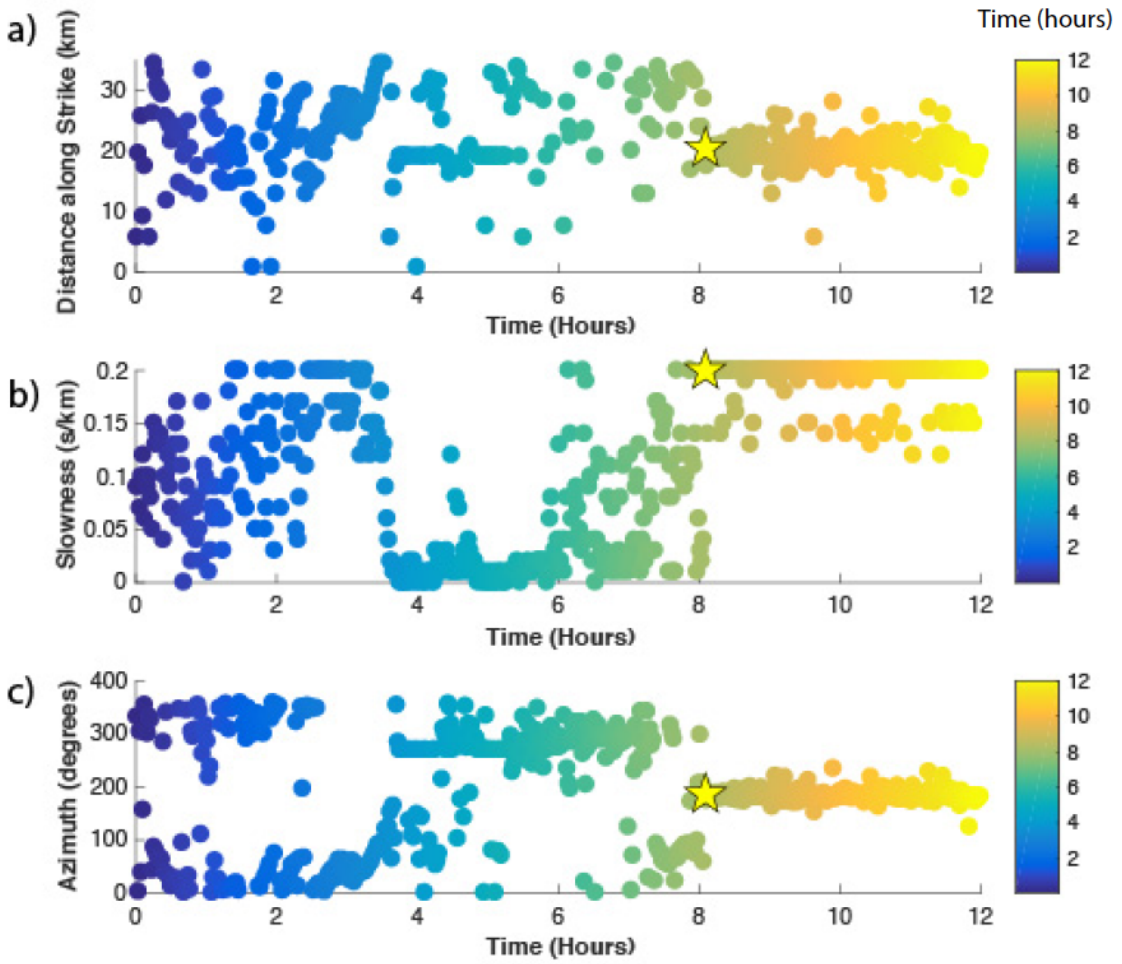

Figure 3.9: This plot shows the information that can be determined from slowness values for the first half of June 10, 2016. The color bars represents time, with blue indicating earlier in the day and the colors becoming more yellow as time passes. The Borrego Earthquake is given with a yellow star. These analyses are conducted at 20s intervals between a 1-10 Hz frequency band to best capture the microseismic events. Panel a) gives the locations of the time windows along strike. At approximately 4 hours, with the arrival of teleseismic energy, a pattern emerges where the signal remains at a distance of 20 km along strike for two discrete periods for a total of two hours (until 6 hours). Panel b) gives slowness and it is clear that around the same time that energy in the 1-10 Hz frequency band begins to concentrate around 20 km along strike, this location corresponds to a very low slowness value indicating a high velocity, and likely, a deep source. Panel c) gives the back azimuth of the energy from the array to the maximum energy in the slowness space (the approximate azimuth of the source location). Again, during these two long duration periods and thereafter, the energy is focused towards towards to northwest edge of the Anza Gap, where ambient tremor and triggered tremor have been detected in the past.

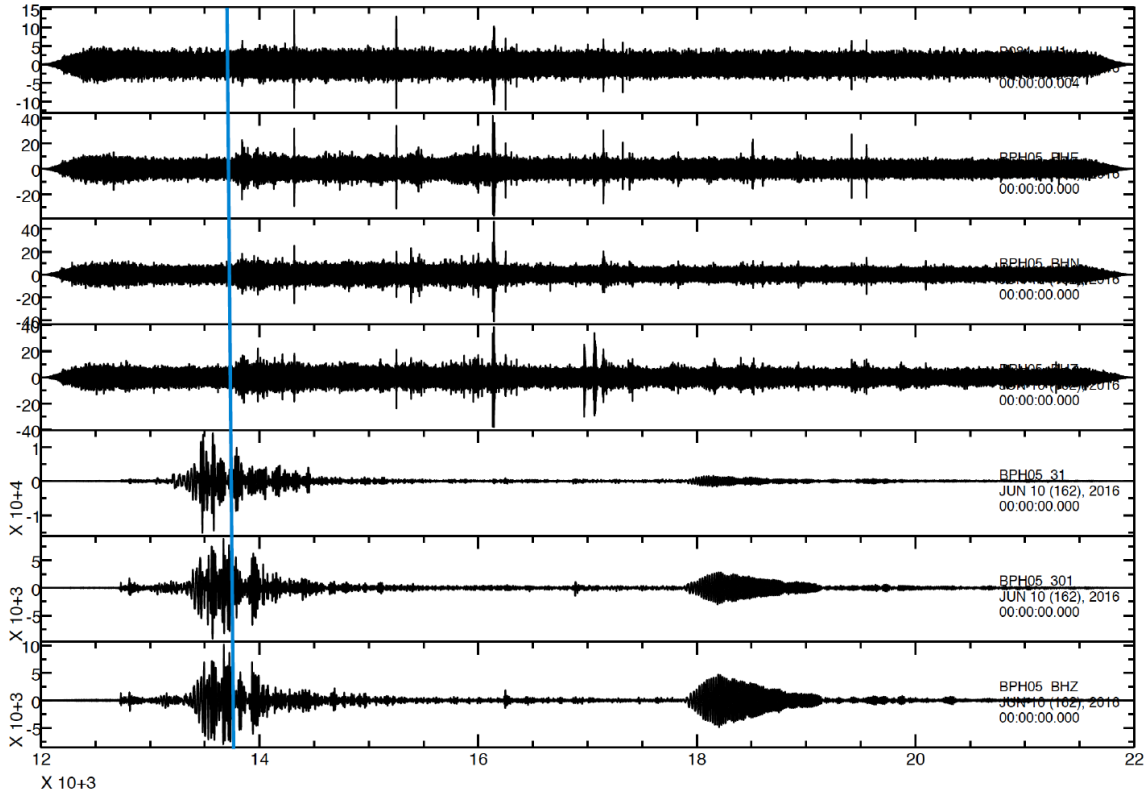

Figure 3.10: The top four seismograms are filtered between 5-15 Hz, and the bottom three are raw data. The top seismogram is the east component from PB.B084, a borehole station near the fault and the following three are the east, north, and vertical components (respectively) from PY.BPH05. The last three represent the transverse, radial, and vertical component of the raw seismic data from PY.BPH05. Here, the tremor and microseismic events are evident in both the array station and in the network borehole station. There is also a relationship evident between the Rayleigh wave arrival and the tremor.

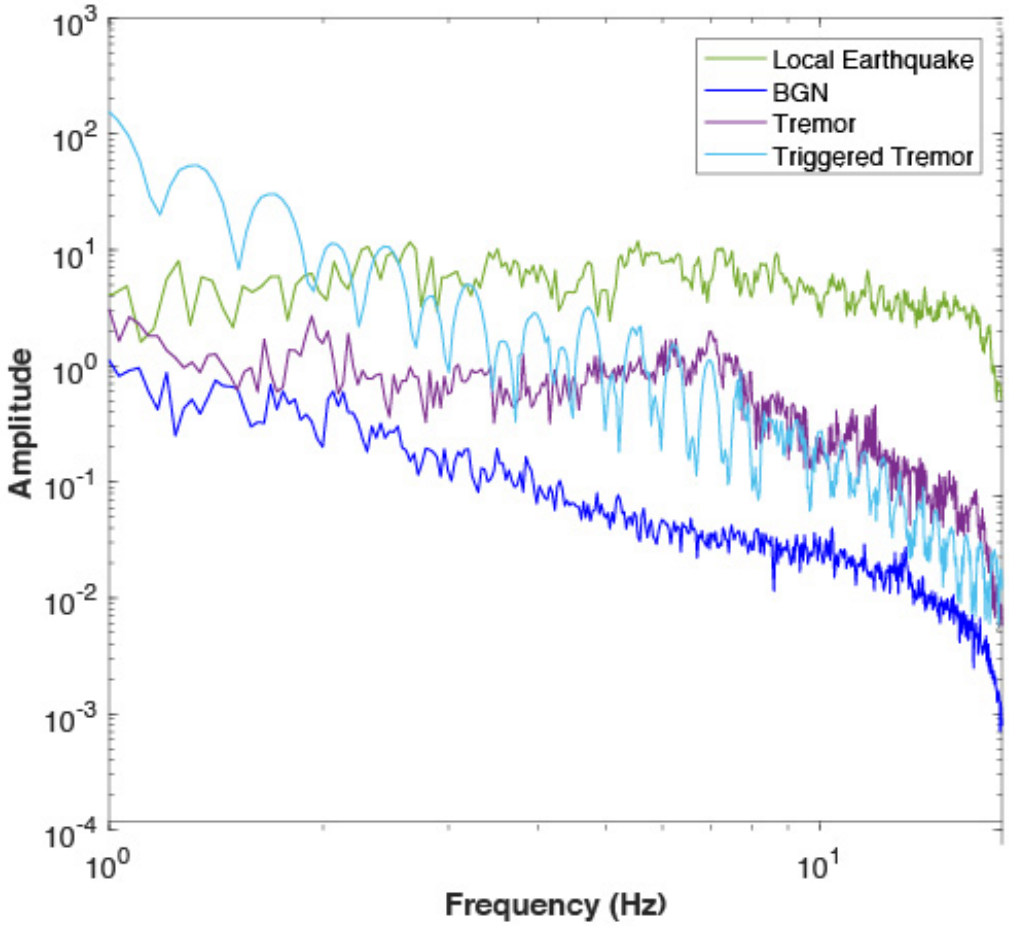

Figure 3.11: This displacement frequency spectra shows the data from teleseismically triggered tremor (light blue) versus ambient tremor from June 8, 2011 [Hutchison and Ghosh, 2017] (purple) versus a local ML 1.69 earthquake that occurred on June 4, 2011 at 14.6 km depth (green) versus stacked background noise (blue). Characteristically tremor depletes of energy in high frequencies more quickly than regular earthquakes [Shelly *et al.*, 2007]. In this case, both instances of tremor are consistent with this empirical observation. Both are also above the background. The triggered tremor however, has high energy in low frequencies, though this is to be expected from teleseismic energy as the energy is carried such long distances through long period signals. It should be noted, however, that the shape of the triggered tremor is unique in that it is somewhat harmonic, distinguishing it from ambient tremor and other signals in the region.

Part III

Very Low Frequency Earthquakes in Cascadia

Chapter 4

Very low frequency earthquakes spatiotemporally asynchronous with strong tremor during 2014 episodic tremor and slip event in Cascadia

4.1 Abstract

We find very low frequency earthquakes (VLFEs) in Cascadia during the 2014 episodic tremor and slip (ETS) event under Washington and Vancouver Island using a grid-search centroid moment tensor inversion method [Ito and Obara, 2006]. In sharp contrast to

previous findings of VLFE and tremor activity in Cascadia [Ghosh *et al.*, 2015] and Japan [Ito *et al.*, 2007], we find that VLFE and strong tremor activity are not spatially coincident. This challenges our current understanding of the dynamic relationship between the different types of slow earthquakes, and their relationship to slow-slip. We interpret these findings to suggest that VLFEs and tremor may have their own 'seismic cycles,' resulting from asperities of different sizes or characteristics that respond quasi-independently to stress loading.

4.2 Introduction

Episodic tremor and slip (ETS) events are defined by periodic intervals of slip along the plate interface, Unlike regular earthquake, large ETS events last about a month or so and are characterized by low frequency seismic activity [Rogers and Dragert, 2003], such as tremor, LFEs and VLFEs [Ide *et al.*, 2007b; Ghosh *et al.*, 2015]. These seismic signals have been extensively used to study fault slip, triggering and structure [e.g., Bostock *et al.*, 2012; Ghosh *et al.*, 2010a; Huesca-Perez and Ghosh, 2015; Vidale *et al.*, 2011; Zhang *et al.*, 2011]. The slip originates in the transition zone of the fault that lies down-dip of the seismogenic zone [e.g. Ito *et al.*, 2007]. The low frequency seismic events that comprise the ETS event include non-volcanic tremor and low frequency earthquakes that emit energy in the 2-8 Hz frequency band. It also includes very low frequency earthquakes, which are characterized by energy in the 20-50s band [Ghosh *et al.*, 2015], but are depleted of energy at higher frequencies compared to regular earthquakes of similar magnitude. Studies at many plate boundary faults have shown that LFEs and tremor are spatially and temporally

coincident [Brown *et al.*, 2009; Sweet *et al.*, 2014], and further that tremor is likely a result LFE swarms, resulting from shearing during slow slip [Shelly *et al.*, 2007]. VLFEs, however, are responsible for a larger portion of the moment release during an ETS event than the cumulative tremor activity during that ETS [Ghosh *et al.*, 2015]. It is thus paramount we study VLFE activity to better understand the role of these more elusive seismic events in the grander scheme of an ETS event. Many tremor and LFE imaging studies have revealed consistent migration patterns of tremor during ETS events [Sweet *et al.*, 2014; Thomas *et al.*, 2013; Ghosh *et al.*, 2010b, 2012]. Thus far in Cascadia, we have observed VLFEs during the 2011 ETS event, which showed a clear spatial-temporal relationship between tremor and VLFE activity [Ghosh *et al.*, 2015]. In Japan, the same spatial-temporal relationship between tremor and VLFE is often observed [e.g. Hirose and Obara, 2010]. Here, we present an unusual case of VLFE activity during the 2014 ETS event in Cascadia.

4.3 Data & Methods

Seismic data of the 2014 ETS event used in this study come from three-component broadband stations from multiple seismic networks including the US Transportable Array (TA), the Pacific Northwest Regional Seismic Network (UW), and the Canadian National Seismograph Network (CN). To initially detect VLFEs and estimate their source parameters, including the location, time, and moment tensor, we apply a grid search centroid moment tensor inversion method [Ito and Obara, 2006; Ghosh *et al.*, 2015] using US stations. Canadian stations tend to be inconsistent for detection due to noise during this time period so they are not used in the initial inversion. The grid consists of nodes in a 3-D

volume with dimensions of 0.1° x 0.1° horizontally, and 5 km vertically. Once events are detected, a second grid-search centroid moment tensor solution is determined using US and Canadian stations for better azimuthal coverage and to confirm that the solution is stable. We consider a stable solution a time window that will reproduce similar focal mechanisms and reasonable CLVD and variance reduction with a variety of different station configurations. Lastly, using the station configuration with the highest variance reduction, a finer grid that has 0.025 ° x 0.025° horizontal resolution and 1 km vertical resolution is used in a final inversion to determine more accurate locations. Optimal station configurations are only determined once an event has been identified through initial detection using the majority of stations. The grid stretches to the edges of the subducting slab, and are well outside the along-strike bounds of tremor observed during the 2014 ETS event, such that the results are not artificially confined to the tremor-active section of the subduction zone. Before the inversion is performed, we remove instrument response and filter the data in 0.02-0.05 Hz frequency band. We use 90-second sliding time-windows with a 1 second time step. For each time window, a moment tensor is calculated for each node using Green's function derived from a regional 1-D velocity model [Crosson, 1976]. The algorithm can thus produce synthetic waveforms for each grid-node for all stations. A grid-node is determined to be the source when there is a high variance reduction, i.e. low misfit, between the synthetic waveform produced for that grid-node and the observed seismograms for each station and each component. All teleseisms ($M_w > 5.5$) and regional events are removed through comparison to the Advanced National Seismic System catalog and through the visual inspection of the data in different frequency bands. Only solutions that remain stable

with different station configurations are kept in the catalog. While we cannot entirely rule out that some of the initial detections are in fact real, we only include events with robust moment tensor solution.

4.4 Results

4.4.1 Very Low Frequency Earthquake Characteristics and Distribution

We analyzed about one-and-half months of seismic data and found eight VLFEs. All the VLFEs we detect occur between December 2 and December 14, 2014, despite applying our detection algorithm to the entire ETS time period (November 3 - December 14). Their moment magnitudes range from M_w 3.7 - 4.1, similar but slightly larger than the events detected by Ghosh *et al.*, [2015] during the August, 2011 ETS event. As are expected of VLFEs [Ito *et al.*, 2009], they exhibit higher energy in the 20-50s band pass, and are depleted of energy in higher frequency bands compared to local regular earthquakes of similar magnitude. Seven of the eight VLFEs occur under southern Vancouver Island, while one occurs east of Vancouver Island, just north of the San Juan Islands. These locations mark a distinct change in the subduction of the Juan de Fuca Plate, slightly north of where the strike of the fault changes from north-south to northwest-southeast. Interestingly, VLFEs are preferentially active in the same general area during 2011 ETS event in this region [Ghosh *et al.*, 2015]. The depths of the events range from 25 – 60 km, though depth resolution is poor. The focal mechanisms of the events are striking NNW-SSE, and dip shallowly towards the east, consistent with general plate motion in this area. As an example, VLFE source parameters of an event on December 11, 2014 are shown in figure

4.1. The best solutions typically use primarily US stations because Canadian stations tend to be noisy during this time period in the VLFE frequency band.

4.4.2 VLFEs in Relation to Tremor and Slow Slip During the 2014 ETS Event

Many studies have suggested that slow earthquake activity, including tremor [Ghosh *et al.*, 2012], low frequency earthquakes (LFEs) [Shelley *et al.*, 2007], slow slip events (SSEs) [Ide *et al.*, 2007b], and VLFEs [Ito *et al.*, 2007; Ghosh *et al.*, 2015] are all manifestations of the same shearing process along the plate interface. It is thus expected that they occur coincidentally. However, the locations of these VLFEs occur in an area characterized by a lack of strong tremor activity. In 2014, episodic tremor and slip activity occurred in this area from November 3, 2014 to December 14, 2014. Based on observations of tremor and slow-slip during previous ETS events, it is expected that during an ETS event, tremor will migrate along the entire northern segment of the Cascadia margin, between Puget Sound in the south and well inside the Vancouver Island in the north, leaving no gaps in tremor or slip activity along strike. However, 2014 ETS does show a gap in tremor activity near southern Vancouver Island. The 2014 ETS event was atypical in that the tremor migration that occurred was not continuous, and its migration had an unusual propagation pattern. Tremor began in central Vancouver Island on November 3, and propagated south but never reached the southern end of Vancouver Island. Tremor activity then began in central Washington and propagated to the north, where it stopped under the Strait of Juan de Fuca, leaving a gap in tremor activity between southern Vancouver Island and the northern Strait

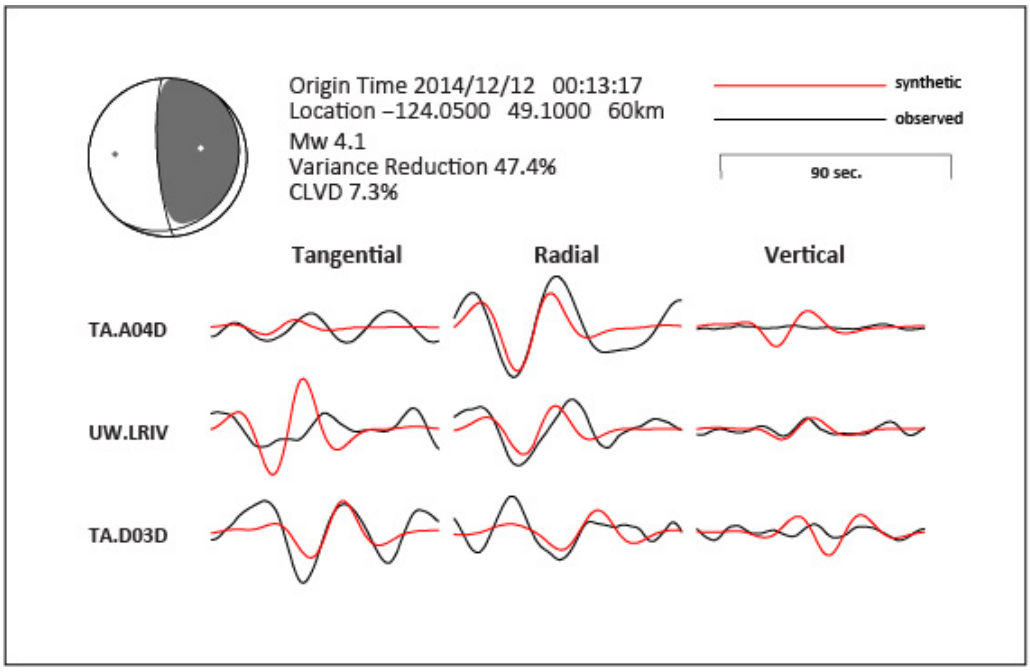

Figure 4.1: Example of a VLFE event detected using the grid-search centroid moment tensor inversion method

of Juan de Fuca. Tremor locations used in this study are provided by pnsn.org.

The VLFEs detected during this ETS event all occurred during the second phase of the ETS after the tremor died down in central/southern Vancouver Island and was activated in central Washington. It is important to note that our catalog may be incomplete in central Vancouver Island due to station distribution in our preliminary grid search centroid moment tensor inversion analysis. All but one of the VLFEs occur under southern Vancouver Island, with the exception of one that occurred north of the San Juan Islands on December 11 at 12:21pm UTC (figure 4.2). A spatiotemporal distribution of tremor versus VLFE activity clearly indicates that VLFEs occur along the edge in within the tremor gap (figure 4.3).

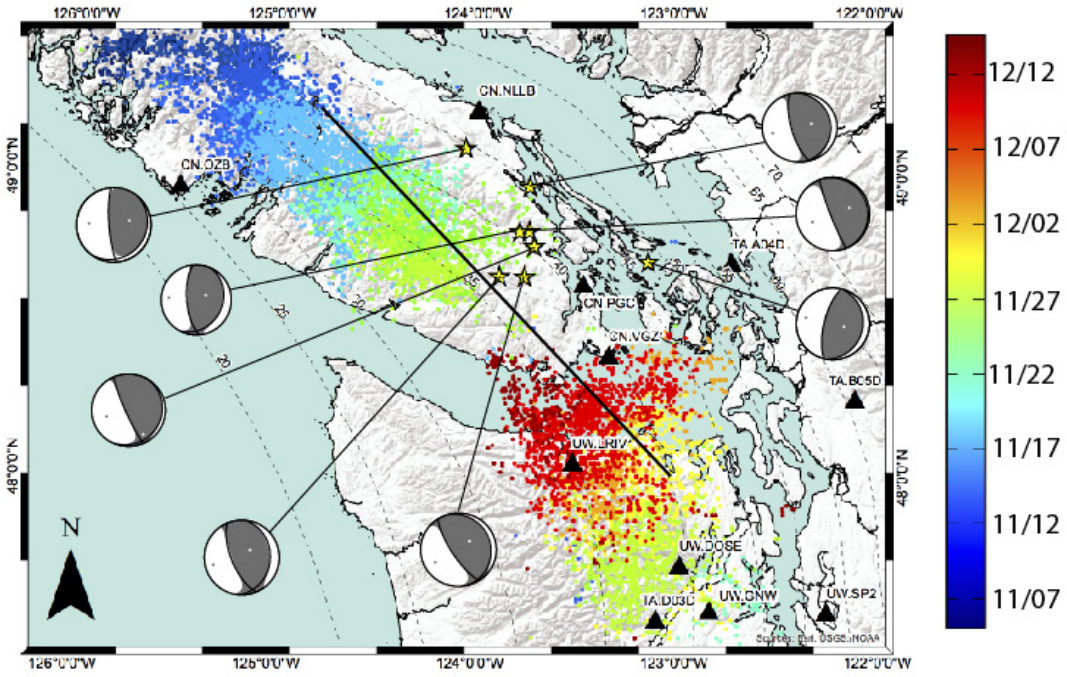

Figure 4.2: A plot of the spatiotemporal evolution of tremor (dots) during 2014 ETS activity that occurred from early November through mid-December. VLFE locations (yellow stars – note that this color does not correspond to the colorbar), fall in a gap where there is little to no tremor detected. The contours of the subducting slab are designated by dashed black lines. The black solid line is approximately parallel to the average strike of subduction in the region of interest, based on a depth contour of 25 km. Tremor data is retrieved from the Pacific Northwest Seismic Network (pnsn.org/tremor).

4.5 Discussion

There are multiple physical mechanisms that may explain how both tremor and VLFEs can be triggered by slow slip. Relatively small changes in Coulomb failure stress (ΔCFS), 0.1-0.5 kPa, were shown to induce VLFEs in models of SSEs on the Ryuku trench [Nakamura and Sunagawa, 2015]. Stress redistribution also resulted in VLFEs without the appearance of tremor in northern Tohoku as a response to afterslip of the 2011 Tohoku earthquake [Matsuzawa *et al.*, 2015]. Fluid over-pressurization is often cited as a mechanism

for inducing slow slip in an otherwise conditionally stable environment. For example, in the Nankai Trough, VLFEs only occur in the region where fluid pressure is the highest, but this region is also known to produce tremor [Saffer and Wallace, 2015]. The section of Cascadia where we observe VLFEs in the 2014 ETS event corresponds to a 4 km thick section of highly reflective shear zones that likely indicate fluid mobilization [Dragert *et al.*, 2004; Nedimovic *et al.*, 2003]. None of these properties or mechanisms, however, can fully explain the generation of one type of slow earthquake without another.

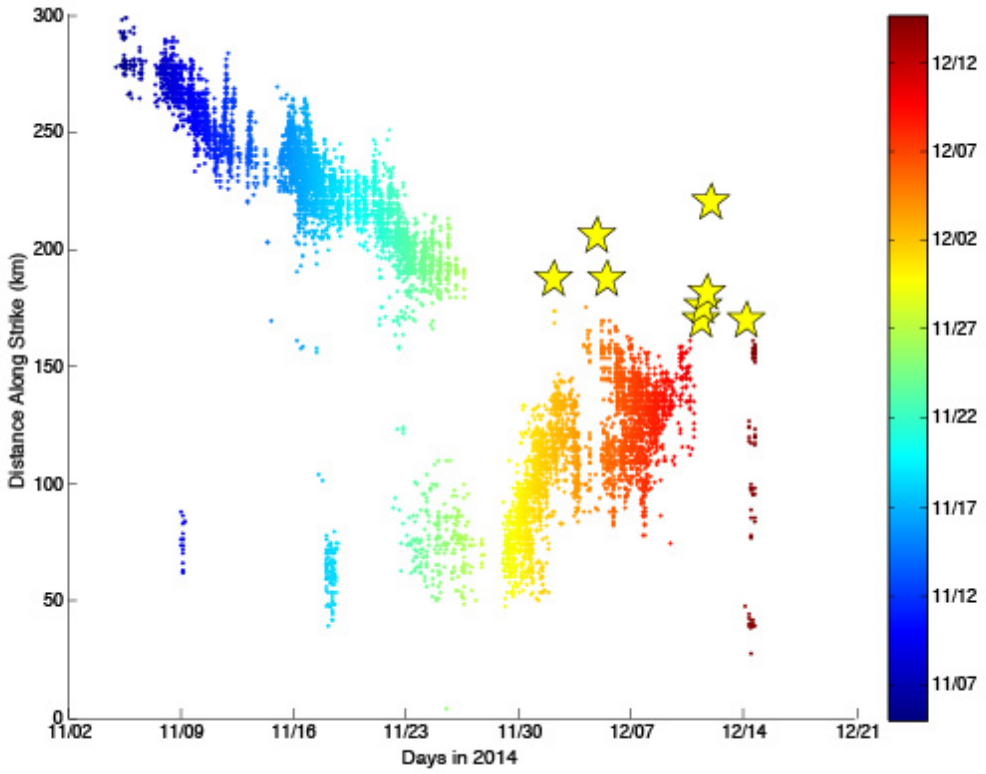

Figure 4.3: A spatiotemporal distribution of tremor (dots) versus VLFE (yellow stars). The color gradient and x-axis represent time and the y-axis represents distance along the average strike indicated in figure 4.2. Here, all of the VLFE activities occur in the second half of the ETS period, in a region along strike where there is little to no tremor activity.

VLFEs are typically coincident with high degree of tremor activity in space and time [Ito *et al.*, 2007; Ghosh *et al.*, 2015]. The common coincidence of different types of seismic radiations such as tremor, LFEs and VLFEs during slow slip led to the suggestion that they represent energy from different parts of the frequency spectrum during the same shearing process [i.e. Shelley *et al.*, 2006; Ito *et al.*, 2009]. The observations shown here indicating no direct correlation between VLFEs and strong tremor activity during the 2014 ETS event in Cascadia add an element of complexity to this potential relationship (figure 4.4). Notably, however, during the inter-ETS period prior to the 2014 ETS event, there was a brief tremor burst (June 20 – June 26, 2014) in the region where we observe VLFEs without coincidental tremor during the November – December 2014 ETS event. Tremor is often observed without VLFEs, but VLFEs are rarely observed without tremor in locations where both types of seismic behaviors are observed (figure 4.5). These observations show that they can occur independently even though the conditions necessary to generate tremor and VLFE signal can coexist in a locale. This requires additional conditions that allow radiations of seismic energy in one relatively narrow frequency band and not in others. Alternatively, it is possible that low amplitude tremor activity is occurring during VLFEs, but is below the detection level of conventional methods of tremor detection and location with the existing seismic network [Obara, 2002; Wech and Creager, 2008]. Ghosh *et al.* [2012, 2009] show quasi-continuous tremor in this area using a beam-beackprojection technique, which detects 5-times the duration of coherent tremor activity compared to a conventional approach. Even if this is the case, such a strong level of VLFE activity with such a low level of tremor is intriguing and challenges our current understanding of mechanism controlling tremor and

VLFEs.

Structures and asperities of various sizes affect the moment release of an event, such that larger asperities would theoretically generate a larger slow earthquake [Nakata *et al.*, 2011]. VLFEs are longer period events than tremor, suggesting that they would result from the rupture of a larger asperity than tremor, which is thought to be a combination of multiple concurrent LFEs [Shelley *et al.*, 2007]. LFEs are short period events that last a few seconds, indicating a smaller rupture area. When slow slip occurs, it is possible that both types of patches rupture simultaneously, producing both VLFEs and tremor.

However, because the area that produced VLFEs without tremor during the ETS period in 2014 exhibited tremor activity earlier in the year (June, 2014), it is possible that stress had not accumulated sufficiently on these smaller asperities to reactivate with the rest of the transitional plate interface (along-strike) producing the multitude of LFEs required to generate tremor. This implies that tremor and VLFE patches slip quasi-independently, even though they are both closely associated with slow slip. In other words, different sized asperities may fail at different times with respect to the same amount of stress loading (e.g. smaller asperities may rupture more quickly, while stress continues to accumulate on larger patches until those are sufficiently stressed to produce a rupture – the loading rate remaining uniform along the fault). It is notable that a significant amount of slow slip is detected by a geodetic network in the area of intense VLFE activity during this ETS event [Liu *et al.*, 2015], although tremor activity is low in that area. Slow slip without strong tremor has also been observed in Cascadia [Wech and Bartlow, 2014]. Occurrence of VLFEs without strong tremor indicates that patches generating VLFEs and tremor may have their own 'seismic

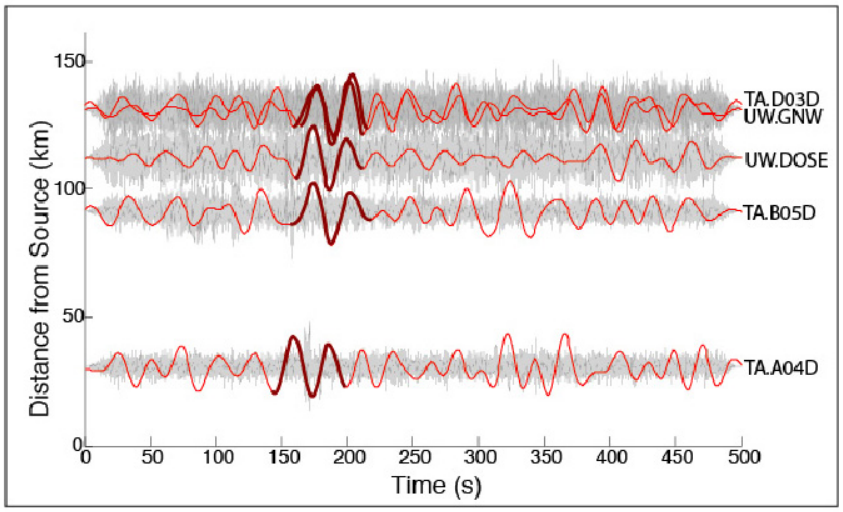

Figure 4.4: A comparison of tremor (grey) and VLFE (red) seismograms from the BHE channel. The seismograms are plotted by stations distance from the location of the VLFE (same event shown in figure 4.1). VLFE seismograms are plotted between 0.02-0.05 Hz, and tremor seismograms are filtered in a 2-8 Hz bandpass. There is no temporal correlation in amplitude between the two frequency bands as is typically observed in tremor and VLFE [Ghosh *et al.*, 2015]. All seismograms give show ground velocity are normalized.

cycle' and are characterized by quasi-independent stress dynamics. If the stress evolution in both types of patches is too asynchronous, they may show instability (producing seismic radiation) independent of each other. This model also explains why tremor is not always

accompanied by VLFE activity.

VLFEs are responsible for a significantly greater portion of the total seismic moment released during an ETS event than tremor activity [Ghosh *et al.*, 2015; Ide *et al.*, 2007a]. Understanding the behavior of VLFEs can thus provide great insight into the stress

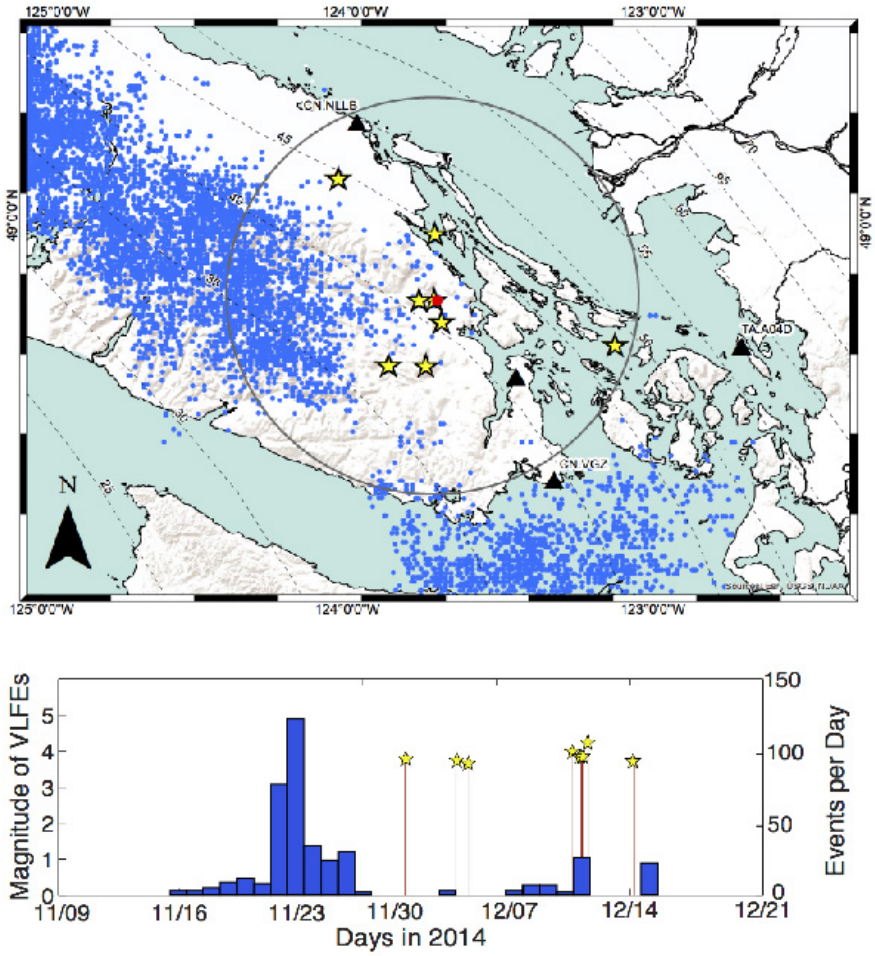

Figure 4.5: The upper map shows VLFEs (yellow stars) from the 2014 ETS event with their geographic mean indicated by a red point. The blue points show tremor. We draw a 50km radius around the geographic mean of the VLFEs to evaluate the spatiotemporal relationship between tremor and VLFE. The lower plot shows the temporal distribution of tremor (blue bars) versus the temporal distribution of VLFEs (stars) and their magnitude. Based on this test, there is not a spatiotemporal relationship between tremor and VLFE during this ETS.

dynamics and major physical processes that occur near the plate interface during an ETS event. The occurrence of VLFEs that is not directly coincident with tremor shows that the relationship between low frequency seismic activity and slip in Cascadia is more complex than previously thought and may be related to separate rupture processes, with distinct stress dynamics along the plate interface.

4.6 Conclusions

Using a grid-search centroid moment tensor inversion method, we detect and locate VLFEs during the November-December 2014 ETS activity in Cascadia. Previously, VLFEs and tremor in Cascadia have been spatiotemporally coincident [Ghosh *et al.*, 2015]. These VLFEs, however, occur in a spatiotemporal gap where there is very little to no tremor. Thus, VLFEs are observed without tremor, indicating that VLFEs can occur independently of tremor even though the conditions necessary to generate both types of events exist in an area. We suggest that the asperities producing VLFEs and tremor may have their own seismic cycles requiring different stress conditions to activate instability during slow-slip.

Chapter 5

Repeating VLFEs during ETS events in Cascadia track slow slip and continue throughout inter-ETS period

5.1 Abstract

Episodic tremor and slip (ETS) events in Cascadia include slow earthquake phenomena such as slow-slip events (SSEs), tremor, low frequency earthquakes (LFEs), and very low frequency earthquakes (VLFEs) [Rogers and Dragert, 2003; Ghosh *et al.*, 2015]. Using VLFEs detected from a grid-search centroid moment tensor inversion algorithm in the 2011 [Ghosh *et al.*, 2015] and 2014 [Hutchison and Ghosh, 2016] ETS events as tem-

plates, we apply a matched filter algorithm to create a VLFE catalog for each ETS event. We also use the 2011 template events to create a VLFE catalog from July 2011 through the end of 2012, which encompasses both the 2012 ETS event and an inter-ETS period. The successful application of the method intrinsically suggests that VLFEs are repeating events, of which thousands were detected during each ETS event. The findings contained herein come shortly after the successful application of a similar matched filter methodology in Western Japan where a number of VLFEs were also successfully detected [Baba *et al.*, 2018]. The high temporal resolution of these VLFE catalogs show a significant increase in VLFE activity during ETS events that drops off immediately before and after the ETS period. A comparison of VLFE activity to GPS data shows that VLFE tracks slow slip, even when tremor is not occurring or is behaving anomalously during ETS periods. Finally, we also find continued VLFE activity during the inter-ETS period for all template events, though the extent of reactivation of VLFE asperities and their spatiotemporal coincidence with tremor is varied amongst the template events.

5.2 Introduction

Very low frequency earthquakes (VLFEs), like low frequency earthquakes (LFEs) and tremor (a cluster of LFEs) are a type of seismic event that are interpreted to represent shearing on the fault plane, typically in the transition zone [e.g. Shelly *et al.*, 2006; Ide *et al.*, 2007; Ito *et al.*, 2009; Ghosh *et al.*, 2015]. VLFEs and LFEs are types of earthquakes that are thought to obey an empirically derived slow earthquake linear moment scaling law that differentiates these events from regular earthquakes [Ide *et al.*, 2008]. Slow earthquakes

are an umbrella term that encompasses aseismic slow slip events (SSEs), VLFEs, LFEs, and tremor, which consists of clustered arrivals of LFEs. There remains uncertainty as to the source properties of these events, their relationships to each other, if they are differing manifestations of the same event [Gomberg *et al.*, 2016], or if the slow earthquake scaling relationship is even a valid characterization of such events.

Many studies indicate spatiotemporal correlations between tremor and VLFE activity in Japan [Ito *et al.*, 2009], Cascadia [Ghosh *et al.*, 2015], and Costa Rica [Walter *et al.*, 2013]. These observations prompted the development of a model suggesting that VLFEs might be the result of filtering a seismic signal of clustered LFEs in the 20 - 50 s period band and do not represent discrete seismic events [Gomberg *et al.*, 2016]. Hutchison and Ghosh, [2016], however, detected VLFEs during the 2014 ETS event in Cascadia that occurred asynchronously with peak tremor/LFE activity, contradicting this alternative source model for VLFEs. Nonetheless, determining the nature of VLFEs is significant as they contribute the largest seismic moment in ETS events and because slow earthquakes can increase the probability of regular earthquakes [Obara & Kato, 2016]. Moreover, a recent study in Alaska revealed a VLFE acting as a transition between a foreshock sequence and the nucleation of a M_w 3.7 earthquake in a strike-slip setting in Cascadia [Tape *et al.*, 2018].

The characteristic period band of VLFEs is 20 - 50 s, unlike the more commonly studied LFEs and tremor that have a characteristic frequency band of 2 -8 Hz [Ide *et al.*, 2007]. It is notable that this characteristic period band for VLFE is derived empirically from observations of signal to noise ratios and that the mechanism, if one exists, for such a distinctive frequency output is still unknown. VLFE signal duration in a seismogram

can last from 50 – 200 s, though in Cascadia, their signal duration is typically 90 s. Magnitudes of VLFEs in Cascadia range between M_w 3.1 and 4.3; thus for an individual event, its moment release is greater than that of any other discrete slow seismic event. Like other types of slow seismic events, VLFEs are thought to result from the rupture of rate weakening patches within a rate strengthening background [Ghosh *et al.*, 2015]. The rupture duration of a VLFE can last from several to tens of seconds [Ide *et al.*, 2007]. Slow earthquakes that occur down-dip of the locked zone are shown to load stress up-dip to the locked part of the fault, potentially increasing the probability of generating a megathrust earthquake [Rogers and Dragert, 2003]. [Beroza and Ide, 2011]

Cascadia is the first region where VLFEs have been observed as occurring both spatiotemporally coincidentally and asynchronously with tremor during different ETS events. Ide *et al.*, [2016] stacked tremor events and filtered the signal in the very low frequency band (0.02 – 0.05 Hz), inverting the results for VLFE locations. The VLFE source locations were consistent with tremor locations, indicating that VLFE signals were abundant throughout the region of this study during periods of tremor and slow slip. Given the detection method, findings of from this study inherently suggest a relationship between tremor and VLFE. Further, during the 2011 ETS event, VLFEs and tremor were spatiotemporally coincident [Ghosh *et al.*, 2015]. However, in the 2014 ETS event, VLFEs and tremor were spatiotemporally asynchronous [Hutchison and Ghosh, 2016]. Given the contrasting activity during the 2011 and 2014 ETS events in Cascadia, it is important to characterize VLFE behavior in order to determine more about their source mechanics and elucidate their role in ETS activity. Currently, a limited catalog of VLFE events exists for the 2011 and 2014

ETS events. Here, we expand the catalog during these ETS events using the existing VLFEs as templates using a matched filter method [Shearer, 1994]. Additionally, we analyze the inter-ETS period between the 2011 and 2012 ETS events, which suggest inter-ETS VLFE activity for all template events.

5.3 Data and Methods

5.3.1 Data

The seismic data used for this study is from three-component broadband stations in the Pacific Northwest Regional Network (UW), the Canadian National Seismograph Network (CN), and the U.S. Transportable Array (TA). For the 2011 ETS event, we analyze July 1, 2011 – October 1, 2011 though the ETS event occurred from July 23, 2011 – September 6, 2011; for the 2014 ETS event, we analyze October 1, 2014 – February 1, 2015, though the ETS occurred from November 3, 2014 – December 10, 2014 and was divided into two subevents, which are separated into distinct events on November 23, 2014 . We also generate a catalog that begins on July 1, 2011 and ends on December 1, 2012. This time period includes two ETS periods and one inter-ETS period, which we define as July 23, 2011 – September 6, 2011, August 30, 2011 – October 11, 2012, and September 6, 2011-August 30, 2012, respectively. These date ranges are based on tremor data from the Pacific Northwest Seismic Network (PNSN) [Wech, 2010].

5.3.2 Grid Search Centroid Moment Tensor Inversion

Before searching for additional VLFEs, instrument response is removed and data is filtered between 0.02-0.05 Hz. Our template events were detected using a grid search centroid moment tensor inversion method [Ito and Obara, 2006; Ghosh *et al.*, 2015; Hutchison and Ghosh, 2016] that provides parameters such as the location, time, and moment tensor solution. The grid, with horizontal spacing of 0.1° x 0.1° and 5 km in depth, extends from the trench to just east of Cascade Range. The moment tensor inversion algorithm uses a 90 s time window with a 0.1 s time step, and a solution is calculated for each node using a Green's function derived from a 1-D velocity model [Crosson, 1976]. Initially detected events are confirmed with a second grid search centroid moment tensor inversion that contains a finer grid with node dimensions of 0.025° x 0.025° and 1 km depth to maximize spatial resolution. We also ensure stability of the solution by using different sets of stations to confirm the same solution. The optimal solution (i.e. the best configuration of stations) will have the highest variance reduction (a measure of similarity between the synthetic and observed seismograms) and a low compensated linear vector dipole value.

5.3.3 Matched Filter Method

Using the 5 template VLFEs detected during the 2011 ETS event and the 8 templates during the 2014 ETS, we perform a cross correlation, or matched filter, analysis [e.g. Shearer, 1994; Shelly *et al.*, 2007]. It should be noted that the source location of these template events can be up to 100 km apart (figure 5.1). Each template event is generated using three component broadband data from the stations included in the best moment

tensor inversion solution. Each template event is compared to continuous waveform data from the same respective stations and channels as the template event with a sliding time window. A summed cross correlation coefficient value is calculated for each time step (1s). Time windows with values above a determined threshold value are catalogued as VLFEs.

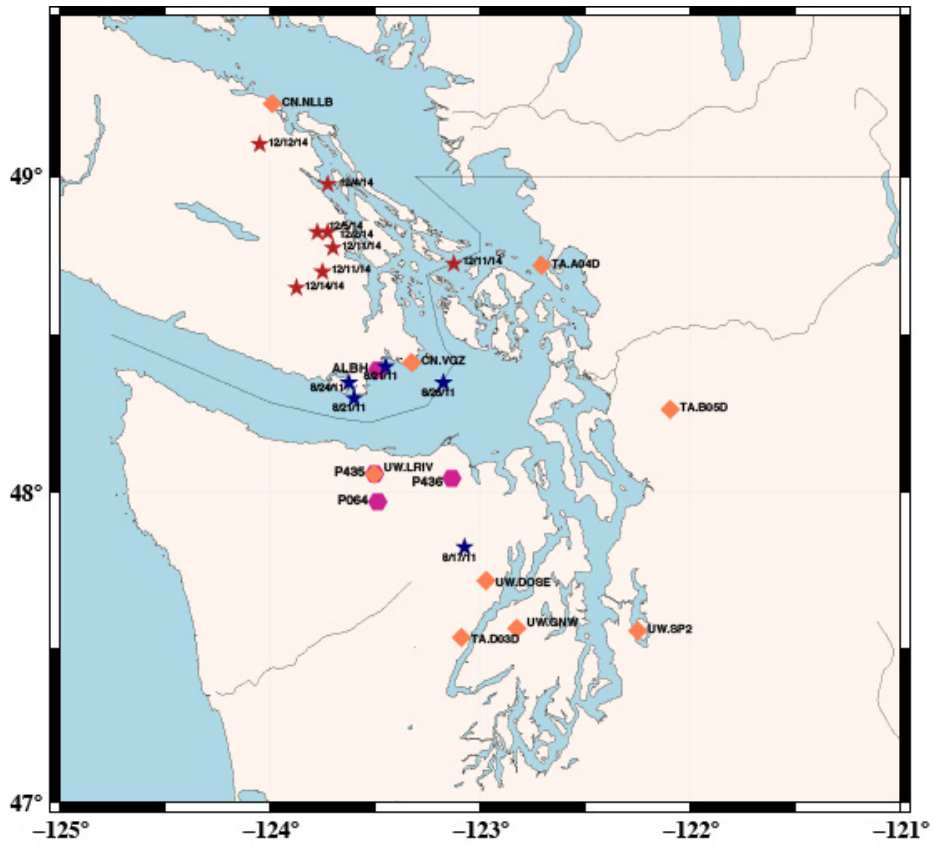

Figure 5.1: A map of the study area. Seismic stations used for grid-search centroid moment tensor inversion and matched filtering are represented by orange diamonds and the GPS stations used to compare VLFE activity to SSEs are given in pink octagons. The template events from 2011 are shown in navy blue stars and the template events from 2014 are represented with dark red stars. Each template event, GPS station and seismic station are labeled on the map accordingly.

We perform an extensive matched filter analysis of background noise to select cross-correlation threshold values. Theoretically, VLFEs should have higher cross-correlation val-

ues than background noise because they are real repeating events. If correct, this hypothesis can provide a quantitative method to derive cross-correlation threshold values for selecting VLFEs above the background. We select 100 random time windows that presumably consist of background noise because they were not detected by the template events. Using the station configuration for each respective template event, we create background noise catalogs for all 100 background noise time windows during the same time period (June 1, 2011 – December 1, 2013) as the template events. We then determine the mean of the third highest summed cross-correlation coefficients (third only to the maximum) for each configuration of stations for each respective VLFE template event,. We use this value, which varies for each template event as a cross correlation threshold value for VLFEs. We chose this value because it conservatively enforces a direct comparison to the background noise levels in the VLFE frequency band, but it nonetheless yielded somewhat similar results to using six times the median absolute deviation (MAD) of all the summed cross correlation values. Using this value will allow for more automated VLFE cataloging in the future. Applying Gaussian statistics, six times the MAD of the summed cross correlation values is equal to 4 standard deviations, equating to a false detection probability of 3 x 10-5. This corresponds to a false detection rate of 0.6 per template/per day if using the MAD approach for selecting a cross correlation threshold, which accurately captures our findings using our own noise threshold selection method.

Once a catalog of matched filter detected VLFEs is generated, we stack the detections from each template at each station from each individual channel (figure 5.2). We invert the stacked seismograms from the VLFE matched filter detections for each individual

template event, using its respective station configuration. Theoretically, since the stacked seismogram should be very similar to that of the original template event, the stacked inversion and original template event should be similar. This process is conducted to ensure that our matched filter process was completed properly and because the results of the stacked inversion can reveal source properties of the matched filter detections including the focal mechanism and location of the events (though these should mimic that of the original template event).

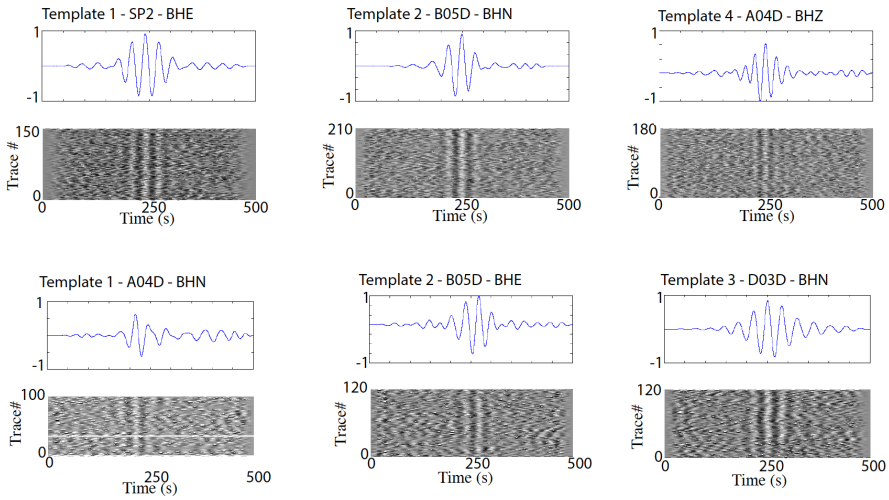

Figure 5.2: Each of these six panels (a-f) show VLFE detections from individual stations and channels from different template events as grayscale plots and stacked. In the grayscale plots each matched filter detected VLFE trace is plotted such that white is positive and black is negative in order to show the semblance of the time windows. Each top seismogram (blue) shows the stacks that resulted from combining the detections shown in the grayscale plots. The top row (a-c) gives examples from individual template events and channels from the 2011 ETS event, while the bottom row (d-f) gives examples from individual template events and channels from the 2014 ETS event.

5.3.4 Spatiotemporal Analysis of VLFE v. Tremor v. Slow Slip

Using the enhanced VLFE catalogs, we perform spatiotemporal analyses to explore the relationship between VLFE, tremor, and slow slip. The stacked moment tensor inversion solutions for each stacked event are inferred as the source location of the repeating events detected by the respective template event. Then, a 50 km radius is taken around the inferred epicenter of the repeating VLFEs. To establish a relationship between VLFE and tremor, we perform a spatiotemporal comparison of the tremor that falls within the 50 km radius of the source location for each stacked solution for both ETS events. Given the poorer temporal constraints on geodetic data, we simply compare position data from the closest GPS (stations ALBH, P435, P436, P064) against the VLFE and tremor data.

5.4 Results

Using the matched filter method, we were able to efficiently detect thousands of new VLFEs during each ETS. For both ETS events, we observe increased VLFE activity during ETS events and decreased VLFE activity when ETS events are not occurring (figure 5.3). Spatial analyses comparing VLFE to tremor and slow-slip as recorded by GPS, however, show that each ETS event has a distinct relationship between tremor and VLFE activity (figures 5.4-5.7). Some activity, however, is detected in the inter-ETS period from 2011-2012 (figure 5.8)

Time windows above the summed cross correlation coefficient threshold value are cut and stacked (figure 5.2). The grid-search centroid moment tensor inversion algorithm

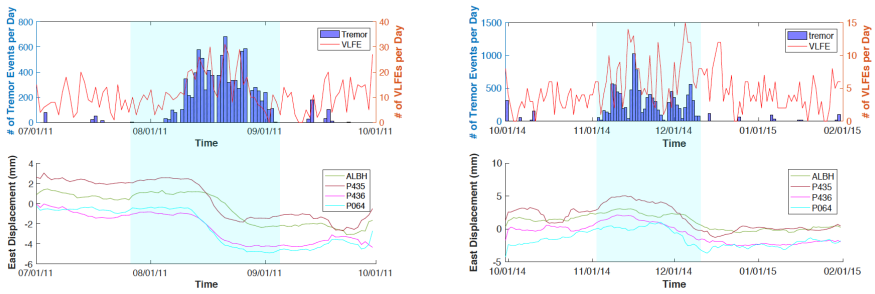

Figure 5.3: These time series plots show the relationship between tremor, slow slip, and VLFEs in Cascadia during the 2011 (left) and 2014 (right) ETS events. In the top panel in both graphs, the red line indicates daily VLFE activity, while the blue histogram shows the number daily tremor events within a 100 kilometer radius of the geographic center of the template events. The bottom panel gives GPS motion from four stations (ALBH, P435, P436, P064) near the VLFE source locations. In both cases, there is a clear increase in VLFEs during ETS, but VLFE activity decreases when there is no ETS activity indicating there exists a temporal relationship between VLFE and ETS.

is then applied to the stacks to ensure that the stacked solutions closely match that of the original template event in terms of their moment tensor, location, variance reduction and compensated linear vector dipole value. The similarity of stacked and the original moment tensor solutions further confirm that the VLFEs are repeating events. We performed this analysis for each template event across the entire catalog, then also for ETS periods and inter-ETS periods to confirm that both time periods were producing similar inversion solutions.

5.4.1 2011 ETS Event

For the 2011 ETS event, matched filtering produced 1394 new detections. The 2011 ETS event began on July 23, 2011 and ended on September 6, 2011, based on tremor activity reported by the PNSN. Notably, there is an increase in VLFE activity during the

ETS event. The number of VLFEs decrease immediately before and after the ETS event. Spatiotemporal analyses of the 2011 ETS event show a clear spatiotemporal relationship between tremor, slow slip, and VLFEs. Not only do the VLFE detections gradually ramp up, peak, and ramp back down with tremor, but the same trend exists for each individual template event, but with moderate variations. For example, in one template event, there is a sudden burst of VLFE activity in the middle of peak tremor activity, but for another there is a more gradual increase and decline in VLFE activity that closely mirrors surrounding tremor activity (figures 5.4 and 5.5, respectively). This spatiotemporal consistency amongst slow earthquake activity is largely consistent with past studies and also reflects the behavior of the template events [Ghosh *et al.*, 2015]. During the 2011 ETS event, VLFE and tremor activity are also consistent with slow slip. The GPS motion on 4 GPS stations indicates westward motion begins and ends at approximately the same time that tremor and VLFE activity pick up and drop off (figures 5.3-5.5).

5.4.2 2014 ETS Event

Matched filtering produced 2001 new detections for the 2014 ETS event. The story of VLFEs with respect to tremor and slow slip during the 2014 ETS event is quite different than 2011. First, however, it is evident that VLFE activity once again increases during the ETS event and weakens immediately before and after the ETS period (figure 5.3). It should be noted that this ETS event can be divided into two sub-events. Tremor first emerges in northern Vancouver Island on November 3, 2014, then migrates south to central/southern Vancouver Island through November 23, 2014. Tremor picks up again in

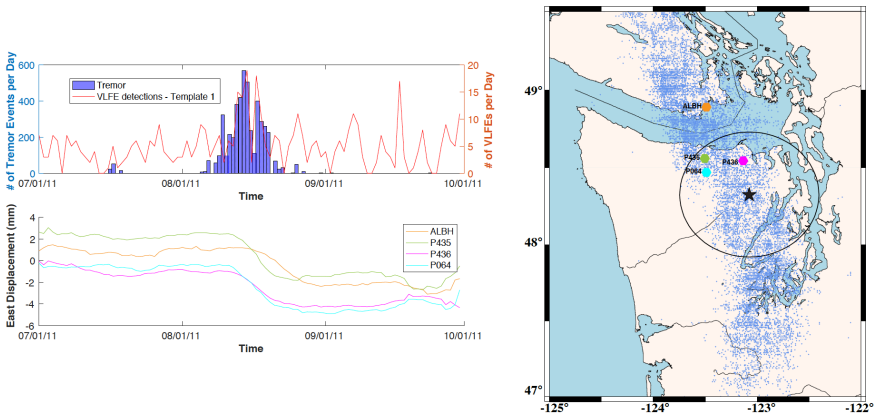

Figure 5.4: This figure illustrates the relationship between an individual template event's VLFE detections with tremor and VLFE. The temporal distribution of VLFE (red) detected by an individual template event (August 17, 2011, 04:30:28) is compared to tremor (blue) within a 50km radius of the inferred source location shown on the map (right). GPS data is also given from four GPS stations (ALBH, P435, P436, P064) in the bottom panel. The geodetic data is consistent with both the tremor and the VLFE activity indicating that these three types of slow earthquakes are spatiotemporally coincident during the 2011 ETS event.

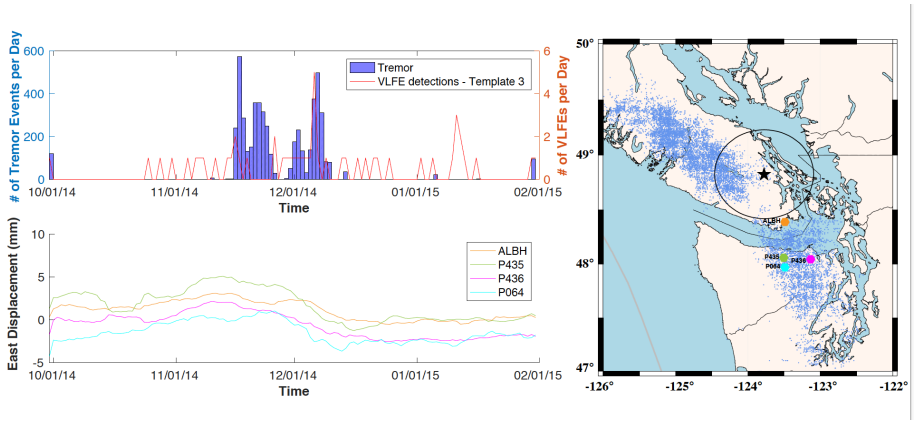

Figure 5.5: Similarly, the matched filter detections (red) from VLFE template from August 21, 2011, 04:09:03 compares well spatiotemporally with tremor (blue) that occurs within a 50km radius of the template event and GPS stations ALBH, P435, P436, and P064 (bottom panel). This behavior is consistent with the VLFE activity observed throughout the 2011 ETS event.

central Washington on November 23, 2014, propagating northwards towards Puget Sound, where the tremor stops on December 10, 2014. VLFEs occur throughout the entirety of both ETS events, however, the maximum VLFE activity occurs during the end of the ETS event. This matched filter catalog provides an improved temporal catalog of VLFE activity. The matched filter locations for the 2014 ETS event are inferred to be similar or the same to the template events given in Hutchison & Ghosh [2016]. Here, individual template events also behave differently with respect to tremor while cumulatively they show an overall increase in VLFE activity during the ETS event. One set of detections from an individual template event show little activity during the first half of the ETS event, but a large peak in the second half (figure 5.6). A different set of detections from a VLFE template that occurred after the ETS event ended (i.e. tremor stopped), on December 14, show a high peak in activity before the onset of tremor and then increases again during the second sub-ETS event (figure 5.7). By the end of the second ETS event, as it is defined by PNSN, tremor has shut off, but there is slow slip in the direction opposite subduction that is still detected by multiple GPS stations (figures 5.3, 5.6, 5.7). As such, during this ETS event, VLFE more accurately tracks slow slip than tremor. Further, VLFE tracks slow slip, even if tremor is not occurring at all. Some individual templates show peak VLFE activity that is coincidental with the second ETS period, wheres other template events show VLFE activity that peaks after tremor has shut off.

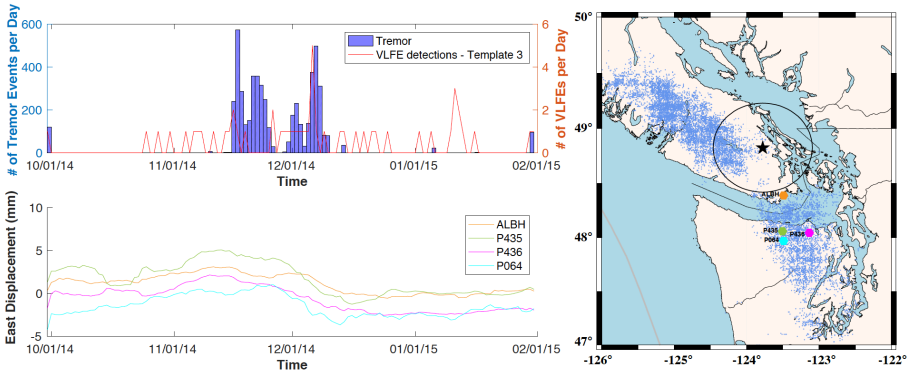

Figure 5.6: The matched filter detections from the template event of December 5, 11:56:58, of the 2014 ETS event behave quite differently than the detections from the individual matched filter detection of the 2011 ETS event. First, there is an almost negligible increase in VLFE activity (red) from the background when tremor (blue) activity starts. GPS data (ALBH, P435, P436, P064) are plotted on the bottom left panel. There is not a significant increase in VLFE activity until the second half of the ETS event, when there is truly a transient in slow slip in the west direction. This is a unique ETS event in that tremor does not gradually increase then decrease, but rather follows a trend of several dramatic peaks and troughs that completely shut off before the end of slow slip that can really be broken up into individual ETS events. We propose that this is because VLFE activity is consistently linked to slow slip, but not always linked to tremor.

5.4.3 Inter-ETS VLFE Activity

Using the same five template events from the 2011 ETS event, we perform matched filtering from June 1, 2011 – December 31, 2012. This period includes a second ETS event in 2012 that occurred from August 30, 2012 – October 11, 2012, based on tremor data obtained from the PNSN. We thus define the inter-ETS period as October 1, 2011-August 30, 2012. A fair amount of VLFE activity is detected between the two ETS periods (figure 5.8). However, only three of five of the template events detected show an increase in activity during the second ETS event. The other two template events showed no increase in the rate of VLFE activity per day during the inter-ETS period or the 2012 ETS event.

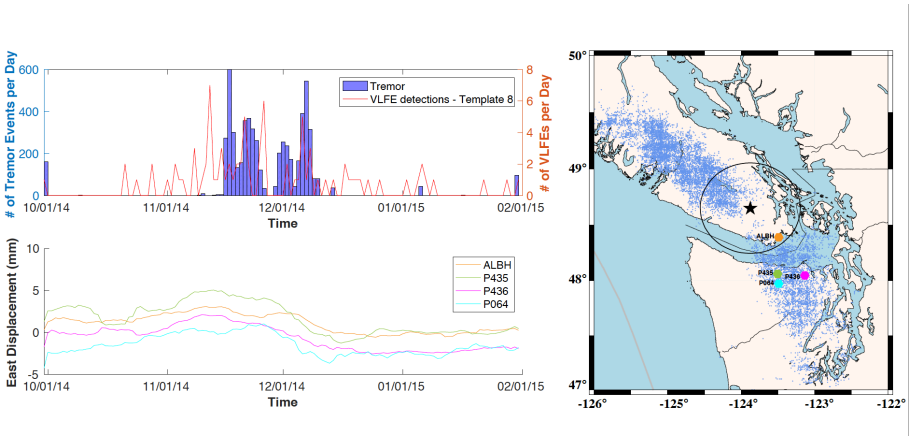

Figure 5.7: The top panel shows a comparison of matched filter VLFE detection (red) from the template event on December 14, 2014, 05:23:52 to tremor within a 50 km radius (blue). Curiously, the VLFE activity detected from this template event spans the entire ETS event, despite the fact this template event occurred shortly after the end of the ETS (as defined by PNSN based on tremor data). Notably, one of the largest peaks in activity occurs before the onset of the tremor first sub-ETS event. The following peaks in VLFE activity, however, roughly correspond to tremor activity, unlike the other template event examined in this ETS. This demonstrates that individual template events are inclined to behave differently with respect to tremor.

To ensure that such detections were not noise, we select at random 100 time windows during the 2011 ETS event that are not included in our VLFE catalog and create noise template events. We analyze these noise catalogs as well for the entire time period and found no clear trend in the noise detections during ETS events and inter-ETS time period. These are also the noise detections we use to determine our cross-correlation threshold values. The stacked noise template detections average and VLFE template detections are plotted together against tremor within a 100km radius of the geographic center of the VLFE template source locations in figure 5.8. As previously noted, we stack the inter-ETS VLFE time windows and inverted for locations, magnitudes and focal mechanisms. These events closely resembled their original template events, to validate that they are indeed VLFEs

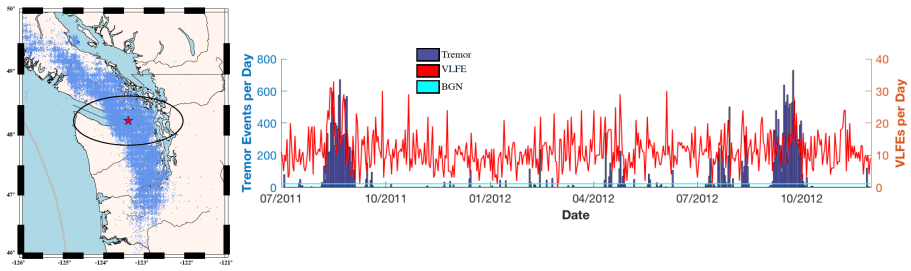

Figure 5.8: The map on the left gives the geographic center of all template events from 2011 (red star) and a 100 km ellipse around the star indicates the tremor included in the time series comparison of tremor (blue) to VLFE (red) detected by all template events from the 2011 ETS event [Ghosh *et al.*, 2015]. The cyan line represents the average number of noise (cyan) detections per day summed for all the template events. The VLFE activity clearly increases during both ETS events with tremor, however, there is sustained VLFE activity throughout the inter-ETS period that is above the background. There are also significant periods of time during the inter-ETS where VLFE activity is greater than the background.

and to infer their source locations.

5.4.4 Discussion

The similarity between the waveforms and the moment tensor inversion solutions of the template events and their respective matched filter detection stacks indicate that VLFEs are repeating events. They rupture on the fault plane on the same or nearby patches, which have similar mechanical and frictional properties. Thus, we consider the VLFEs detected through matched filtering events with source locations that are nearby, but not necessarily exactly the same. Further, the matched filter results indicate that many VLFEs occur below the background of what is detectable using the grid-search centroid moment tensor inversion approach. Beyond matched filtering simply proving an effective method for VLFE detection, it also enables the observation VLFE activity with a significantly higher degree of temporal resolution. Thus, this method and subsequent results should be considered for inclusion in a public database of slow earthquakes [Kano *et al.*, 2018]

It is largely thought that VLFEs, tremor, and slow slip are all manifestations of a greater, quasi-periodic shearing activity that occurs on the plate interface that obey a unique linear moment scaling law [Shelly *et al.*, 2007; Ide *et al.*, 2008]. More recently, Hawthorne and Bartlow, [2018] estimate the spectral distribution of moment rates in Cascadia for large slow slip events using the sums of other types of slow earthquakes as subevents in the moment rate distribution. The findings of this study further supported the findings of the linear moment scaling relationship of slow earthquakes and an interconnectedness of events.

Tremor is already thought to be a good proxy to locate and track the movement of a slow slip event along the plate interface [Aguiar *et al.*, 2009]. Previously, it was only possible to make broad inferences about the relationship between VLFE, tremor, and SSEs in Cascadia due to the small handful of VLFEs detected through grid-search centroid moment tensor inversion. Further, more recent studies, such as that of Hawthorne and Bartlow, [2018] further suggest that VLFEs are an inherent part of SSEs due to their moment scaling relationships. Fortunately, as a result of this research thousands of events detected through matched filtering make it possible to more deeply examine the role of VLFEs in ETS cycling. Many of the VLFE patches, which are separated by up to 100km, rupture simultaneously, indicating that they are being triggered by the passage of the same slow slip event, a behavior also observed in LFEs [Shelly *et al.*, 2007].

In both the 2011 and 2014 ETS catalogs, VLFEs are occurring throughout the ETS event and their activity weakens immediately prior to and after the ETS period. However, because VLFEs behave differently with respect to tremor during the 2011 and 2014 ETS events, but show consistent behavior with slow slip, it appears the VLFEs may be a reliable

indicator for a more detailed spatiotemporal analysis of the progression of slow slip through seismic monitoring even when tremor is behaving anomalously or is not occurring at all.

In 2011, there is a very clear relationship between tremor, VLFE, and slow slip. There is also a clear a rise and fall where tremor and VLFE activity gradually increase and then taper off. These findings are all consistent with previous studies that found similar spatiotemporal behavior between types tremor and VLFEs [Shelly *et al.*, 2007; Ghosh *et al.*, 2015, Ito *et al.*, 2009; Ide *et al.*, 2008; Hawthorne and Bartlow, 2018]. These results are strong evidence in favor of the model suggesting that VLFEs are the result of the same source process as other slow earthquakes and do not contradict models that suggest VLFEs are a result of filtering clustered LFEs in a 20-50s period band [Gomberg *et al.*, 2016]. Because the VLFEs in 2011 are spatiotemporally coincident with tremor and have moment tensor solutions similar to that of the plate interface with a spatial distribution that matches with the transition zone, we infer that these VLFEs are the result of shear slip occurring on rate weakening patches in a creeping segment of the plate interface.

During the 2014 ETS event, the relationship between the various types of slow earthquakes is more complex. In this case, tremor almost entirely terminates before slow slip, such that VLFEs give a better spatiotemporal representation of the progression of the slow slip event (figure 5.3). Tremor occurs within the window of slow slip, but shuts off before the slow slip event ends. VLFEs, however, mirror the slow slip throughout the entire ETS event, even after tremor has shut off. Once tremor stops, there is a large increase in VLFE activity that corresponds to a large westward slow slip transient during the ETS event. This behavior indicates that the asperities responsible for generating both VLFEs

and tremor are likely driven by slow slip, but are not necessarily intrinsically linked to one another [Hutchison and Ghosh, 2016]. This observation conflicts with the model proposing that VLFEs are a result of filtering clustered LFEs in the 20 – 50s period band [Gomberg *et al.*, 2016]. The other VLFE detections in the region are unable to make an inference either way with regards to this model because template event generation in this study relies on stacking and filtering tremor detections in the region in a very low frequency period band [Ide, 2016], or they have simply been spatiotemporally coincident with tremor [Ghosh *et al.*, 205]. Given the longer source duration of VLFEs relative to LFEs, their source patches likely have a larger area, or different mechanical properties, than the asperities responsible for generating LFEs and thus tremor [Ito *et al.*, 2007]. It follows that asperities of significantly varied areas or mechanical properties are likely to take different amounts of time and require differing amounts of (slow) slip on the surrounding rate strengthening region along the plate interface to reach their yield stress. In other words, LFE patches may slip more quickly once a slow slip front begins to pass through, whereas the regions responsible for VLFE require a different amount of slip or slip rates in the surrounding creeping region of plate interface before they are ready to rupture. Because the VLFE activity during the 2014 ETS event more accurately tracks slow slip (as measured by the closest GPS station) than tremor, VLFEs were better proxy for the seismic observation of slow slip event behavior in this particular ETS event. In both the 2011 and 2014 ETS events, VLFE activity was consistent with geodetic data of slow slip from the closest GPS stations. As such, VLFE is an alternative proxy for slow slip transient observation even when tremor is not active or not behaving consistently with the geodetic observations during ETS events. This probably

suggests that VLFEs are directly related to slow-slip, though not necessarily directly to tremor.

When observing VLFE activity over both the 2011 and 2012 ETS events, we observe continuous VLFE activity detected by all template events (figure 5.8), though the behavior of VLFEs detected by each template event is distinctive (figure 5.9). Three of the template events detect an increase in activity that corresponds with the second ETS event while two of the template events do not. We interpret this to suggest that those template events that show an increase in activity during the latter (2012) ETS event occur on a part of the plate interface that was reactivated during the propagation of slow-slip; while those which did not show an increase in activity during the second ETS event were on a part of the fault that did not reactivate. This is likely a result of geometric heterogeneities along the fault plane, and/or other variations such as the presence of fluids or differences in frictional properties. In the San Andreas Fault, activity amongst LFE clusters is observed in a similar manner [Shelly *et al.*, 2009]. Additionally, it should be noted that the lack of template events in other regions does not rule out the possibility that there may also be activity there. Additionally, it is possible that some VLFEs do not produce signals with sufficiently large SNRs to stand out above the background with the station coverage currently available. Thus, this picture of VLFE activity may be a piece of the puzzle, but is likely still an incomplete picture of VLFE behavior.

Across all of the template events, our application of the matched filter method during the inter-ETS period between the 2011 and 2012 ETS events indicates continuous VLFE activity (figure 5.8). While several of the template events detect a distinctive increase

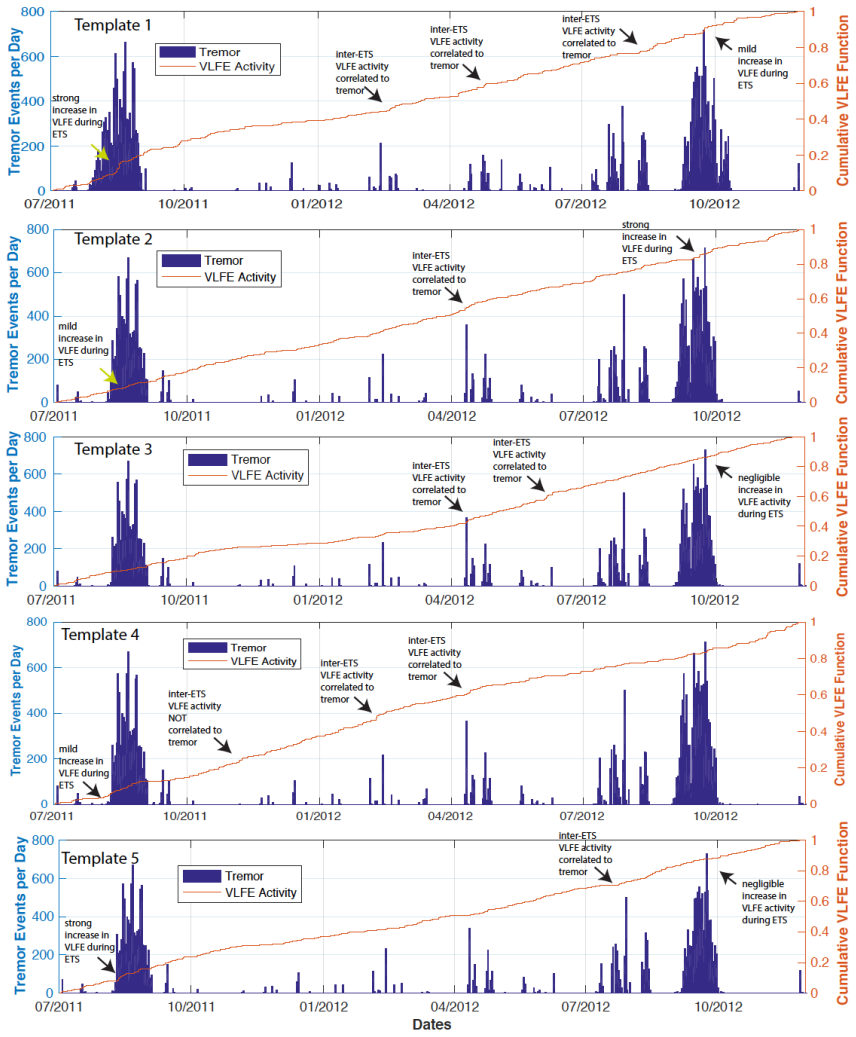

Figure 5.9: These plots give tremor within a 100km radius of each template event's source location (blue) versus a cumulative function of the VLFE detected by each template event (red). Each VLFE template behaves differently during the inter-ETS period with respect to reactivation during tremor bursts and with respect to an increase in activity during the first and second ETS events. The template events are numbered 1-5 from the top to bottom.

in VLFE activity during tremor, our observation of continuous VLFE activity throughout the inter-ETS period for when there is no tremor present further indicates that VLFEs are discrete events that can occur with or without tremor. This is particularly valid in the context of the extensive noise analyses conducted to ensure that the signals detected by the

template events are above the noise background level.

5.4.5 Conclusion

The results of this study show that VLFEs in Cascadia are repeating events. Further, the matched filtering technique provides an efficient and computationally effective VLFE detection method, capable of making thousands of detections, which can provide a more comprehensive understanding of the behavior of slow earthquakes. Such findings should be considered for addition to the public database of slow earthquake activity [Kano *et al.*, 2018]. We find that VLFE activity increases during ETS events and drops off when ETS events are not occurring. In other words, these events can track slow slip at the plate interface during ETS events. The 2011 ETS event shows that VLFE and tremor can correspond spatiotemporally, while the 2014 ETS event shows that VLFE activity does not always correspond to peak tremor activity during an ETS, but in both cases VLFE activity mimics GPS observations of slow slip. VLFEs thus have potential to act as an alternative seismic proxy to study the evolution and passage of an SSE during an ETS event, particularly when tremor is behaving anomalously. We interpret this to signify that both tremor and VLFE might be related to SSE processes, but not necessarily to each other. Finally, we observe that during the inter-ETS period, VLFEs show continuous activity, though each template event has distinctive behavior when it comes to reactivation during the subsequent ETS event and with respect to activity that is spatiotemporally coincident with inter-ETS tremor. This suggests that some patches are more susceptible to slip than others.

5.4.6 Acknowledgements

Thank you to Dr. Yoshihiro Ito, Dr. Jessica Hawthorne and Dr. Heidi Houston who have all provided useful and complementary insights into this investigation.

Chapter 6

Analysis of Long-Term Very Low Frequency Earthquake Behavior in Cascadia over 3 Year Period Suggests Ongoing Slow Earthquake Activity during Inter-ETS Period

6.1 Abstract

Very low frequency earthquakes (VLFEs) are merely one kind of seismic slip event that fits within a umbrella of events called slow earthquakes, which are unified through a unique linear moment rate scaling law [Ide *et al.*, 2007]. These events are observed along

most subduction zones including Japan [Ito *et al.*, 2007], Costa Rica [Walter *et al.*, 2013], and Cascadia [Ghosh *et al.*, 2015]. They are observed both up-dip in the accretionary prism [Ito *et al.*, 2007; Matzusawa *et al.*, 2015] and down-dip of the locked section of the fault [Hutchison and Ghosh, 2016]. Typically, tremor and VLFEs have been observed together in space and in time. Thus far, Cascadia VLFE has only been closely examined during episodic tremor and slip (ETS) events, when tremor and slip occur simultaneously [Rogers and Dragert, 2003]. During the 2014 ETS event, VLFE and tremor both occurred during the ETS event, but they were not spatiotemporally coincident suggesting that tremor and VLFE may have discrete source properties [Hutchison and Ghosh, 2014]. This study utilizes grid search centroid moment tensor inversion to generate a VLFE catalog to cover the period from the end of the 2011 ETS event [Ghosh *et al.*, 2011] to the beginning to the 2014 ETS event [Hutchison and Ghosh, 2016], allowing for VLFE observation during two ETS events and three inter-ETS periods. Continually, VLFE activity increases with within the time frame of the ETS event, but there is not always a direct relationship between migration of tremor and VLFE. This is interpreted to indicate that VLFEs are connected to tremor through underlying slow-slip processes, though the two types of slow earthquakes may not be directly related to each other. Finally, inter-ETS VLFEs sometimes follow a similar trend to that observed during the ETS, where VLFE will either migrate spatiotemporally with tremor, quasi-spatiotemporally with tremor, or sporadically. Given recent findings of small SSEs during the inter-ETS period [Frank, 2016], and models showing that low magnitude SSEs have scattered distributions along strike [Colella *et al.*, 2011], we suggest that the gap between large SSEs and VLFEs on the slow earthquake spectrum (of moment

vs. duration) may actually be a continuum filled in by "mini-ETS" events, driven by small SSEs, but manifested by a variety of seismic slow earthquakes. Further, we may go so far as to suggest that all slow earthquake activity is some scaled version of an SSE with or without seismic expressions, but further research is required to determine what controls the slow slip and its seismic expressions.

6.2 Introduction

Very low frequency earthquakes (VLFEs) have been detected down-dip of the locked zone in Cascadia [Ghosh *et al.*, 2015, Hutchison and Ghosh, 2016] and both in other subduction zones around the globe including in Japan (both up-dip and down- dip) and offshore in Costa Rica [e.g. Ito *et al.*, 2009; To *et al.*, 2015; Asano *et al.*, 2008; Walter *et al.*, 2013]. When VLFEs have been detected down-dip of the locked zone, their activity is coincident with slow-slip and tremor, i.e. during episodic tremor and slip events [Ghosh *et al.*, 2015; Takeo et al, 2010; Hutchison and Ghosh, in revision.]. This observation, however, is not necessarily due to physics, but rather to limitations in observations and studies. Hutchison and Ghosh, in review detected a number of VLFEs occurring during the inter-ETS period, when aseismic slip is below measurable levels. Additionally, VLFEs were detected as a segue way between a foreshock sequence and a M_w 3.7 earthquake in a strike-slip setting environment in Alaska. VLFEs are becoming a more frequently observed phenomenon in more fault settings. Using a traditional method of VLFE detection, grid-search centroid moment tensor inversion, we conduct an exhaustive search of VLFEs in the Puget Sound region of Cascadia between the 2011 and 2014 ETS events to identify VLFEs

that may occur during the inter-ETS period, or may occur off the plate interface.

6.3 Data and Methods

6.3.1 Data

This study utilizes three component broadband data from the Pacific Northwest Seismic Network (UW), the US Transportable Array (TA), and the Canadian National Seismograph Network(CN), and the United States National Seismic Network (US) (figure 6.1). Before analyses, all seismic data has instrument response removed and is filtered in the 20-50s period band to best detect VLFEs because their energy output is concentrated in this very low frequency band., for analyses in the context of other slow earthquake, this research includes automatically generated tremor data from the Pacific Northwest Seismic Network (PNSN) [Wech, 2010]. This study covers the time span of September 1, 2011 – October 1, 2014 to cover the time period between the 2011 and 2014 ETS events, which have both been studied in detail for VLFE activity, particularly with respect to tremor [Ghosh *et al.*, 2015; Hutchison and Ghosh, 2016]. This study covers two ETS periods and several inter-ETS periods.

6.3.2 Methods

Similar to previous studies in Cascadia [Ghosh *et al.*, 2015; Hutchison and Ghosh, 2016] and Japan [Ito *et al.*, 2007], this study employs a grid search centroid moment tensor inversion method. The study area, which stretches from 124.5° W to 122° W and 47° N to 49° N is divided into a 0.1° x 0.1° grid horizontally and every 5 km laterally. Using a

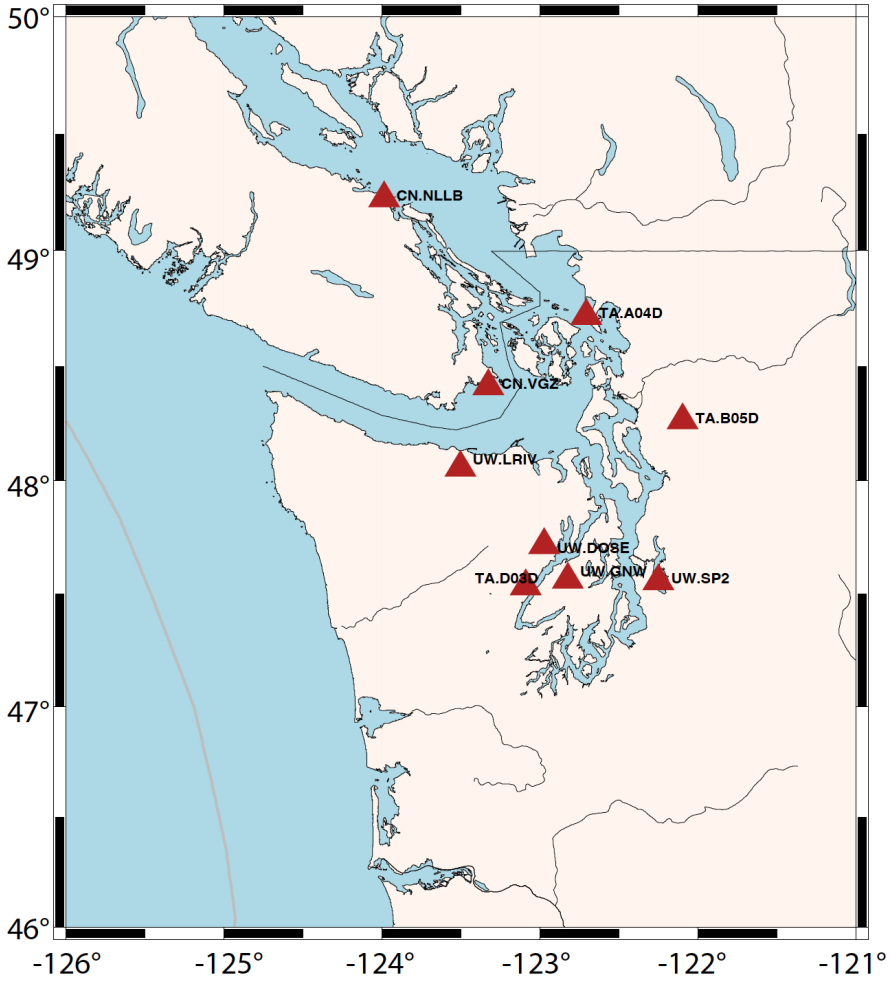

Figure 6.1: The Puget Sound region of the Cascadia subduction zone is shown here. The seismic stations used in this study are given by red triangles.

laterally homogenous velocity model for the region [Crosson, 1976], synthetic waveforms are calculated from each grid node to each station using a convolution of a delta function with Earth's structural response and a source time function. Real broadband seismograms are compared to the synthetic data and for each time window, only the value with the highest variance reduction (VR) (i.e. the best match between real and synthetic seismograms) is recorded. As VLFEs in Cascadia are tend to have a signal duration of 90s [Hutchison

and Ghosh, 2016; Ghosh *et al.*, 2015], we use a sliding time window of that duration and recalculate the centroid moment tensor inversion every 1 s. The results include location, depth, strike, dip, rake, variance reduction, compensated linear vector dipole (CLVD), moment tensor and a focal mechanism. Typically, only VLFEs that are reproducible with multiple station configurations that also do not conflict with local, regional, or teleseismic events are added to the catalog. However, this is a timely process that was not completed for every VLFE in this catalog. Therefore, only the VLFEs for the ETS periods and inter-ETS events discussed in this dissertation have been confirmed to this extent. Additionally, all events that occurred along the edge of the moment tensor inversion grid are removed. A more conservative catalog will be established at a later date. For all of the moment tensor inversion solutions, please see the electronic supplement. For cross-referencing the earthquake catalog, we utilize the Advanced National Seismic System (ANSS) earthquake catalog. For earthquakes after December 31, 2012, we reference the ANSS ComCat Catalog available through the United States Geological Survey.

Typically, manual inspection of the results is required, however for this study the code was somewhat modified for more effective review of results. The code was modified to automatically generate figures for all time windows with high values for variance reduction and low CLVD values and to record all time windows fitting predetermined criteria for VR and CLVD. This allows for faster and easier processing. Since VLFEs are expected to occur along the plate interface [Ide *et al.*, 2007], having a figure with the focal mechanism readily available aids in faster determination of whether a candidate event is indeed a VLFE.

6.4 Results

This robust catalog for the Puget Sound region contains data from September 1, 2011 through October 1, 2014. The dataset contains two ETS events: the 2012 ETS event, which lasts from August 30, 2012 – October 10, 2012, and the 2013 ETS event, which occurs from September 7, 2013 – October 8, 2013 as defined by tremor activity automatically collected by PNSN [Wech, 2010]. As noted in previous studies observing VLFEs in Cascadia, there is an overall increase in VLFE activity during ETS events [Hutchison and Ghosh, 2016; Ghosh *et al.*, 2015]. There are thus multiple periods to make observations of inter-ETS period VLFE activity, for which there is currently little observation in Cascadia. This study shows sustained VLFE activity throughout the inter-ETS periods. There are some VLFE bursts associated with tremor, though their occurrence is not consistently spatiotemporally coincident with the tremor. Additionally, VLFEs also occur throughout the ETS event without relation to tremor (figure 6.2). In total, we observe more than 450 new VLFEs, with 373 occurring during the inter-ETS periods.

The most novel findings of this observational experiment involve inter-ETS VLFE detections. Here we find multiple examples of VLFE without tremor, but also examples of inter-ETS tremor bursts that are quasi-spatiotemporally coincident with tremor. The first instance of this begins on December 18, 2011 and continues through December 31, 2011 including both tremor and VLFE activity. During this first instance of tremor, there is a clear burst of tremor activity that occurs in central Vancouver Island and several events that occur off the southeastern edge of Vancouver Island. When observing the relationship between the geographic center of the VLFE events and the tremor that occurs within a

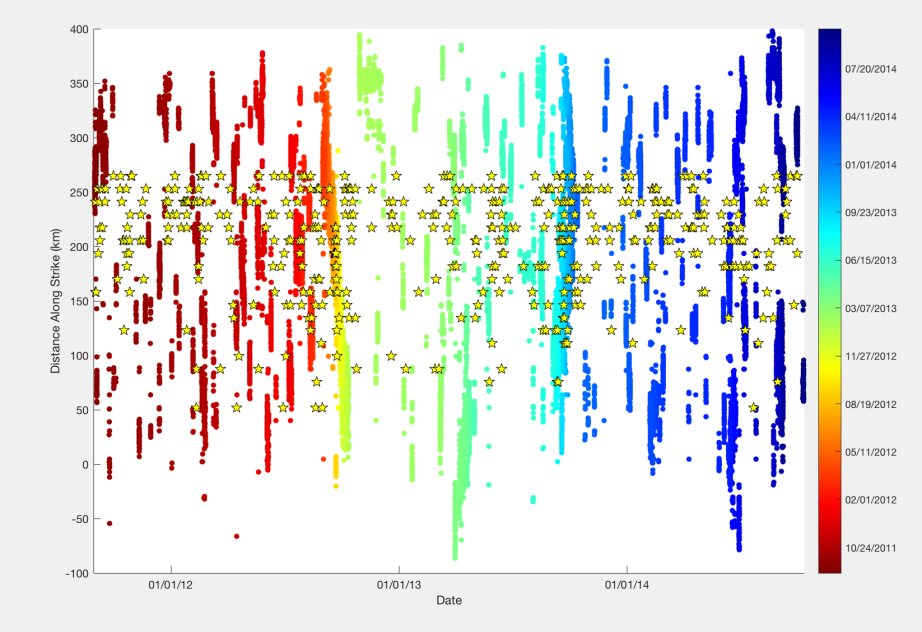

Figure 6.2: The colored dots represent tremor plotted along strike versus time. Their color also corresponds to time (see colorbar on right). VLFEs are plotted in yellow stars.

100 km radius, there is not much of a relationship to be established. However, if that radius is expanded to 200 km, there begins to be a clear temporal relationship between the tremor activity and the VLFEs (figure 6.3). This implies a temporal relationship, but not necessarily a close spatial relationship.

The second time this is observed is in February 2012. During this inter-ETS tremor, there are several short bursts of tremor between February 2, 2012 and February 13, 2012. There are a number of VLFEs as well that occur within, and after this period (until February 18) at a similar location along strike. Including both VLFEs and tremor, this inter-ETS event lasts from February 2, 2012 – February 19, 2012. Curiously, while the VLFEs are occurring spatially in a similar location, they seem to occur in the temporal gap when there is no tremor occurring and after the tremor activity shuts off in the region

(figure 6.4, figure 6.5). In other words, sometimes there is a temporal correlation without a spatial one and other times there is a temporal correlation without a spatial correlation.

Some VLFEs occur during the inter-ETS period and are not associated with any tremor. These events tend to have equally high variance reduction to the other VLFEs and focal mechanisms that also suggest a source location of the plate interface (e.g. figure 6.6). Many of the inter-ETS VLFEs are centroid moment tensor solutions are quite similar to the ETS VLFE solutions in that they occur in similar locations and have high variance reductions. One qualitatively noticeable difference is that the inter-ETS VLFEs tend to have higher CLVD values. A future statistical analysis may help to quantify this difference and understand possible reasons for such a difference. It also appears the inter-ETS VLFEs have higher magnitudes, though this is also worth a deeper quantitative investigation that this dissertation does not allow time for.

During the 2012 ETS event, tremor migrates unilaterally along strike, which is a typical feature of tremor during ETS events. VLFE, however, does not appear to have a specific migration pattern or relationship with respect to tremor. There are small gaps in the tremor activity towards the end of the ETS, however, when VLFE activity occurs in a different section of the subduction zone. This VLFE activity, though, occurs where tremor has previously migrated along strike during the same ETS event (figure 6.7). This can be observed towards the end of the ETS event when there are two brief interuptions in tremor activity during the first week of October and at the end of the ETS event. There is also some scattered VLFE activity prior to the onset of ETS event, which temporally does not

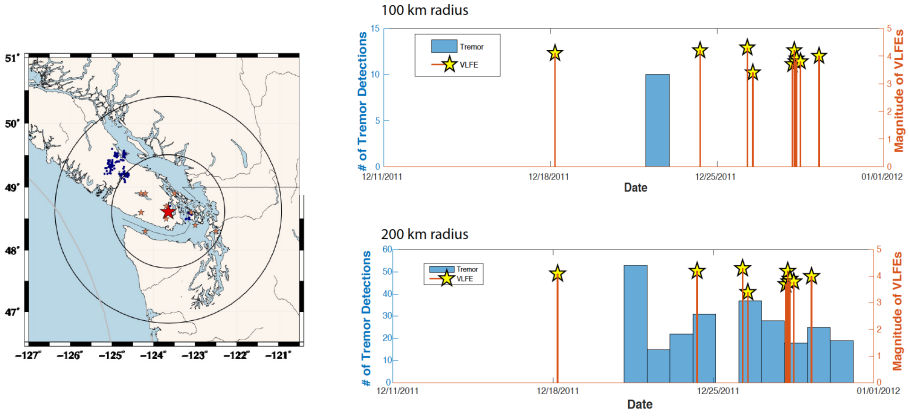

Figure 6.3: The map on the left gives tremor from this tremor burst, which begins on December 21, 2011 and continues through December 30, 2011, in navy blue dots, VLFE in orange stars and the geographic center of the VLFEs. There is a 100 km radius circle around the center of the VLFE and a 200 km radius circle. On the right,are two time series plots showing tremor within the two contours (light blue) and VLFEs (yellow stars) with their magnitudes) versus time. The top panel corresponds to the tremor (light blue) within a 100km radius of the geographic center of the VLFEs and the bottom panel represents at 200km radius from the geographic center of the VLFEs. This plot indicates that there is a temporal relationship between VLFEs and tremor in this instance, but not necessarily a spatial one

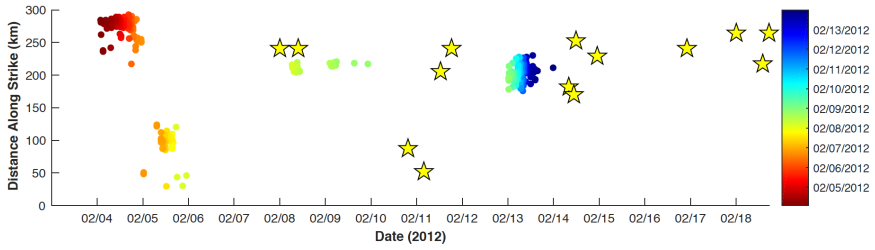

Figure 6.4: The x-axis is time and the y-axis is distance along strike. Tremor is plotted in points and the color also represents time (see colorbar at right). VLFEs are plotted in yellow stars. During this inter-ETS tremor burst, there is VLFE occurring nearly in the same location along strike, but it is occurring in the temporal gaps when there is no VLFE occurring

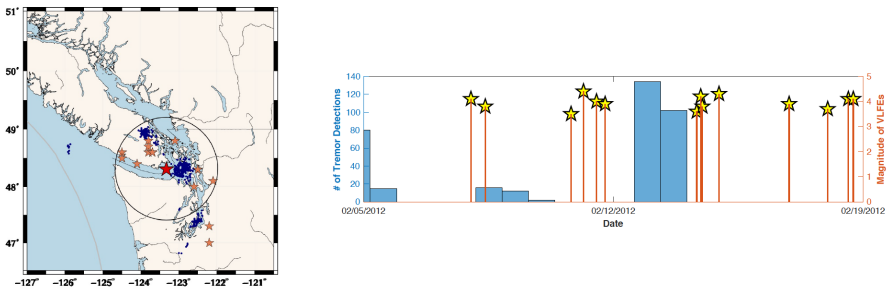

Figure 6.5: Left) A map giving the geographic center (red star) of VLFE activity (orange stars) during an inter-ETS event tremor (blue) burst from February 5, 2012 - February 14, 2012. A 100 km radius is drawn around the center of the VLFE activity. Right) A time series showing the tremor (blue) and VLFEs and their respective magnitude (red with yellow stars). As a general observation, VLFEs occur in the time gap within the tremor burst and after it ends.

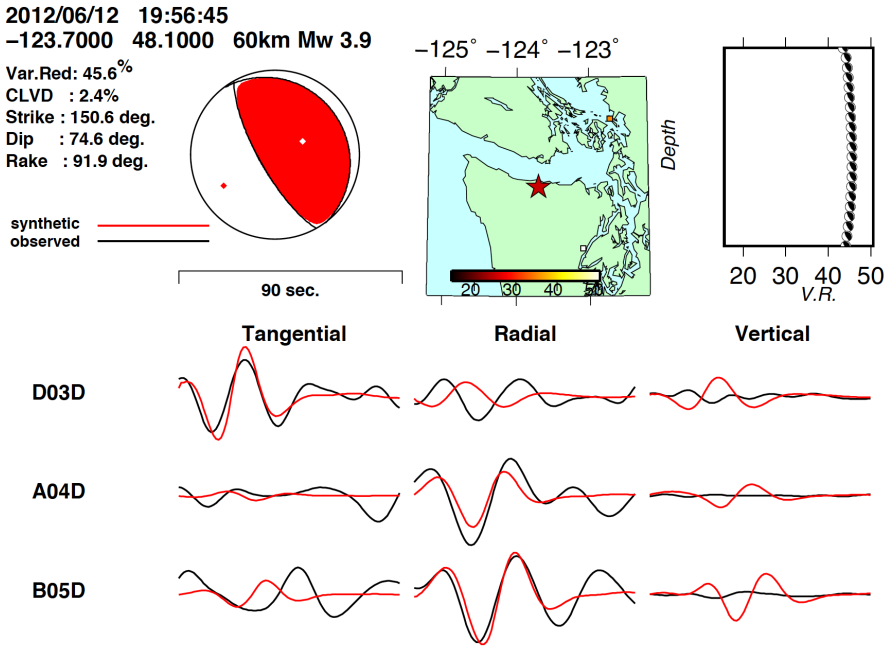

Figure 6.6: An inter-ETS VLFE centroid moment tensor solution. There is high variance reduction, low CLVD, and the location is similar to some VLFEs detected during ETS events (see fig. 6.8)

appear to have a specific pattern, though spatially these events span the section, along-strike, that will slip during the ETS event. Most of the VLFEs during this ETS event have

high variance reduction and occur in a similar region and are detected on most stations, particularly in the middle of the ETS event (figure 6.8)

The temporal distribution of VLFEs during this ETS event are also notable in that they cluster towards the middle of the ETS and again at the end of the events. There are a large number of events at the middle of the event and relatively few between the middle and the end. Moreover, the peak VLFE activity occurs with peak tremor activity (figure 6.9).

The behavior in this ETS event is unique in that, unlike the majority of ETS events where tremor migrates unilaterally along strike, the tectonic tremor migrates along strike such that is begins independently in multiple locations, convering towards a single location where VLFE is occuring throughout the ETS [Wech, 2010]. The VLFE activity primarily migrates spatiotemporally with the tremor in both directions, but also sometimes occurs outside of the tremor region (figure 6.10). Unlike the 2012 and 2014 ETS events [Hutchison and Ghosh, 2016], where VLFE activity is clustered in discrete parts of the ETS event, the VLFE activity is more evenly distributed throughout the ETS event as it is during the 2011 ETS event (figure 6.11) [Ghosh *et al.*, 2015].

6.5 Discussion

The VLFEs during the 2013 ETS event, for the most part, migrate spatiotemporally with tremor. This is a widely observed relationship that has been seen in Cascadia

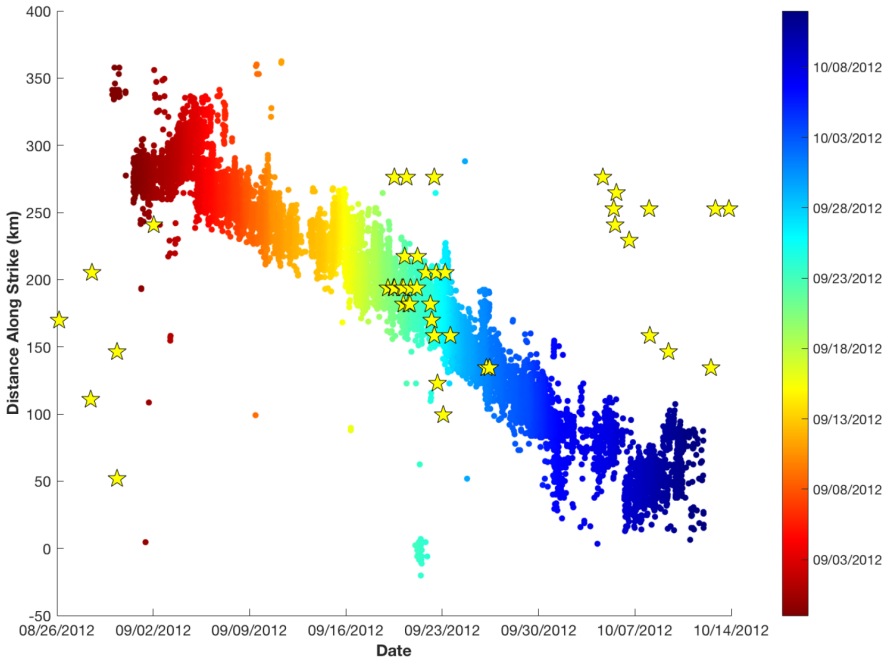

Figure 6.7: The x-axis is time and the y-axis is distance along strike. Tremor is plotted in points and the color also represents time (see colorbar at right). VLFEs are plotted in yellow stars. Here, tremor clearly migrates unilaterally, however, VLFE spatially tends to occur across the entire margin where tremor occurs without a specific migration pattern.

[Ghosh *et al.*, 2015], Costa Rica [Walter *et al.*, 2013], and Japan – even linking up-dip VLFE and down-dip tremor [Hirose *et al.*, 2010]. This near ubiquitous observation might lead to interpretations about non-uniqueness with respect to the source properties of these events. For example, one possible interpretation might be that both events have the same source patches with the same rupture mechanisms – such as the passage of slow slip [Hirose *et al.*, 2010] – or even that VLFE is an artificial artifact caused by filtering tremor in a very low frequency band [Gomberg *et al.*, 2016]. These conclusions, however, are likely incorrect as this catalog amongst other observations show discrete locations for tremor and VLFE both during ETS events and during the inter-ETS period.

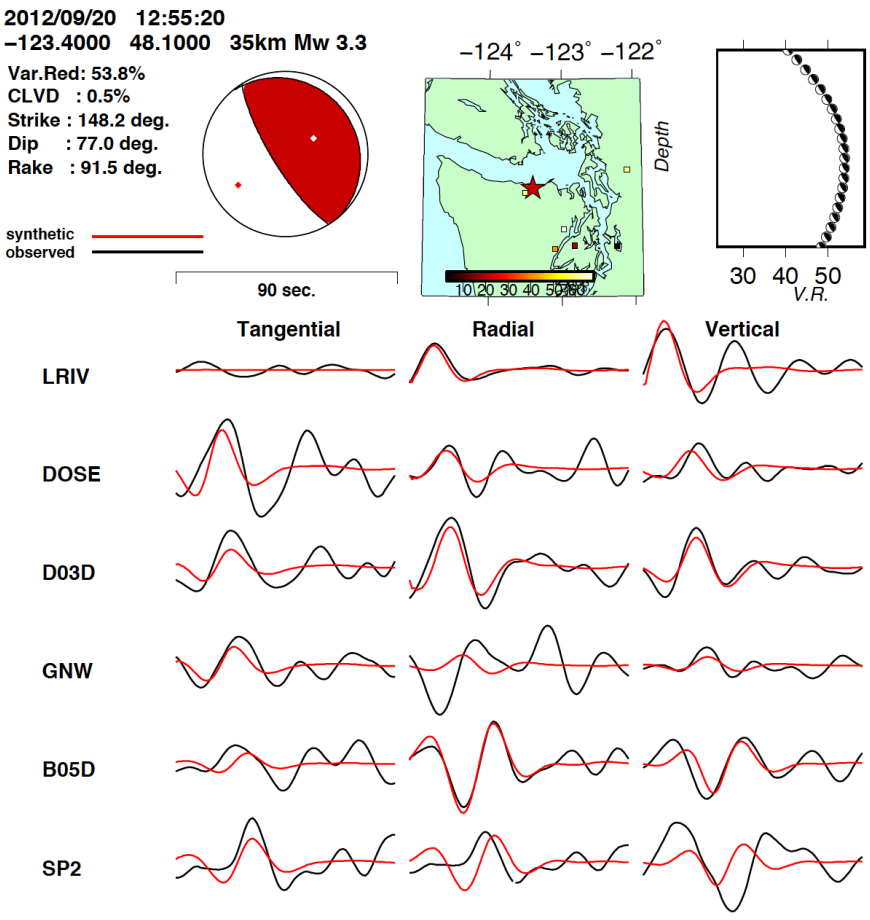

Figure 6.8: The centroid moment tensor inversion solution gives a focal mechanism that is consistent with the plate interface. It also has a high variance reduction and low CLVD. Many of the VLFEs during this ETS event, particuarly during the peak of tremor activity are very similar to this solution

The VLFEs during the 2012 ETS, curiously, display behavioral elements of both the 2011 ETS event and the 2014 ETS event. VLFEs are consistent with tremor in the spatiotemporally consistent with tremor during the peak of tremor activity, but there are long periods where there are no VLFEs. As noted, there are several short gaps in tremor activity during the 2012 ETS event, when VLFEs occur along strike in locations where tremor has previously occurred during the towards the end of the ETS event (figure 6.7).

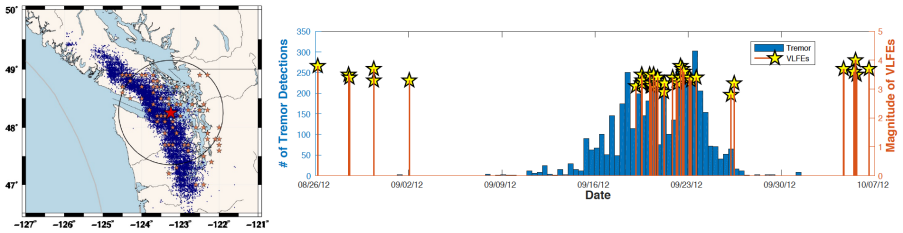

Figure 6.9: Left) A map giving the geographic center (red star) of VLFE activity (orange stars) during an inter-ETS event tremor (blue) burst from February 5, 2012 - February 14, 2012. A 100 km radius is drawn around the center of the VLFE activity. Right) A time series showing the tremor (blue) and VLFEs and their respective magnitude (red with yellow stars). The majority of VLFEs occur during the peak of tremor, a relationship that is consistent with many past studies showing a close spatiotemporal relationship between VLFEs and tremor

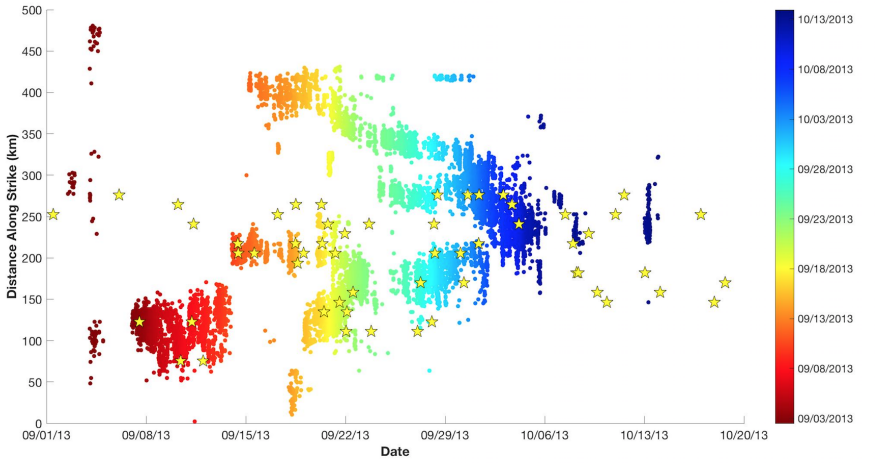

Figure 6.10: The x-axis is time and the y-axis is distance along strike. Tremor is plotted in points and the color also represents time (see colorbar at right). VLFEs are plotted in yellow stars. This is a unique ETS event in that tremor appears in multiple locations independently and converges towards a single locations around where the VLFE occurs throughout the ETS event. VLFEs are somewhat spatiotemporally coincident with tremor, but at times they have a quasi-spatiotemporally coincident relationship with tremor

Interestingly, these particular VLFEs at the end of the 2012 ETS event occur during a period when tremor is not occurring, activity is significantly decreased, or after tremor has shut off. One interpretation of this result is that it represents a delayed redistribution of stress. The

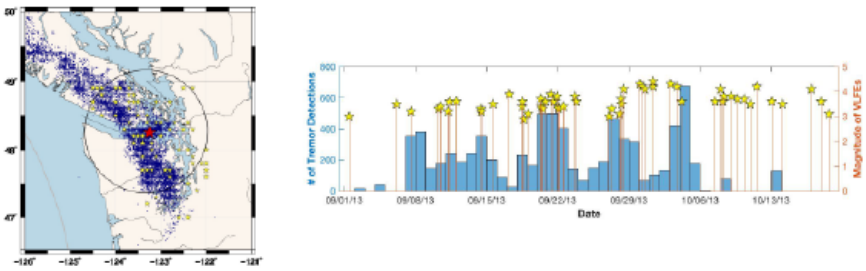

Figure 6.11: Left) A map giving the geographic center (red star) of VLFE activity (yellow stars) during the 2013 ETS event tremor (blue). A 100 km radius is drawn around the center of the VLFE activity. Right) A time series showing the tremor (blue) and VLFEs and their respective magnitude (red with yellow stars). The VLFEs occur consistently throughout the duration of tremor activity during the ETS events, behavior consistent with many previous findings where VLFE and tremor behavior mirror each other.

asperities responsible for VLFE generation following the passage of tremor through that particular segment of the plate interface likely required a different yield stress to rupture as a result of (or a combination of) one of the following features: fault geometry, mechanical properties, or local stresses. The quasi-spatiotemporal coincidence of tremor and VLFE (as opposed to a clear relationship in space and time) led to a similar conclusion regarding the delayed rupture of asperities during the 2014 ETS event [Hutchison and Ghosh, 2014]. One other possible explanation is that perhaps it is possible that the tremor and slow slip, which occurred earlier in the ETS event left a static stress change in its wake that resulted in post-slow earthquake deformation accommodated by VLFEs.

VLFEs were observed before and after the 2011 Tohoku earthquake in the Japan Trench. One cluster of VLFEs was observed before the event near the center of the rupture patch, but following the event, there were two clusters, one on either end of the rupture that were interpreted to be correlated to postseismic stress redistribution processes [Matzusawa

et al., 2015]. In cases where tremor, or a slow-slip transient has already passed through a region, it is possible that VLFEs may be a manifestation of or response to the longer-term stress redistribution process that can occur during or after a seismic event (or creep event, SSE, etc.). Thus, through this interpretation, the VLFEs that are quasi-spatiotemporally coincident with tremor may reflect just that: post- or co-slow earthquake redistributions of stress. I refrain from using the terms "coseismic" and "post-seismic" as slow earthquakes do not always produce seismic energy.

Sometimes, it seems that the onset of VLFEs is delayed, or occurs in temporal gaps with respect to tremor, as is the case in the inter-ETS period in February 2012 and the 2014 ETS event [Hutchison and Ghosh, 2016]. Significantly, at times VLFEs occur while there is an indication that other slip processes are occurring in the transition zone (i.e. tremor), though, not necessarily in the same place as VLFE. This relationship has even been observed both with up-dip VLFE and down-dip tremor indicating that there is an along-dip process relating these transient events [Hirose *et al.*, 2010]. It is also observed along strike several times during the inter-ETS periods in this study. For example, during the December 2011 inter-ETS tremor/VLFE burst, VLFE occurs simultaneously with tremor, though the majority of tremor occurs 100-200 km away from the geographic center of the VLFE source locations. These observations suggest that there is an along strike process that is occurring linking the two types of seismic slow earthquakes. It is possible that if the tremor activity alone is causing enough of a change in the static stress field that the VLFEs are a response to such stress perturbations, though given the magnitude of tremor alone and the distance of these VLFEs, this seems unlikely. A more logical scenario is that there are

small underlying SSEs occurring that are driving deep creep which in turn results in these quasi-spatiotemporally rupture patterns for VLFEs and tremors. In this case, such inter-ETS periods that include tremor and VLFE may instead be deemed "mini-ETS" events, where small SSEs are likely occurring episodically and driving the seismic manifestations of slow-slip, such as tremor and VLFE. Using a rate- and state- dependent friction earthquake modeling system, RSQSim, it was showing that small magnitude SSEs ($<M_w$ 5.6) have a scattered distribution along strike, as opposed to a coherent and connected rupture pattern like that of larger SSEs and ETS events [Colella *et al.*, 2011]. Such small SSEs would be near impossible to detect geodetically. However, decomposition of interaseismic GPS data from Northern Cascadia and Guerrero, Mexico showed small SSEs occurring during the inter-ETS period [Frank, 2016]. The time windows of the inter-ETS VLFEs contained in this three year catalog coincide, though often quasi-spatiotemporally, with inter-ETS tremor bursts, indicating a correlation between the tremor and the VLFEs, thus opening the door to a potential relationship between the VLFEs and the inter-ETS SSEs. The fact that high fault slip rates tend to correspond to the appearance of tremor also supports that fact that inter-ETS SSEs are likely responsible for inter-ETS tremor and VLFE bursts, or "mini-ETS" events [e.g. Bartlow *et al.*, 2009; Wech and Bartlow, 2014].

If indeed these "mini-ETS events" are scattered incoherent SSEs occurring along strike in a similar time period, it requires a further investigation of the accuracy of the linear moment rate empirically derived scaling properties of slow earthquakes [Ide *et al.*, 2007] that suggest an apparent linear relationship between duration, T, and moment. The RSQSim model results show a moment proportional to $T^{1.5}$ for events smaller than M_w 5.6,

and a moment proportional to T^2 for events greater than M_w 5.6. It is further shown that these particular values for moment rate scaling fit the Ide *et al.*, [2007] values of ETS events and SSEs, but not necessarily the seismic expressions of these events. Peng and Gomberg, [2010] propose an alternative to the empirical slow earthquake scaling relationship that entails a continuum of slip between those of regular earthquakes and what is shown in the slow earthquake scaling relationship, which include other types of slow-slip including glacial tremor and gravity driven landslides. These inter-ETS observations of "mini-ETS" events support the occurrence of small SSEs driving their seismic slow earthquake counterparts. Perhaps as SSE magnitude increases, its characteristic moment to duration ratio changes such that a larger moment corresponds to shorter duration. For small magnitude SSEs, it is at this point impossible to resolve this empirically, particularly since these events are scattered along strike and each individual event may have its own moment rate. Nonetheless, the observation of "mini-ETS" events supports the idea of a slip continuum where these events may actually begin to populate the void between regular earthquakes and slow earthquakes. Further, "mini-ETS" events support the notion of discrete aseismic slow earthquake processes driving the seismic processes, an observation supported by several studies, but that is extremely difficult to resolve given current instrumentation and observational methods [Fukada *et al.*, 2008; Obara and Kazigushe, 2010].

The difference in distribution of VLFEs during the ETS and inter-ETS periods is notable. VLFEs during the inter-ETS periods tend to occur further up-dip than the ETS VLFEs (figure 6.12), though the sample size here is limited to several ETS and inter-ETS events. This observation is inconsistent with tremor activity observed during ETS versus

inter-ETS periods, though the interpretation remains elusive and the sample size small [Wech *et al.*, 2009]. This further serves to support that an underlying process (i.e. an SSE) is occurring in discrete locations during both the ETS and inter-ETS periods linking tremor and VLFE. It should be considered, however, that these processes may be serving to transfer stress in a different direction during the inter-ETS period. The actual direction of stress loading during this period remains to be determined. "Mini-ETS" events may serve to relieve excess stress not released during large ETS events, or they may be relieving stress in the direction of subduction. Without additional geodetic data, this is difficult to constrain. If it is determined they are loading the locked zone, they may have implications in seismic hazard assessment.

The quasi-spatiotemporal relationship between the tremor and the VLFE during inter-ETS activity plays an important role in establishing the underlying role of SSEs. The fact that these events are often occurring quasi-contemporaneously or nearly in the same place, but not the exact same place would indicate distinct source locations, but an underlying process linking these discrete types of events. An SSE can affect a large region, or scattered patches along strike [Colella *et al.*, 2011] potentially causing many VLFE and tremor patches to slip within a close time window, causing distinctive rupture patterns based on unique fault geometries, frictional properties and geologic characteristics [e.g. Shelly, 2010].

LFEs, the smallest of the slow earthquakes according to the linear moment scaling law [Ide at al., 2007], are thought to be driven by aseismic slow-slip [Shelly *et al.*, 2006] and many LFEs compose tremor. VLFEs are also likely driven by slow-slip given their indepen-

dence from tremor during ETS events, such as during the 2014 ETS event [Hutchison and Ghosh, 2016]. Repeatedly, and on multiple scales within the framework of the slow earthquake scaling relationship, seismic slow earthquakes seem driven by slow-slip, as though they are "mini"-ETS events. Inter-ETS activity manifested by tremor, small SSEs and now VLFE can confirm that there are ongoing processes uniting the slow earthquake, or gray area, of the slip spectrum. Ultimately, everything within the slow earthquake spectrum seems tied together by slow slip and exists on a continuum, with distinctive characteristics of asperities dictating the seismic outputs from the slow slip transient. The real importance of the inter-ETS VLFEs is that they provide evidence for ongoing slow earthquake activity beyond the typical ETS, indicating that there is likely slow slip occurring much more frequently than previously thought. These findings help tie together other work showing inter-ETS slow earthquake activity such as inter-ETS tremor [Wech *et al.*, 2009], and interaseismic SSEs [Frank, 2016; Rouet-Leduc *et al.*, 2018], and the predicted behavior of small SSEs based on rate- and state- friction [Colella *et al.*, 2011].

It is widely thought that tremor is a good proxy for SSEs, but an increasing number of studies are suggesting that actually SSEs can occur without tremor [Wech and Bartlow, 2014; Hutchison and Ghosh, in revision]. During a large tremor-genic slow earthquake, tremor stops during decreased slip speeds and picks up again as the slip rate increases. Hawthorne and Rubin, [2013] found that during ETS events, higher slip amplitudes corresponded to higher rates of seismicity – indicating that while seismicity may indicate slow-slip, it is not a requirement. Again, these are further evidence that seismic slow earthquakes are slow-slip driven processes, but it remains unclear what exactly causes one type

of seismic slow earthquake as opposed to another. Another lingering problem is how best to constrain a largely aseismic process in the absence of a consistent proxy or a reliable observational method for discerning such small aseismic events at depth.

One possible solution for explaining why slow-slip may result in discrete seismic behaviors at different times is that the same asperities are responsible for generating VLFEs and tremor, but that the type of signal they produce is dependent on the slip rate as the slip front passes through. A possible mechanism that might describe such a hypothesis is that the presence or migration of fluids can increase the effective normal stress, and can weaken the strength of the fault, making it more susceptible to slip [Szelgia *et al.*, 2004] and that may itself be dictated or controlled by SSEs. This may also explain why at different times, depending on the presence of fluids, the same asperities may display discrete seismic and aseismic behaviors.

6.6 Conclusions and Future Research

The research contained herein analyzes a three year catalog of VLFE activity in Cascadia between the 2011 and 2014 ETS events using grid-search centroid moment tensor inversion. During the ETS events, VLFE behaves both spatiotemporally with tremor and also quasi-spatiotemporally with tremor. This catalog also confirms the existence of inter-ETS VLFEs. Some of these events are spurious while others are quasi-correlated to inter-ETS tremor. The fact that VLFEs can behave either spatiotemporally coincidentally, quasi-coincidentally, or not coincidentally with tremor indicates that they have discrete source mechanisms, but not necessarily discrete source locations, as some VLFEs occur in

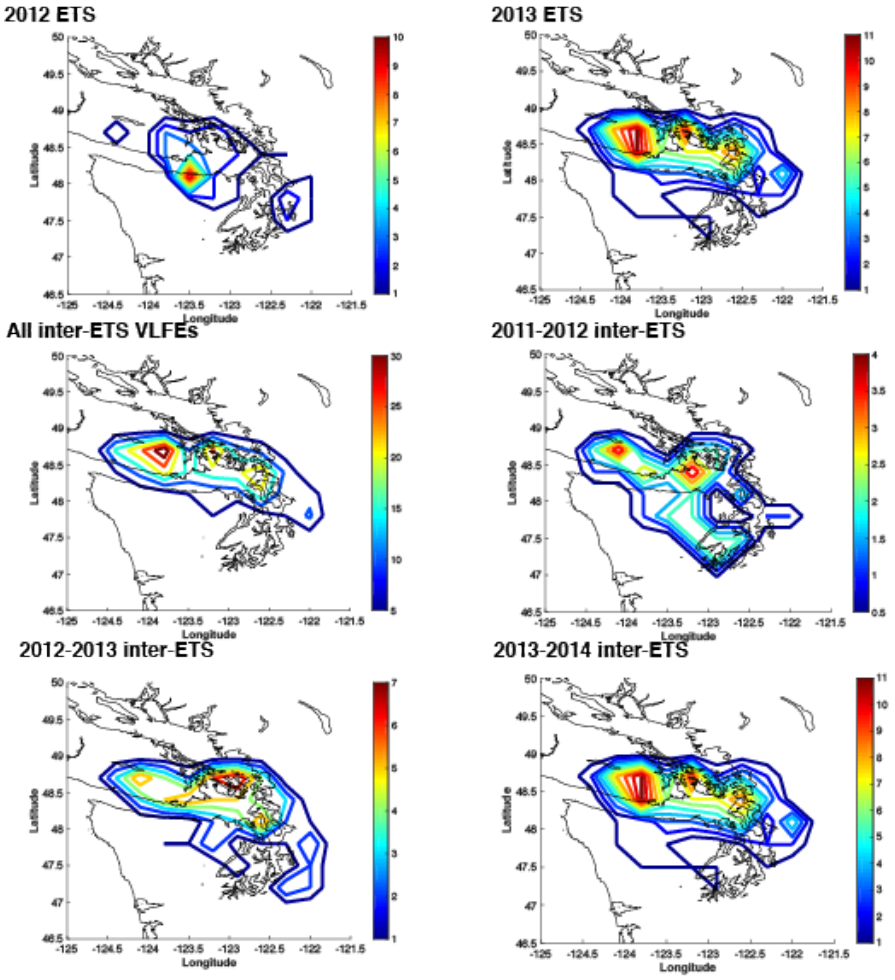

Figure 6.12: Each of these plots gives contours for the number of VLFEs in a 0.3 x 0.3 degree region. The ETS events tend to have more activity down-dip than the inter-ETS periods. A significant number of inter-ETS VLFE actvity is concentrated at the southern tip of Vancouver Island. These findings show a distinct difference between inter-ETS VLFE locations and ETS VLFE locations indicating that they may be part of distinct stress transfer processes.

locations where tremor occurs. Due to the fact that some interaseismic SSEs have been observed in Cascadia [Frank, 2016], despite their small size, we propose that inter-ETS VLFEs are likely a manifestation of slow-slip activity in the transition zone. This is also consistent with rate- and state- friction based models of small SSEs in Cascadia [Colella *et al.*, 2011]. The quasi-coincidental bursts of VLFEs and tremor during inter-ETS periods can

be considered "mini-ETS" events, filling in the gap in the slow earthquake scaling law [Ide *et al.*, 2007]. Further, we hypothesize that slow-slip is the primary driving mechanism behind all observable activity described in the slow earthquake scaling law study [Ide *et al.*, 2007] suggesting that moment rate for slow versus regular earthquake is actually a continuum as opposed to a linear versus cubic (respectively) relationship.

It would be useful to use all of the events in this catalog as template events to generate a more comprehensive catalog for the region using matched filter analysis [e.g. Shelly *et al.*, 2007]. This method has been successfully applied to the region by Ide *et al.*, [2016] using stacked tremor time windows and filtering them between a 20-50 s period band to generate template events. VLFEs were identified across the entire subduction margin. Template events from 13 years of VLFE cataloging in Shikoku, Japan also yielded promising matched filter results, revealing a correlation between long term SSEs and VLFEs [Baba *et al.*, 2018; Matzusawa *et al.*, 2015].

Finally, a deeper comparison between inter-ETS VLFE and tremor activity versus ETS VLFE and tremor may help elucidate the role of each other these events. GPS activity during ETS events indicates that the activity during these periods in the transition zone is loading stress onto the locked zone, but an analysis to determine if mini-ETS play the same role would be important to deepen our understanding of plate mechanics and the role of slow earthquakes in the greater earthquake cycle. An analysis of slip rate distribution versus VLFE and tremor activity may also reveal a relationship between slip rate and seismic manifestations of slow slip.

It should be noted that given the findings of Tape *et al.*, [2018], where a VLFE was

found on a non-plate boundary fault line, which spatiotemporally preceded an earthquake, it is possible that a number of other VLFEs occurred in this region that were not included in this catalog. The generation of this catalog explicitly looked for events that were occurring on the plate interface and were thus limited to focal mechanisms that fit the regional tectonic setting. Further investigation should be conducted to examine VLFEs on other faults in the region, and perhaps if even VLFEs included in this catalog may occur on subfaults close to the plate interface.

Chapter 7

Conclusions

7.1 Conclusion

The entire center of the slip spectrum remains largely unexplored. There are still many things that we know we don't know, and surely more things that we don't know that we don't know (to paraphrase Donald Rumsfeld). This dissertation, with several case studies, provides only a minor look at observations that might help ascertain information about the mechanics driving this enigmatic transient fault behavior. These studies alone cannot provide any direct insights into the relationship between slow earthquakes and regular earthquakes. They do, however, if analyzed from a second order perspective, have a common theme: the underlying role of deep creep and slow-slip being an ever-present factor in these seismic phenomena (VLFEs, tremor, triggered foreshock sequences, etc.). Before any of my research was conducted, there has been abundant evidence that that slow-slip and deep creep are at the very least coincident with the seismic varieties of slow earthquakes [Rogers and Dragert, 2003; Wech *et al.*, 2012; Bartlow *et al.*, 2011; Ide *et al.*, 2007; Obara

et al., 2004; Shelly, 2009; Beroza and Ide, 2011]. This dissertation provides additional evidence that the seismic kinds of slow earthquakes (and microseismic events) are likely a product of slow slip. That is to say, seismic slow earthquakes require slow slip and are not necessarily related to each other, but slow slip does not mandate seismic manifestations. This is especially true based on the observations of the relationships of VLFE to tremor and SSEs in Cascadia, though the studies in the Anza Gap also help suggest this possibility as well.

The observation of tremor alone in the Anza Gap can merely reveal the fact that this region can behave within the transitional regime of the slip spectrum. In the greater context of the studies in the region, however, we see a reason that tremor may be generated. Increasingly, studies in this region have identified slow-slip [Inbal *et al.*, 2017], and have provided ample evidence for deep creep [Lindsay *et al.*, 2014; Jiang and Fialko, 2016; Meng and Peng, 2016]. Further studies with geodetic data and more comprehensive tremor catalogs would help elucidate this relationship in the region. The onslaught of diverse seismic events preceding the Borrego earthquake on June 10, 2016, though, indicate some process occurring at depth, perhaps as a result of dynamic triggering from teleseismic energy. Triggered creep events have been proposed as a triggering mechanism for earthquakes and tremor [Shelly *et al.*, 2011], both of which were observed in this context and are heavily supported with observational evidence. Again, in the context of the literature, the observations of non-end member seismic activity in this region seems reliant, or at the very least, heavily correlated to deep creep and slow-slip.

In Cascadia, there is substantial evidence that all seismic types of slow earthquakes

are related directly to SSEs, but not necessarily to each other. Both the 2011 and 2014 ETS events show a close relationship between VLFEs and SSEs. Moreover, tremor and VLFE consistently fall within the SSE time frame, but in 2014 there is not a direct relationship between tremor and VLFE. This would logically, granted based on a small sample size, indicate that SSEs may dictate both these events, though independently. Furthermore, if a seismic slow earthquake is indeed a rate weakening patch within a slowly moving rate strengthening background, it also follows different patches may rupture at different times based on their physical, or frictional properties as an SSE transient passes through. We also must consider the role of fluids and that slow earthquakes may manifest fluid transport and dehydration processes. Examining the 3 year VLFE catalog in the final chapter of this thesis, the variety of VLFE activity in the ETS and inter-ETS period could all be interpreted as various manifestations of SSEs of various sizes, filling in the "empty part" of the slow earthquake scaling law [Ide *et al.*, 2007]. This interpretation may be further supported by rate- and state- friction based models of slow earthquakes, from an earthquake simulator, RSQSim, that shows that SSEs below M_w 5.6 tend to rupture in incoherent patches along strike [Colella *et al.*, 2011]. These models are consistent with observations with bursts of tremor and VLFE activity during the inter-ETS periods that here I term "mini-ETS" events.

A separate study also found VLFEs clustered on either end of the 2011 M_w 9.0 Tohoku rupture patch after the main shock, suggesting that they may be associated with postseismic relaxation and stress redistribution. This may also be true for VLFEs during and after SSEs. VLFEs may, at times, represent redistributions of stress with response to surrounding VLFE activity, and might explain why they can occur at times in spatial and

temporal gaps when there is no tremor.

Ultimately, there is still much to be explored within the "gray area" of the slip spectrum in terms of moment scaling laws and physical source properties. These studies, though, are beginning to elucidate that fact that while these events may exhibit distinctive observational properties, the studies contained within this dissertation suggest that they are all essentially some scaled version of an ETS event and moreover, that these events of different magnitudes are happening all the time.

Bibliography

Aguiar, A. C., T. I. Melbourne, and C. W. Scrivner (2009). Moment release rate of cascadia tremor constrained by gps. Journal of Geophysical Research: Solid Earth 114(B7).

Allam, A. and Y. Ben-Zion (2012). Seismic velocity structures in the southern california plate-boundary environment from double-difference tomography. Geophysical Journal International 190(2), 1181–1196.

Anooshehpoor, A. and J. N. Brune (2001). Quasi-static slip-rate shielding by locked and creeping zones as an explanation for small repeating earthquakes at parkfield. Bulletin of the Seismological Society of America 91(2), 401–403.

Asano, Y., K. Obara, and Y. Ito (2008). Spatiotemporal distribution of very-low frequency earthquakes in tokachi-oki near the junction of the kuril and japan trenches revealed by using array signal processing. Earth, Planets and Space 60(8), 871–875.

Baba, S., A. Takeo, K. Obara, A. Kato, T. Maeda, and T. Matsuzawa (2018). Temporal activity modulation of deep very low frequency earthquakes in shikoku, southwest japan. Geophysical Research Letters 45(2), 733–738.

Bartlow, N. M., S. Miyazaki, A. M. Bradley, and P. Segall (2011). Space-time correla-

tion of slip and tremor during the 2009 cascadia slow slip event. Geophysical Research Letters 38(18).

Beroza, G. C. and S. Ide (2011). Slow earthquakes and nonvolcanic tremor. Annual review of Earth and planetary sciences 39, 271–296.

Bostock, M., A. Royer, E. Hearn, and S. Peacock (2012). Low frequency earthquakes below southern vancouver island. Geochemistry, Geophysics, Geosystems 13(11).

Bouchon, M., H. Karabulut, M. Aktar, S. Özalaybey, J. Schmittbuhl, and M.-P. Bouin (2011). Extended nucleation of the 1999 mw 7.6 izmit earthquake. science 331(6019), 877–880.

Brodsky, E. E. and N. J. van der Elst (2014). The uses of dynamic earthquake triggering. Annual Review of Earth and Planetary Sciences 42, 317–339.

Brown, J. R., G. C. Beroza, S. Ide, K. Ohta, D. R. Shelly, S. Y. Schwartz, W. Rabbel, M. Thorwart, and H. Kao (2009). Deep low-frequency earthquakes in tremor localize to the plate interface in multiple subduction zones. Geophysical Research Letters 36(19).

Brown, J. R., S. G. Prejean, G. C. Beroza, J. S. Gomberg, and P. J. Haeussler (2013). Deep low-frequency earthquakes in tectonic tremor along the alaska-aleutian subduction zone. Journal of Geophysical Research: Solid Earth 118(3), 1079–1090.

Chen, T. and N. Lapusta (2009). Scaling of small repeating earthquakes explained by interaction of seismic and aseismic slip in a rate and state fault model. Journal of Geophysical Research: Solid Earth 114(B1).

Colella, H. V., J. H. Dieterich, and K. B. Richards-Dinger (2011). Multi-event simulations of slow slip events for a cascadia-like subduction zone. Geophysical Research Letters 38(16).

Crosson, R. S. (1976). Crustal structure modeling of earthquake data: 1. simultaneous least squares estimation of hypocenter and velocity parameters. Journal of geophysical research 81(17), 3036–3046.

Delahaye, E., J. Townend, M. Reyners, and G. Rogers (2009). Microseismicity but no tremor accompanying slow slip in the hikurangi subduction zone, new zealand. Earth and Planetary Science Letters 277(1-2), 21–28.

Doser, D. I. (1992). Historic earthquakes (1918 to 1923) and an assessment of source parameters along the san jacinto fault system. Bulletin of the Seismological Society of America 82(4), 1786–1801.

Dragert, H., K. Wang, and G. Rogers (2004). Geodetic and seismic signatures of episodic tremor and slip in the northern cascadia subduction zone. Earth, planets and space 56(12), 1143–1150.

Fialko, Y. (2006). Interseismic strain accumulation and the earthquake potential on the southern san andreas fault system. Nature 441(7096), 968.

Frank, W. B. (2016). Slow slip hidden in the noise: The intermittence of tectonic release. Geophysical Research Letters 43(19).

Fraser-Smith, A. C., A. Bernardi, P. McGill, M. Ladd, R. Helliwell, and O. Villard (1990). Low-frequency magnetic field measurements near the epicenter of the ms 7.1 loma prieta earthquake. Geophysical Research Letters 17(9), 1465–1468.

Fukuda, M., T. Sagiya, and Y. Asai (2008). A causal relationship between the slow slip event and deep low frequency tremor indicated by strain data recorded at shingu borehole station. In AGU Fall Meeting Abstracts.

Gershenzon, N. I., G. Bambakidis, E. Hauser, A. Ghosh, and K. C. Creager (2011). Episodic tremors and slip in cascadia in the framework of the frenkel-kontorova model. Geophysical Research Letters 38(1).

Ghosh, A., E. Huesca-Pérez, E. Brodsky, and Y. Ito (2015). Very low frequency earthquakes in cascadia migrate with tremor. Geophysical Research Letters 42(9), 3228–3232.

Ghosh, A., J. E. Vidale, and K. C. Creager (2012). Tremor asperities in the transition zone control evolution of slow earthquakes. Journal of Geophysical Research: Solid Earth 117(B10).

Ghosh, A., J. E. Vidale, Z. Peng, K. C. Creager, and H. Houston (2009). Complex nonvolcanic tremor near parkfield, california, triggered by the great 2004 sumatra earthquake. Journal of Geophysical Research: Solid Earth 114(B12).

Ghosh, A., J. E. Vidale, J. R. Sweet, K. C. Creager, and A. G. Wech (2009). Tremor patches in cascadia revealed by seismic array analysis. Geophysical Research Letters 36(17).

Ghosh, A., J. E. Vidale, J. R. Sweet, K. C. Creager, A. G. Wech, and H. Houston (2010). Tremor bands sweep cascadia. Geophysical Research Letters 37(8).

Ghosh, A., J. E. Vidale, J. R. Sweet, K. C. Creager, A. G. Wech, H. Houston, and E. E. Brodsky (2010). Rapid, continuous streaking of tremor in cascadia. Geochemistry, Geophysics, Geosystems 11(12).

Gomberg, J., D. Agnew, and S. Schwartz (2016). Alternative source models of very low frequency events. Journal of Geophysical Research: Solid Earth 121(9), 6722–6740.

Gomberg, J., P. Reasenberg, P. Bodin, and R. Harris (2001). Earthquake triggering by seismic waves following the landers and hector mine earthquakes. Nature 411(6836), 462.

Gomberg, J., J. L. Rubinstein, Z. Peng, K. C. Creager, J. E. Vidale, and P. Bodin (2008). Widespread triggering of nonvolcanic tremor in california. Science 319(5860), 173–173.

Guilhem, A. and R. M. Nadeau (2012). Episodic tremors and deep slow-slip events in central california. Earth and Planetary Science Letters 357, 1–10.

Hawthorne, J. and N. Bartlow (2018). Observing and modeling the spectrum of a slow slip event. Journal of Geophysical Research: Solid Earth.

Hawthorne, J. C. and A. M. Rubin (2013). Short-time scale correlation between slow slip and tremor in cascadia. Journal of Geophysical Research: Solid Earth 118(3), 1316–1329.

Hayakawa, M., R. Kawate, O. A. Molchanov, and K. Yumoto (1996). Results of ultra-low-frequency magnetic field measurements during the guam earthquake of 8 august 1993. Geophysical Research Letters 23(3), 241–244.

Hill, D., P. Reasenberg, A. Michael, W. Arabaz, G. Beroza, D. Brumbaugh, J. Brune, R. Castro, S. Davis, W. Ellsworth, et al. (1993). Seismicity remotely triggered by the magnitude 7.3 landers, california, earthquake. Science 260(5114), 1617–1623.

Hill, D. P. (2012). Dynamic stresses, coulomb failure, and remote triggering—corrected. Bulletin of the Seismological Society of America 102(6), 2313–2336.

Hill, D. P. and S. Prejean (2015). Dynamic triggering.

Hirose, H., Y. Asano, K. Obara, T. Kimura, T. Matsuzawa, S. Tanaka, and T. Maeda (2010). Slow earthquakes linked along dip in the nankai subduction zone. Science 330(6010), 1502–1502.

Hirose, H. and K. Obara (2010). Recurrence behavior of short-term slow slip and correlated nonvolcanic tremor episodes in western shikoku, southwest japan. Journal of Geophysical Research: Solid Earth 115(B6).

Houston, H., B. G. Delbridge, A. G. Wech, and K. C. Creager (2011). Rapid tremor reversals in cascadia generated by a weakened plate interface. Nature Geoscience 4(6), 404.

Huesca-Pérez, E. and A. Ghosh (2015). Crustal anisotropy from tectonic tremor under washington state in the cascadia. Geophysical Research Letters 42(7), 2228–2234.

Hutchison, A. A. and A. Ghosh (2016). Very low frequency earthquakes spatiotemporally asynchronous with strong tremor during the 2014 episodic tremor and slip event in cascadia. Geophysical Research Letters 43(13), 6876–6882.

Hutchison, A. A. and A. Ghosh (2017). Ambient tectonic tremor in the san jacinto fault, near the anza gap, detected by multiple mini seismic arraysambient tectonic tremor in the san jacinto fault, near the anza gap, detected by multiple mini seismic arrays. Bulletin of the Seismological Society of America 107(5), 1985–1993.

Hyndman, R. D. and S. M. Peacock (2003). Serpentinization of the forearc mantle. Earth and Planetary Science Letters 212(3-4), 417–432.

Ide, S. (2016). Characteristics of slow earthquakes in the very low frequency band: Application to the cascadia subduction zone. Journal of Geophysical Research: Solid Earth 121(8), 5942–5952.

Ide, S., A. Baltay, and G. C. Beroza (2011). Shallow dynamic overshoot and energetic deep rupture in the 2011 mw 9.0 tohoku-oki earthquake. Science 332(6036), 1426–1429.

Ide, S., G. C. Beroza, D. R. Shelly, and T. Uchide (2007). A scaling law for slow earthquakes. Nature 447(7140), 76.

Ide, S., K. Imanishi, Y. Yoshida, G. C. Beroza, and D. R. Shelly (2008). Bridging the gap between seismically and geodetically detected slow earthquakes. Geophysical Research Letters 35(10).

Ide, S., D. R. Shelly, and G. C. Beroza (2007). Mechanism of deep low frequency earthquakes: Further evidence that deep non-volcanic tremor is generated by shear slip on the plate interface. Geophysical Research Letters 34(3).

Inbal, A., J.-P. Ampuero, and J.-P. Avouac (2017). Locally and remotely triggered aseismic slip on the central san jacinto fault near anza, ca, from joint inversion of seismicity and strainmeter data. Journal of Geophysical Research: Solid Earth 122(4), 3033–3061.

Ito, Y. and K. Obara (2006a). Dynamic deformation of the accretionary prism excites very low frequency earthquakes. Geophysical Research Letters 33(2).

Ito, Y. and K. Obara (2006b). Very low frequency earthquakes within accretionary prisms are very low stress-drop earthquakes. Geophysical Research Letters 33(9).

Ito, Y., K. Obara, T. Matsuzawa, and T. Maeda (2009). Very low frequency earthquakes related to small asperities on the plate boundary interface at the locked to aseismic transition. Journal of Geophysical Research: Solid Earth 114(B11).

Ito, Y., K. Obara, K. Shiomi, S. Sekine, and H. Hirose (2007). Slow earthquakes coincident with episodic tremors and slow slip events. Science 315(5811), 503–506.

Jiang, J. and Y. Fialko (2016). Reconciling seismicity and geodetic locking depths on the anza section of the san jacinto fault. Geophysical Research Letters 43(20).

Kano, M., N. Aso, T. Matsuzawa, S. Ide, S. Annoura, R. Arai, S. Baba, M. Bostock, K. Chao, K. Heki, et al. (2018). Development of a slow earthquake database. Seismological Research Letters.

Kato, A. and S. Nakagawa (2014). Multiple slow-slip events during a foreshock sequence of the 2014 iquique, chile mw 8.1 earthquake. Geophysical Research Letters 41(15), 5420–5427.

Kato, A., K. Obara, T. Igarashi, H. Tsuruoka, S. Nakagawa, and N. Hirata (2012). Propagation of slow slip leading up to the 2011 mw 9.0 tohoku-oki earthquake. Science, 1215141.

Lindsey, E. O., V. J. Sahakian, Y. Fialko, Y. Bock, S. Barbot, and T. K. Rockwell (2014). Interseismic strain localization in the san jacinto fault zone. Pure and Applied Geophysics 171(11), 2937–2954.

Liu, Z., Y. Fu, Y. Bock, Y. Jiang, A. Moore, S. Owen, and S. Kedar (2015). Investi-

gate the spatiotemporal relationship between slow slip transients and tremor in cascadia subduction zone. In AGU Fall Meeting Abstracts.

Lohman, R. B. and J. J. McGuire (2007). Earthquake swarms driven by aseismic creep in the salton trough, california. Journal of Geophysical Research: Solid Earth 112(B4).

Matsuzawa, T., Y. Asano, and K. Obara (2015). Very low frequency earthquakes off the pacific coast of tohoku, japan. Geophysical Research Letters 42(11), 4318–4325.

McGuire, J. J., M. S. Boettcher, and T. H. Jordan (2005). Foreshock sequences and short-term earthquake predictability on east pacific rise transform faults. Nature 434(7032), 457.

Meng, X. and Z. Peng (2015). Increasing lengths of aftershock zones with depths of moderate-size earthquakes on the san jacinto fault suggests triggering of deep creep in the middle crust. Geophysical Journal International 204(1), 250–261.

Nadeau, R. M. and D. Dolenc (2005). Nonvolcanic tremors deep beneath the san andreas fault. Science 307(5708), 389–389.

Nadeau, R. M. and A. Guilhem (2009). Nonvolcanic tremor evolution and the san simeon and parkfield, california, earthquakes. science 325(5937), 191–193.

Nakamura, M. and N. Sunagawa (2015). Activation of very low frequency earthquakes by slow slip events in the ryukyu trench. Geophysical Research Letters 42(4), 1076–1082.

Nakata, R., R. Ando, T. Hori, and S. Ide (2011). Generation mechanism of slow earth-

quakes: Numerical analysis based on a dynamic model with brittle-ductile mixed fault heterogeneity. Journal of Geophysical Research: Solid Earth 116(B8).

Nedimović, M. R., R. D. Hyndman, K. Ramachandran, and G. D. Spence (2003). Reflection signature of seismic and aseismic slip on the northern cascadia subduction interface. Nature 424(6947), 416.

Obara, K. (2002). Nonvolcanic deep tremor associated with subduction in southwest japan. Science 296(5573), 1679–1681.

Obara, K. (2010). Phenomenology of deep slow earthquake family in southwest japan: Spatiotemporal characteristics and segmentation. Journal of Geophysical Research: Solid Earth 115(B8).

Obara, K., H. Hirose, F. Yamamizu, and K. Kasahara (2004). Episodic slow slip events accompanied by non-volcanic tremors in southwest japan subduction zone. Geophysical Research Letters 31(23).

Obara, K. and A. Kato (2016). Connecting slow earthquakes to huge earthquakes. Science 353(6296), 253–257.

Payero, J. S., V. Kostoglodov, N. Shapiro, T. Mikumo, A. Iglesias, X. Pérez-Campos, and R. W. Clayton (2008). Nonvolcanic tremor observed in the mexican subduction zone. Geophysical Research Letters 35(7).

Peng, Z. and J. Gomberg (2010). An integrated perspective of the continuum between earthquakes and slow-slip phenomena. Nature Geoscience 3(9), 599.

Peng, Z., J. E. Vidale, A. G. Wech, R. M. Nadeau, and K. C. Creager (2009). Remote triggering of tremor along the san andreas fault in central california. Journal of Geophysical Research: Solid Earth 114(B7).

Rogers, G. and H. Dragert (2003). Episodic tremor and slip on the cascadia subduction zone: The chatter of silent slip. Science 300(5627), 1942–1943.

Rost, S. and C. Thomas (2002). Array seismology: Methods and applications. Reviews of geophysics 40(3).

Rouet-Leduc, B., C. Hulbert, and P. A. Johnson (2018). Breaking cascadia's silence: Machine learning reveals the constant chatter of the megathrust. arXiv preprint arXiv:1805.06689.

Rubin, A. M. (2011). Designer friction laws for bimodal slow slip propagation speeds. Geochemistry, Geophysics, Geosystems 12(4).

Rubinstein, J. L., M. La Rocca, J. E. Vidale, K. C. Creager, and A. G. Wech (2008). Tidal modulation of nonvolcanic tremor. Science 319(5860), 186–189.

Ruiz, S., M. Metois, A. Fuenzalida, J. Ruiz, F. Leyton, R. Grandin, C. Vigny, R. Madariaga, and J. Campos (2014). Intense foreshocks and a slow slip event preceded the 2014 iquique mw 8.1 earthquake. Science 345(6201), 1165–1169.

Ryberg, T., C. Haberland, G. Fuis, W. Ellsworth, and D. Shelly (2010). Locating nonvolcanic tremor along the san andreas fault using a multiple array source imaging technique. Geophysical Journal International 183(3), 1485–1500.

Saffer, D. M. and L. M. Wallace (2015). The frictional, hydrologic, metamorphic and thermal habitat of shallow slow earthquakes. Nature Geoscience 8(8), 594.

Sanders, C. O. and H. Kanamori (1984). A seismotectonic analysis of the anza seismic gap, san jacinto fault zone, southern california. Journal of Geophysical Research: Solid Earth 89(B7), 5873–5890.

Scott, J. S., T. G. Masters, and F. L. Vernon (1994). 3-d velocity structure of the san jacinto fault zone near anza, california—i. p waves. Geophysical Journal International 119(2), 611–626.

Shearer, P. M. (1994). Global seismic event detection using a matched filter on long-period seismograms. Journal of Geophysical Research: Solid Earth 99(B7), 13713–13725.

Shelly, D. R. (2009). Possible deep fault slip preceding the 2004 parkfield earthquake, inferred from detailed observations of tectonic tremor. Geophysical Research Letters 36(17).

Shelly, D. R. (2010). Periodic, chaotic, and doubled earthquake recurrence intervals on the deep san andreas fault. Science 328(5984), 1385–1388.

Shelly, D. R., G. C. Beroza, and S. Ide (2007). Non-volcanic tremor and low-frequency earthquake swarms. Nature 446(7133), 305.

Shelly, D. R., G. C. Beroza, S. Ide, and S. Nakamula (2006). Low-frequency earthquakes in shikoku, japan, and their relationship to episodic tremor and slip. Nature 442(7099), 188.

Shelly, D. R., W. L. Ellsworth, T. Ryberg, C. Haberland, G. S. Fuis, J. Murphy, R. M.

Nadeau, and R. Bürgmann (2009). Precise location of san andreas fault tremors near cholame, california using seismometer clusters: Slip on the deep extension of the fault? Geophysical Research Letters 36(1).

Suzuki, T. and T. Yamashita (2009). Dynamic modeling of slow earthquakes based on thermoporoelastic effects and inelastic generation of pores. Journal of Geophysical Research: Solid Earth 114(B6).

Sweet, J. R., K. C. Creager, and H. Houston (2014). A family of repeating low-frequency earthquakes at the downdip edge of tremor and slip. Geochemistry, Geophysics, Geosystems 15(9), 3713–3721.

Szeliga, W., T. I. Melbourne, M. M. Miller, and V. M. Santillan (2004). Southern cascadia episodic slow earthquakes. Geophysical Research Letters 31(16).

Takeo, A., K. Idehara, R. Iritani, T. Tonegawa, Y. Nagaoka, K. Nishida, H. Kawakatsu, S. Tanaka, K. Miyakawa, T. Iidaka, et al. (2010). Very broadband analysis of a swarm of very low frequency earthquakes and tremors beneath kii peninsula, sw japan. Geophysical Research Letters 37(6).

Tape, C., S. Holtkamp, V. Silwal, J. Hawthorne, Y. Kaneko, J. P. Ampuero, C. Ji, N. Ruppert, K. Smith, and M. E. West (2018). Earthquake nucleation and fault slip complexity in the lower crust of central alaska. Nature Geoscience, 1.

Thatcher, W., J. A. Hileman, and T. C. Hanks (1975). Seismic slip distribution along the san jacinto fault zone, southern california, and its implications. Geological Society of America Bulletin 86(8), 1140–1146.

Thomas, T. W., J. E. Vidale, H. Houston, K. C. Creager, J. R. Sweet, and A. Ghosh (2013). Evidence for tidal triggering of high-amplitude rapid tremor reversals and tremor streaks in northern cascadia. Geophysical Research Letters 40(16), 4254–4259.

To, A., K. Obana, H. Sugioka, E. Araki, N. Takahashi, and Y. Fukao (2015). Small size very low frequency earthquakes in the nankai accretionary prism, following the 2011 tohoku-oki earthquake. Physics of the Earth and Planetary Interiors 245, 40–51.

Toppozada, T. R., C. R. Real, S. P. Bezore, and D. L. Parke (1981). Preparation of isoseismal maps and summaries of reported effects for pre-1900 california earthquakes. Technical report, US Geological Survey.

Van Der Elst, N. J. and E. E. Brodsky (2010). Connecting near-field and far-field earthquake triggering to dynamic strain. Journal of Geophysical Research: Solid Earth 115(B7).

Vidale, J. E., A. J. Hotovec, A. Ghosh, K. C. Creager, and J. Gomberg (2011). Tiny intraplate earthquakes triggered by nearby episodic tremor and slip in cascadia. Geochemistry, Geophysics, Geosystems 12(6).

Wallace, L. M. and J. Beavan (2010). Diverse slow slip behavior at the hikurangi subduction margin, new zealand. Journal of Geophysical Research: Solid Earth 115(B12).

Walter, J. I., S. Y. Schwartz, J. M. Protti, and V. Gonzalez (2011). Persistent tremor within the northern costa rica seismogenic zone. Geophysical Research Letters 38(1).

Walter, J. I., S. Y. Schwartz, M. Protti, and V. Gonzalez (2013). The synchronous occurrence of shallow tremor and very low frequency earthquakes offshore of the nicoya peninsula, costa rica. Geophysical Research Letters 40(8), 1517–1522.

Wech, A., C. Boese, T. Stern, and J. Townend (2012). Tectonic tremor and deep slow slip on the alpine fault. Geophysical Research Letters 39(10).

Wech, A. G. (2010). Interactive tremor monitoring. Seismological Research Letters 81(4), 664–669.

Wech, A. G. and N. M. Bartlow (2014). Slip rate and tremor genesis in cascadia. Geophysical Research Letters 41(2), 392–398.

Wech, A. G. and K. C. Creager (2008). Automated detection and location of cascadia tremor. Geophysical Research Letters 35(20).

Wech, A. G., K. C. Creager, and T. I. Melbourne (2009). Seismic and geodetic constraints on cascadia slow slip. Journal of Geophysical Research: Solid Earth 114(B10).

Zhang, J., P. Gerstoft, P. M. Shearer, H. Yao, J. E. Vidale, H. Houston, and A. Ghosh (2011). Cascadia tremor spectra: Low corner frequencies and earthquake-like high-frequency falloff. Geochemistry, Geophysics, Geosystems 12(10).